Utah State University

DigitalCommons@USU

5-2023

Groundwater-Surface Water Interaction to Increase Groundwater Availability

Saeid Masoudiashtiani
Utah State University

Follow this and additional works at: https://digitalcommons.usu.edu/etd

Part of the Civil and Environmental Engineering Commons

Recommended Citation

Utah State University
MERRILL-CAZIER LIBRARY

GROUNDWATER-SURFACE WATER INTERACTION TO INCREASE GROUNDWATER AVAILABILITY

by

Saeid Masoudiashtiani

A dissertation submitted in partial fulfillment
of the requirements for the degree

of

DOCTOR OF PHILOSOPHY

in

Civil and Environmental Engineering

Approved:

_____   _____
Richard C. Peralta, Ph.D.   R. Ryan Dupont, Ph.D.
Major Professor   Committee Member

_____   _____
Niel Allen, Ph.D.   Thomas E. Lachmar, Ph.D.
Committee Member   Committee Member

_____   _____
Stephen Clyde, Ph.D.   D. Richard Cutler, Ph.D.
Committee Member   Interim Vice Provost of Graduate Studies

UTAH STATE UNIVERSITY
Logan, Utah

2023

ABSTRACT

Groundwater-Surface Water Interaction to Increase Groundwater Availability

by

Saeid Masoudiashtiani, Doctor of Philosophy

Utah State University, 2023

Major Professor: Dr. Richard C. Peralta
Department: Civil and Environmental Engineering

Aquifer storage and recovery (ASR), aquifer recharge (AR), and green-infrastructure (GI) recharge system use can increase groundwater availability. Presented are predictive simulation software tools to aid in designing such systems for density-independent groundwater flows. First, for an ASR well at which extraction from an unconfined aquifer begins when injection ceases, are surrogate estimators that predict injectate recovery effectiveness (REN, the time-varying proportion of injectate that has been extracted). The REN estimators are applicable for situations in wide ranges of hydraulic conductivity, specific yield, initial saturated thickness, initial aquifer hydraulic gradient, porosity, and assumed steady rates of injection (61 days) and extraction (91 days). Second, the presented user-friendly Managed Aquifer Storage for Effective Recovery

(MASER) software employs these estimators to enable addressing a wide range of appropriate sites. For other ASR or AR situations, MASER can semi-automatically apply MODFLOW2005 and MT3DMS to simulate groundwater flow and transport after requesting user-input: (un)steady injection (61 days) rates; injectate solute concentration; ambient groundwater solute concentration; duration of storage period before extraction begins; and extraction rates (91 days). MASER provides simulated values of REN and the blended solute concentration of ASR-extracted water, about every 15 days and produces aquifer solute concentration maps.

Third, for predicting impacts of urban GI implementation in Utah (Salt Lake County 1300 South Drainage Basin), is HyperRBC, a MODFLOW2005 stream-aquifer simulation model implementation. Derived from a Salt Lake Valley-wide multilayer groundwater model, but including only the Red Butte watershed, the HyperRBC model also differs from the valley-wide model by having a refined discretization and by using the Streamflow-Routing (SFR) package to simulate Red Butte Creek (RBC) flow. After calibration of the RBC vertical hydraulic conductivity values, HyperRBC was used to predict unconfined aquifer storage changes due to a hypothetical GI implementation of grass swales to reduce stormwater runoff. Assumed was a total of 54.30 ac-ft GI aquifer recharge from April through June of 2016 within a 704-acre area located east of the Jordan River. The simulation predicted that by the end of a year: about three percent of the recharge remained within the unconfined aquifer in the HyperRBC area; 66.6% of the recharge flowed as groundwater northward into the extensive unconfined aquifer; and 30.3% discharged to surface waters.

(166 pages)

PUBLIC ABSTRACT

Groundwater-Surface Water Interaction to Increase Groundwater Availability

Saeid Masoudiashtiani

This study develops procedures for using surface water to increase groundwater availability and sustainable yield, and for evaluating impacts on surface water. Increasing sustainable groundwater yield requires reducing the gap between the volumes of discharge from versus recharge to an aquifer. The study presents procedures for water user(s) to help increase groundwater availability. Toward that end, this study simulates and evaluates: a) aquifer storage and recovery (ASR) of water diverted from Red Butte Creek in Salt Lake Valley, Utah for subsequent turf irrigation; b) ASR injection of residential runoff from daily rainfall for subsequent extraction to irrigate turf; and c) stream-aquifer seepage and aquifer recharge from use of grass swales (green infrastructure).

Employed groundwater and/or surface water modeling tools include finite difference numerical flow and solute transport simulation models, and statistical expressions. Utilized simulation and/or optimization tools show how to best use surface water to increase aquifer recharge and quantify its impacts on stream-aquifer seepage and streamflow.

ACKNOWLEDGMENTS

CONTENTS   Page

Figure   LIST OF FIGURES   Page

CHAPTER 1

INTRODUCTION

Increasing aquifer recharge can potentially increase the sustained availability of groundwater within an aquifer. By using data from Utah's Salt Lake Valley, this research considers three situations for increasing groundwater recharge. Among these situations, two involve replacing or supplementing current water use for summer irrigation. Both of those situations employ aquifer storage and recovery (ASR) to inject surface water when abundant, and then to extract the injectate during the more arid turf irrigation season. The third situation envisions the implementation of grass swales to induce rainfall infiltration and recharge of a shallow aquifer. Simulated are the effects on stored groundwater volume and groundwater seepage to the Jordan River in Utah, USA. Also, the rainfall runoff flows into residential-area outfalls that are connected to pre-existing drainage networks and then routed through the Jordan River without infiltrating.

In Salt Lake Valley (iUTAH, 2012), rainfall and surface water flows are greatest shortly before irrigation water demand becomes large. ASR is a method useful for helping balance the timing of available water and water demand. ASR involves injecting available surface water into an aquifer for later extraction to help satisfy water demand. Considerations affecting the physical and legal feasibilities of ASR injection include the existing uses and qualities of the surface water and the receiving groundwater, and the amount of time that injectate remains stored (injectate longevity) within the receiving aquifer. The longevity is affected by physical aquifer characteristics and flows, and the time series of injection and subsequent extraction. Quantifying remained, and recovered ASR injectate within, and from an aquifer can be important to: a)

prevent undesirable or long-term groundwater quality changes; and b) assure the availability of sufficient aquifer-stored injectate for future use as groundwater, respectively. With the aid of developed estimators in Chapter 2, the recovered injectate (recovery effectiveness, REN), and the remained (1.00 - REN) at different times can be quantified to present the groundwater quality changes.

Chapter 2 defines REN as differing from the recovery efficiency (RE) used to quantify the ratio of ASR-well injectate volume divided by the volume of extracted water (a blend of injectate and native brackish, or saline groundwater), that does not need treatment before its intended use (Pyne, 1995; Bakker, 2010). Estimating injectate recovery (Bockelmann et al., 2003; Ptak et al., 2004; and Visser et al., 2014) can be performed by field tracer tests but results of that process have much uncertainty (Fitts, 1996). The developed Chapter 2 estimators simplify REN-estimation for unconfined aquifers. Chapter 3 presents an easy-to-use tool that can help natural resource developers, planners, and managers to estimate REN, the solute concentrations of extracted water, and the solute concentrations remaining in the aquifer.

In Chapter 3, the presented MASER (Managed Aquifer Storage for Effective Recovery) software applies hydrogeologic-site information to estimate time series of: aquifer head drawup and/or drawdown; concentrations of solutes in water being pumped out of the aquifer and solutes remaining within the aquifer. MASER can simulate (un)steady injection of stormwater versus steady injection of diverted streamflow; and extraction of the same volume or a greater volume than is injected (possibly to protect aquifer groundwater quality). MASER does not inherently address changes in stream-aquifer seepage that can result from diverting flow from a stream or from increasing aquifer recharge, but the option exists to do so. On the other hand, Chapter 4

presents a water simulation model of the 1300 South Drainage Basin in Salt Lake County, Utah. The model can simulate Red Butte Creek (RBC) surface water flow, stream-aquifer seepage, and groundwater flow.

The Chapter 4 HyperRBC simulation model accepts Red Butte Reservoir discharge data as input to represent headwater inflow into RBC. From that inflow location, HyperRBC simulates flows and seepages downstream to and including part of the Jordan River. HyperRBC development involved: a) designating a subsystem of the Salt Lake Valley MODFLOW groundwater flow model calibrated by the U.S.G.S. (Lambert, 1995); b) selecting a refined spatial discretization to increase model accuracy; c) conceptualizing and implementing the addition of Red Butte Creek features to the groundwater subsystem model; d) obtaining available physical system data to describe the coupled aquifer and stream system; e) identifying available and relevant boundary condition data; f) calibrating the streambed vertical hydraulic conductivity values required to simulate stream-aquifer seepage; and g) simulating recharge resulting from infiltration and percolation of applied grass swale in Salt Lake Valley residential areas. The recharge affects stored groundwater volume, and seepages between groundwater and surface waters (e.g., RBC, and the Jordan River) nearby within the Red Butte watershed.

In short, this dissertation provides tools to use aquifer recharge for increasing groundwater availability. Provided tools include estimators and simulators of injectate recovery from unconfined aquifers, and a case study numerical model for quantifying groundwater-surface water seepage resulting from the grass swale recharge to an aquifer.

References

Bakker, M. (2010). Radial Dupuit interface flow to assess the aquifer storage and recovery potential of saltwater aquifers. Hydrogeology Journal, 18, 107-115. https://doi.org/10.1007/s10040-009-0508-1

Bockelmann, A., Zamfirescu, D., Ptak, T., Grathwohl, P., & Teutsch, G. (2003). Quantification of mass fluxes and natural attenuation rates at an industrial site with a limited monitoring network: a case study. Contaminant Hydrology J., 60(1–2), 97-121. https://doi.org/10.1016/S0169-7722(02)00060-8

Fitts, C. R. (1996). Uncertainty in deterministic groundwater transport models due to the assumption of macrodispersive mixing: evidence from the Cape Cod (Massachusetts, U.S.A.) and Borden (Ontario, Canada) tracer tests. Contaminant Hydrology J., 23, 69-84. https://doi.org/10.1016/0169-7722(95)00101-8

Innovate Urban Transitions and Arid region Hydro-sustainability (iUTAH). (2012). https://iutahepscor.org/

Lambert, P. M. (1995). Numerical Simulation of Ground-Water Flow in Basin-Fill Material in Salt Lake Valley, Utah. U. S. Geological Survey Technical Publication No. 110-B. https://pubs.er.usgs.gov/publication/70179464

Ptak, T., Piepenbrink, M., & Martac, E. (2004). Tracer tests for the investigation of heterogeneous porous media and stochastic modelling of flow and transport—a review of some recent developments. Hydrology J., 294(1–3), 122-163. https://doi.org/10.1016/j.jhydrol.2004.01.020

Pyne, R. D. G. (1995). Groundwater Recharge and Wells: A Guide to Aquifer Storage Recovery. CRC Press Inc.

Visser, A., Singleton, M. J., & Esser, B. K. (2014). Xenon Tracer Test at Woodland Aquifer Storage and Recovery Well, Lawrence Livermore National Laboratory, A report to West Yost Associates LLNL-TR-652313. https://www.osti.gov/servlets/purl/1162248

CHAPTER 2

RECONNAISSANCE PREDICTION OF ASR WELL RECOVERY EFFECTIVENESS IN UNCONFINED AQUIFERS

Abstract

Presented polynomial equations aid reconnaissance aquifer storage and recovery (ASR) well design for unconfined aquifers by allowing rapid REN (the time-varying proportion of injectate that has been extracted) prediction without requiring preparation for and execution of solute transport simulations. Knowledge of REN allows predicting the blended concentration of a conservative solute, such as chloride, within the extracted water. Assume that into an isotropic homogenous portion of an unconfined, one-layer aquifer, water is injected for 61 days at a steady rate through a fully penetrating ASR well, and then water is extracted from the well at the same steady rate for up to 91 days. Presented polynomial predictors were designed to match REN values resulting from groundwater flow and solute transport simulations for ranges of factors representative of Great Basin intermountain valley unconfined aquifers (hydraulic conductivity, specific yield, initial saturated thickness, background hydraulic gradient, porosity, and steady rates and durations of injection and extraction). Nonlinear optimization and regression aided the development of dimensionless parameters, and the calibration of one polynomial REN predictor per combination of porosity and extraction duration. The predictors appropriately estimate the REN achievable by one ASR well injecting diverted water during a time of surface water availability, and subsequently extracting groundwater during a 91-day period of high demand.

Total extraction equals total injection at the end of extraction day 61. Subsequently continued extraction presumes a pre-existing groundwater right.

2.1. Introduction

Aquifer storage and recovery (ASR) involves storing available excess surface water within an aquifer and subsequently recovering the water when needed for beneficial uses. Here, it is assumed that when available, surface water is injected into an aquifer via an ASR well. After water availability for injection ceases, the same ASR well immediately begins extracting groundwater for irrigation use. After extraction begins, the ASR recovery effectiveness (REN) is the proportion of the total injected water molecules that is contained within the total volume of water extracted by that time. REN cannot exceed a value of one.

REN differs from a recovery efficiency (RE) used to quantify the performance of ASR wells that inject water into brackish, saline, or coastal aquifers and extract blended water that does not need treatment before its intended use (Pyne, 1995; Bakker, 2010). RE can exceed a value of one because it is the result of dividing the extracted volume that does not need treatment by the injectate volume (Kimbler et al., 1975; Pavelic et al., 2005; Lowry and Anderson, 2006; Ward et al., 2008 and 2009; Lu et al. 2011; Brown et al., 2016).

REN is important in situations requiring knowledge of how much of the injected water is subsequently extracted or how much remains in the aquifer. Sometimes modest mixing of (un)treated surface water or stormwater with groundwater in an aquifer is legally and

environmentally acceptable. Estimating REN helps predict the degree of blending that will

occur. In other situations, legal water rights are involved. In the state of Utah, by injecting

surplus surface water into a confined aquifer during wet months, the Jordan Valley Water

Conservancy District (JVWCD) earns the right to extract more groundwater during dry

months. If JVWCD does not extract the injectate volume within one year after injection,

the volume of the new water right decreases due to assumed losses within the aquifer.

Rather than assessing how much injectate escapes subsequent capture by an extracting

ASR well, Forghani and Peralta (2018) used a counting molecule method to estimate ASR

well recovery effectiveness (REN). The relation between REN and RE is:

$$RE = REN(V_E) + \frac{V(E, amb)}{V_{inj}} \tag{1}$$

where $V(E, amb)$ is the volume of ambient groundwater in the extracted water, V_E is

the total volume of extracted water, and V_{inj} is the total volume of injectate.

Situations in which injected water and native groundwater have similar quality are

particularly challenging for estimating REN in the field. Field tracer tests have been

performed to estimate injectate recovery (Bockelmann et al., 2003; Ptak et al., 2004;

Visser et al., 2014), but involve much uncertainty (Fitts, 1996). A procedure or tool that

simplifies the task of estimating REN for ASR operation in an unconfined aquifer is needed.

The presented suite of predictive equations is such a tool. Employed ranges of input

parameter values exceed the ranges of values reported for a representative 756 km^2 (288 mi^2) shallow unconfined aquifer in an intermountain valley in the U.S. Great Basin.

2.2. Methods and Materials

2.2.1. Parameters and procedures for REN simulation and prediction

2.2.1.1. Overview

It is desired to increase groundwater availability during a dry period (June-August) by injecting available excess surface water into an unconfined aquifer during a preceding wet period (April-May). This subsection defines the factors that impact REN and identifies the ranges of factor values that exist in Salt Lake Valley, Utah.

After selection of approximately half-month durations for flow and solute transport simulations, standard methods are used in estimating: the advective plume length after two months (61 days) of injection; the longitudinal dispersivity; Courant number; maximum time step size; total number of simulation time steps; and time steps per each stress period. These estimates enable preparing a groundwater aquifer model domain sufficiently large that assumed injection and extraction rates will not appreciably affect any employed boundary conditions.

To cover the ranges of REN-affecting factors, 48,000 unique input files were prepared for flow and solute transport simulations that were then processed in

parallel. From simulation results, the procedure required computing simulated REN response, and identifying parameter combinations and dimensionless terms that aid REN prediction. After envisioning those terms within polynomial expressions, nonlinear optimization and regression generated the coefficient values for the polynomial equations. Finally, a statistical comparison of simulated versus polynomial-predicted values of REN was used to determine the accuracy of the predictors.

2.2.1.2. Selection of REN impact factors and their ranges of values

Based upon work by Fetter (1999), Bedient et al., (1999), Pavelic et al., (2005), Ward et al., (2008, 2009), Bakker (2010), Brown et al., (2016), Smith et al. (2017), and Forghani and Peralta (2018), eight impact factors that affect REN were considered: 1) initial aquifer (background) hydraulic gradient; 2) horizontal hydraulic conductivity; 3) initial (original) saturated thickness; 4) porosity; 5) specific yield; 6) steady rates of injection and extraction; 7) durations of injection and extraction; and 8) well diameter. Applying the Table 2.1 parameter values ranges yielded 48,000 different sets of input data for groundwater flow and solute transport simulations.

The ranges of background hydraulic gradient, horizontal hydraulic conductivity, and initial saturated thickness used here, include the values employed for Layer 1 of a Salt Lake Valley groundwater model (Lambert, 1995). To set the 0.1-0.6 range of porosity values, this study also relies upon values from Gelhar et al.

(1992) and Heath (1983). To determine the specific yield range, the porosity range and a 0.375-0.95 range of ((specific yield)/porosity) quotients (Table 2.1) were used. The 5.451 to 327.06 m³/d (1 to 60 gpm) steady injection rate range approximates the range of one percent of the average local Red Butte Creek flow of 2014 through 2016 during April and May, the months of greatest streamflow (iUTAH, 2012). The range of steady extraction rates is equal but opposite in sign to the injection rate range. The extraction duration is three months (Table 2.1).

Table 2.1

Ranges of input parameter values

Input Parameter	Range (SI)	Range (English)
Background hydraulic gradient	0.00001-0.015	0.00001-0.015
Horizontal hydraulic conductivity	4-20 (m/d)	13.124-65.61 (ft/d)
Initial saturated thickness	8-46 (m)	26.25-150.91 (ft)
Porosity	0.1-0.6	0.1-0.6
(Specific yield) / (porosity)	0.375-0.95	0.375-0.95
Specific yield	0.0375-0.57	0.0375-0.57
Daily constant injection rate[*]	5.451-327.06 (m³/d)	0.0022-0.132 (cfs) or 1-60 (gpm)
Well diameter	15.24 (cm)	6 (inch)

[*] *Note.* injection and extraction durations are two months (April and May) and three months (June, July, and August), respectively. Extraction begins when injection ceases.

2.2.1.3.   Modeled system and simulators

In essence, to allow computing REN with reasonable accuracy, the MODFLOW (McDonald and Harbaugh, 1988) finite difference flow model and its Multi-Node Well (MNW2) package; and the MT3DMS solute transport model (Zheng and Wang, 1999) were used. To distinguish the injectate from native groundwater, and to provide a solute for transport simulation, a hypothetical injectate concentration of 100 ppm of imaginary non-reactive solute was assigned. In this study, a fully penetrating ASR well in a homogenous, isotropic, freshwater, one-layer, unconfined aquifer was modeled, and extraction rates that are equal but opposite in sign to injection rates were used. Specified constant-head boundaries on the eastern and western edges of a square model area, no-flow boundaries on the northern and southern edges, and the ASR well at the center (Figures 2.1 and 2.2) were assumed.

Figure 2.1

MODFLOW2005-MT3DMS model study area for ASR well, top view (not to scale)
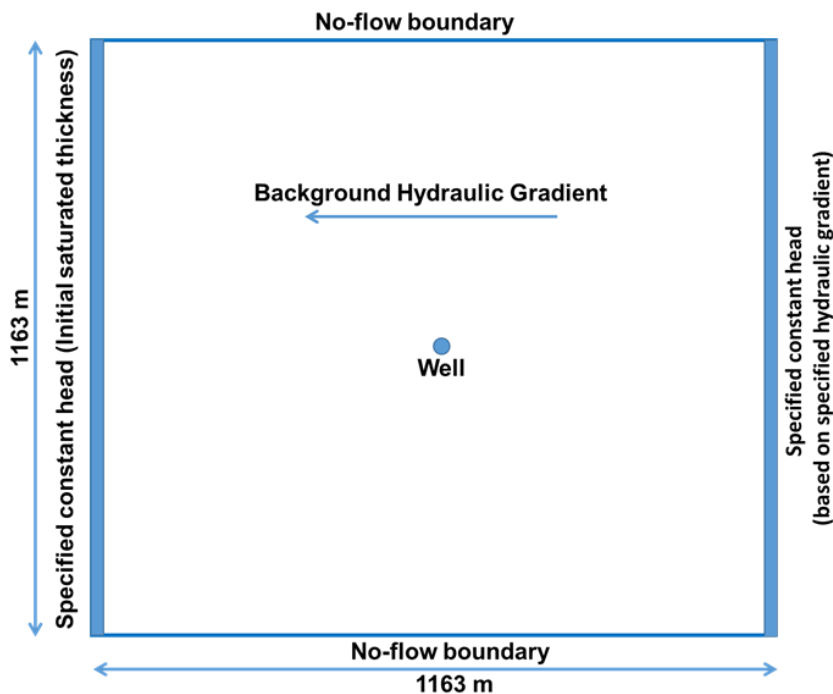
Figure 2.2

MODFLOW2005-MT3DMS model study area for ASR well, side view (not to scale)
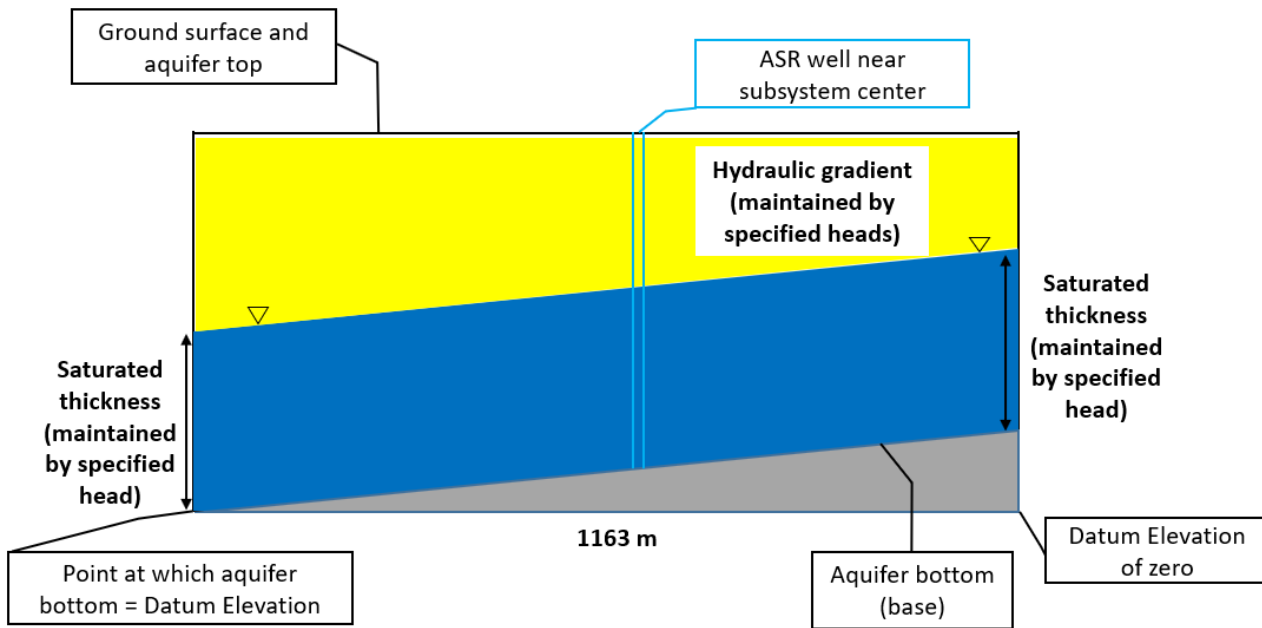
The greatest advective plume length that would occur by the end of the injection period for any set of Table 2.1 parameter values was estimated. Ignoring gradient changes induced by an injection or groundwater mound, and applying hydraulic conductivity of 20 m/d, the greatest pore velocity would be 3 m/d (9.84 ft/d). After 61 days, this would yield a 183 m (600.4 ft) advective plume length.

Longitudinal dispersion will lengthen the plume further. For an advective plume longer than one meter, the longitudinal dispersivity can be estimated as (Wilson et al., 1990; Gelhar et al., 1992; Xu and Eckstein, 1995; U.S. EPA, 2019):

$$\alpha_L = 0.83 \left[\log_{10} L_p\right]^{2.414} \tag{2}$$

where α_L = longitudinal dispersivity (m), and L_p = advective plume length (m). If $L_p \leq 1$ m, $\alpha_L = 0.1 L_p$.

MT3DMS uses a user-input Courant number to control the advective process by decreasing oscillations, improving accuracy, and decreasing numerical dispersion. $C = (v \times \Delta t)/\Delta x$, where v = linear pore velocity, Δx = the grid cell dimension at the well location (0.5 m or 1.64 ft), and Δt is the maximum desirable time step size (Daus et al., 1985).

To determine the simulation time step size in days, suitable for the preferred spatial discretization, the grid Peclet number, P, was estimated as equaling 2C

(Daus et al., 1985). By assuming that P also equals ($\Delta x/\alpha_L$), one can compute the maximum time step size desirable for use during injection.

The first estimation of the total number of time steps needed for the injection period was the integer result of dividing the total injection duration by the time step size. Those steps were then partitioned equally into each injection stress period and then two more steps per period were added to increase the likelihood of successful simulation. All preliminary simulations for all data combinations used the same number of time steps for flow and solute transport simulations.

Preliminary simulations helped determine the horizontal domain size required to avoid appreciable boundary condition impact from groundwater pumping. Simulations employed the broadest extents of values of injection rate, extraction rate, horizontal hydraulic conductivity, initial saturated thickness, and background hydraulic gradient. The resulting selected 1163 m by 1163 m (3815.62 ft. by 3815.62 ft.) model domain has 129 rows and 129 columns that transition smoothly from cell sizes of 10 m by 10 m (32.80 ft. by 32.80 ft.) to 0.5 m by 0.5 m (1.64 ft. by 1.64 ft.). In the center, the central smallest cell is a 7.62 cm (3 inch) radius vertical well. To have a uniform background hydraulic gradient and saturated thickness from the east to the west, the layer bottom elevation paralleled the desired initial water table.

To most easily utilize available rainfall, streamflow, and plant water needs information, 11 half-month stress periods were used in the MODFLOW2005 and

MT3DMS simulations. Period 1 simulated steady state background heads. Transient periods 2-5 employed injection, and periods 6-11 simulated extraction. Both models also used identical numbers of time steps per period, and that number can differ with period. The MODFLOW2005 PCG solver uses a 0.01 m head change criterion, and a 0.01 m residual convergence criterion. To simulate advection and dispersion, MT3DMS employs the total variation diminishing (TVD) package and the generalized conjugate gradient (GCG) solver. The injection stress period has varied time step durations. To avoid excessive processing time, the extraction period had a single time step (using even 300 time steps for extraction increases REN less than 0.005).

From the Table 2.1 parameter value ranges, five background hydraulic gradients, five hydraulic conductivities, eight injection or extraction rates, six porosity values, ten initial saturated thicknesses, and four (specific yield/porosity) ratios were used in this study. For each of the 48,000 possible combinations, a different set of input data for groundwater flow and solute transport simulations were prepared.

As mentioned above, the study assigns 100 ppm of imaginary non-reactive solute to injectate to distinguish it from native groundwater. MT3DMS simulations provide both the mass of solute injected into the ASR well, and the mass of solute recovered from the well. REN equals extracted solute mass divided by injected solute mass.

Because the processing time of a single MODFLOW2005-MT3DMS simulation might exceed an hour, parallel processing was used to drastically decrease computing time was used (Gropp et al., 2014; Ketabchi and Ataie-Ashtiani, 2015; Forghani and Peralta, 2018). To implement parallel processing on multi-cored personal computers and on node clusters of the Center for High Performance Computing (CHPC) at the University of Utah, USA, the study used the Message Passing Interface (MPI) (Snir et al., 1996; Sloan, 2009; Neal et al., 2010) of the C++ programming language. About 47,000 of the 48,000 attempted MODFLOW2005-MT3DMS completed successfully. Each successful simulation provided the total mass of solute injected through the ASR well, and the mass of solute recovered from the well. REN values were computed after 15, 30, 45, 61, 76 and 91 days of simulated extraction (REN15, REN30, REN45, REN61, REN76 and REN91, respectively) from simulation results. Note, the C++ code was tested to apply inputs in MODFLOW2005-MT3DMS simulators correctly.

2.2.2. Development and evaluation of porosity-specific predictors of REN
2.2.2.1. Overview

This section describes development of analytical porosity-specific polynomial estimators that can predict REN rapidly for use in lieu of numerical simulation models. Data employed for this section include Table 2.1 inputs, resulting simulation outputs, and computed RENs. Section activities include: 1) developing an analytical dimensionless volume (DLV) expression that equals the sum of a

constant plus ratios of (extraction/plume) volumes within sigmoid function, a weighted normalized lateral (transverse) capture zone ratio, and a weighted natural logarithm of (capture zone/plume) lengths; 2) developing DLV-containing analytical porosity-specific polynomial equations to predict REN values; and 3) defining statistical indices to evaluate the developed polynomial estimators.

2.2.2.2. Development of dimensionless volume function, f(DLV)

The Table 2.1 input parameters affect REN both in the field and as simulated by MODFLOW2005-MT3DMS. A dimensionless function, f(DLV), was designed to predict dimensionless REN from simulation results. The function consists of the sum of four terms: a) a dimensionless weighting coefficient times the volume of extracted water divided by the injectate plume volume at the time that extraction begins; b) a weighted ratio of the zero-gradient capture zone radius divided by the maximum zero-gradient capture zone radius for that time; c) a weighted natural logarithm of the ratio of the steady-state down-gradient capture zone radius divided by the advective plume length down-gradient of the well; and d) a constant real number.

The volume of extracted water at a moment in time equals the extraction duration to that moment times the extraction rate. The volume of the injectate plume equals its 2D area times a representative vertical thickness. The area, A_p, of an

elliptical injection plume having a normal or Gaussian concentration distribution, length of $3\sigma_x$ and width of $3\sigma_y$, is:

$$A_p = \pi 3\sigma_x 3\sigma_y \qquad (3)$$

where: σ_x, the standard deviation of concentration in the x direction, (L) $= \sqrt{2D_L t}$; σ_y is similarly defined; D_L and D_T are longitudinal and horizontal transverse dispersions (L^2/T) that respectively equal $\alpha_L \times v_x$ and $\alpha_T \times v_y$; α_L and α_T are horizontal longitudinal dispersivity and transverse dispersivity (L), respectively; v_x and v_y are the linear pore velocities in the longitudinal x and transverse y directions (L/T), respectively; and t is the injection duration (T), (Bear, 1961; Fetter, 1999; Bedient et al., 1999). In the field, horizontal transverse dispersivity is typically an order of magnitude smaller than longitudinal dispersivity (Zheng and Wang, 1999; Gelhar et al., 1992). Freeze and Cherry (1979) indicated that the above equations can be used for preliminary estimation of solute migration arising from small contaminant spills in simple hydrogeologic settings.

Assuming the horizontal transverse dispersivity is one tenth the longitudinal dispersivity, by substitution, the plume area is:

$$A_p = \pi 18\sqrt{0.1}\alpha_L vt \qquad (4)$$

where v = linear pore velocity.

An estimate of the 61-day plume volume is the sum of the volumes of a cylinder and a cone (the cylinder, and cone represent the initial saturated thickness, and injection or groundwater mound height). The cylinder volume equals the product of the plume area and the initial saturated thickness (b_{ist}). The cone (injection or groundwater mound) volume equals the plume area times $b_{im}/3$. Thus, the plume volume is:

$$V_p = A_p \left(b_{ist} + \frac{1}{3} b_{im} \right) = \left(\pi 18\sqrt{0.1}\alpha_L vt \right) \times \left(b_{ist} + \frac{1}{3} b_{im} \right) \qquad (5)$$

where V_p is the plume volume, b_{ist} is the initial saturated thickness, and b_{im} (MODFLOW2005 injection or groundwater mound height that is water above the initial water table). For about 48,000 combinations of Table 2.1 parameter values, injection or groundwater mound heights were determined by MODFLOW2005 simulation of the unconfined aquifer.

Herein, employing a two-step equation-based process with a regression equation estimates MODFLOW2005-simulated injection or groundwater mound height (b_{im}), and helps avoid the need to run MODFLOW2005 for the b_{im} value. The two-step process employed: a) the Cooper and Jacob (1946) straight line method to compute the head change (s') in an equivalent confined aquifer; and b) the Jacob correction (1944) to convert the computed confined aquifer head change into an unconfined aquifer head change. The Cooper and Jacob (1946) straight-line method computes

the head change in an equivalent confined aquifer by $s'=\left\{\frac{Q}{4\pi t}LN\left(\frac{2.25Tt}{r^2S_y}\right)\right\}$, where Q

is a constant positive pumping (here, constant negative injection flow); T is

horizontal transmissivity; S_y is the unconfined aquifer specific yield; and t is the

elapsed time after steady pumping began. The Jacob correction (1944) converts

the confined aquifer head change into an unconfined aquifer head change as: s =

$b\left(1-\sqrt{1-\left(\frac{2s'}{b}\right)}\right)$, where b is the initial saturated thickness. This is appropriate

because values of the late-time function (u_B) are much less than 0.01 for the Table

2.1 parameter values (Jacob, 1944; Copper and Jacob, 1946; Fitts, 2002; Schwartz

and Zhang, 2003; Neuman, 1975; Huisman, 1972).

The regression equation estimates b_{im} values with a mean error (ME) of 0.000 (m);

root mean square errors (RMSE) of 0.005 (m); peak weighted root mean square

errors (PWRMSE) of 0.006 (m); R^2 of 0.9999; and percent of bias (PBIAS) of 0.000

(%). Employing this regression equation to estimate MODFLOW2005-simulated

mound height avoids the need to run MODFLOW2005 for new combinations of

aquifer conditions. Hence this expression is used to estimate the mound height

within equations for predicting REN. Thus, the regression equation was defined as:

b_{im} (MODFLOW injection or groundwater mound height estimated by
regression equation) = | {(1.026623 x mound height from the two-step
analytical process) + 0.002061} |

Equation 6 shows the definition of a dimensionless volume (DLV) as the product of dimensionless weighting coefficient W_{DLV}, times the ratio of the volume of the extracted water (V_{ext}) and the plume volume (V_p):

$$DLV = \frac{W_{DLV}V_{ext}}{V_p} \tag{6}$$

where: $V_{ext} = Q \times t$; Q = pumping extraction rate; and t = extraction duration.

For general application using any combination of the Table 2.1 input values, Equation 7 describes the $f(DLV)$ function of DLV.

$$f(DLV) = Term\ 1 + Term\ 2 + Term\ 3 + Term\ 4 \tag{7}$$

Because REN after any duration of extraction is a cumulative relative mass, Term 1 is a logistic sigmoid function (an S-shaped function with response between 0 and 1) of the DLV:

$$Term\ 1 = \frac{1}{1 + e^{-DLV}} \tag{8a}$$

By substituting Equations 5 and 6:

$$Term\ 1 = \left[\frac{1}{1 + e^{-\frac{W_{DLV}V_{ext}}{A_p\left(b_{ist} + \frac{1}{3}b_{im}\right)}}} \right] \tag{8b}$$

Term 2 is a weighted (W_{CZR}) normalized lateral (transverse) capture zone ratio for

a particular time. Equation 9 shows that for a particular simulation run and time,

Term 2 is the product of the weighting coefficient (W_{CZR}) and the ratio of the {(run's

zero-gradient capture zone radius for that time) / (maximum zero-gradient capture

zone radius for that time)}. The zero-gradient capture zone radius (ZGCZR) equals

$\{(Q\ t)/(\pi\ b_{ist}\ n)\}^{0.5}$ (Landmeyer, 1994). The maximum zero-gradient capture

zone radius for that time is the greatest radius resulting from all Table 2.1 input

combinations for that time. Without the W_{CZR} weight, Term 2 is always positive.

Even with the weight, Term 2 plays a small role in modifying the estimated REN

value.

$$\text{Term 2} = W_{CZR} \times \frac{\text{ZGCZR for that time}}{\text{Max. ZGCZR for that time}} \qquad (9)$$

where W_{CZR} is a weighting coefficient; Q is the pumping extraction rate (L^3/T); t is

the pumping extraction time (T); π is 3.1416; n is the aquifer material porosity in

percent (%); b_{ist} is the initial aquifer saturated thickness (L); and Max. ZGCZR is the

maximum zero-gradient capture zone radius of any simulation for that time.

Term 3 is a weighted (W_{CZRL}) natural logarithm of the ratio of the (steady-state

down-gradient capture zone radius) / (length of advective plume down-gradient of

well). Term 3 reduces the f(DLV) value if the plume is so long that some of it escapes

the steady-state capture zone. Without the weight, Term 3 is either a negative or

a positive value. Term 3 significantly affects the REN estimate. W_{CZPL} is always positive (Tables 2.2 to 2.7).

$$\text{Term 3} = W_{CZPL} \times LN\left(\frac{DGCZR}{APL}\right) \tag{10}$$

where W_{CZPL} is the weighting coefficient; LN is natural logarithm; DGCZR is the steady-state down-gradient capture zone radius or $\{Q / (2\pi \times K \times b_{ist} \times i)\}$ (U.S. EPA, 2008); Q is the pumping extraction rate (L^3/T); π is 3.1416; K is horizontal hydraulic conductivity (L/T); b_{ist} is the aquifer initial saturated thickness (L); and APL is the advective plume length down-gradient of the well at the specified time (L).

Term 4 is a constant-value real number (C_{DLV}). After computing Terms 1-3 for each MODFLOW2005-MT3DMS run and assigning values of 1.0 for the weights of Terms 1-3, the value for C_{DLV} was determined that minimized the sum of squared differences between simulated and Equation 7-computed REN values. This process identified -0.7 as the best value for C_{DLV}. Equation 11 shows the resulting $f(DLV)$ that was a crude estimator of REN.

$$f(DLV) = \frac{1}{1 + e^{-\frac{W_{DLV}\ V_{ext}}{A_p\left(b_{ist}+\frac{1}{3}b_{im}\right)}}} + W_{CZR} \times \frac{\sqrt{\frac{Q\ t}{\pi\ b_{ist}\ n}}}{\text{Max.}\left[\sqrt{\frac{Q\ t}{\pi\ b_{ist}\ n}}\right] \text{in that time}}$$

$$+ W_{CZPL} \times LN\left(\frac{\frac{Q}{2\pi k b_{ist} i}}{\frac{Kit_{inj}}{n}}\right) - 0.7 \tag{11}$$

where t_{inj} is 61 (injection duration, day); b_{ist} is the initial saturated thickness (L); and b_{im} is the MODFLOW2005 injection or groundwater mound height after 61 days (two months) of steady injection (L).

Equation 11 did not predict REN as well as had been hoped. Error was especially related to porosity differences.

2.2.2.3. Development of porosity-specific regression equations to predict REN

In an effort to produce an adaptable regression REN-prediction equation for each tested aquifer porosity, f(DLV) was placed within polynomials of 2nd- to 11th-order and tested for each porosity. A 6th-order polynomial regression equation estimated REN most accurately (Eq. 12).

$$REN = af(DLV)^6 + bf(DLV)^5 + cf(DLV)^4 + df(DLV)^3 + ef(DLV)^2 +$$
$$ff(DLV) + g \qquad\qquad (12)$$

To obtain the weighting coefficients of Term 1 (W_{DLV}), Term 2 (W_{CZR}), Term 3 (W_{CZPL}), and polynomial coefficients (a, b, c, d, e, f, and g) for each porosity-specific data set and each time, the Generalized Reduced Gradient (GRG) nonlinear optimization solver within Excel (version 2019, 64-bit) and: a) constraint precision of 0.000001, b) convergence criteria of 0.0001, c) forward derivatives, d) and automatic scaling were used.

Optimizations sought to minimize the root mean square error (RMSE) between simulated (observed) MODFLOW2005-MT3DMS results and responses of polynomial-estimated REN equation (Equation 12) to calibrate values of the variable weights and coefficients. All variable weights and coefficients were bounded to be between -10000 and +10000. Separate input data sets exist for each extraction duration (15, 30, 45, 61, 76, and 91 days), and for each porosity value or range between 0.1 and 0.6 using 0.1 intervals. Thus, nonlinear optimization determined optimal weights and coefficients for six porosity values (0.1, 0.2..., 0.6). For a specific porosity and REN, the initial (start) input value for all variables was 0.1. To achieve optimal values for each optimization model, the GRG algorithm was re-run via using manual multi-start (initial) values as many times as needed for the optimal solution to cease changing.

After the Excel optimizations, and reduction in the number of decimal values in weights, R software (R Core Team, 2019) was used to perform regressions of Equation 12. These regressions obtained precise coefficient values for the rounded weights.

Linear interpolation is recommended to estimate REN for a site having a porosity in an interval between two evaluated porosities. The interpolation would use the RENs predicted for the lower and the higher bounding porosities.

2.2.2.4. Evaluation of developed porosity-specific polynomial estimators

R software (R Core Team, 2019) was used to evaluate how accurately the developed REN-estimators predicted the results of successful MODFLOW2005-MT3DMS simulations. Statistical indices included were (Appendix A):

a) Mean Error, ME (Javan et al., 2015);

b) Root Mean Square Error, RMSE (Mentaschi et al., 2013; Javan et al., 2015; Jimeno-Sáez et al., 2018);

c) Peak Weighted Root Mean Square Error, PWRMSE (Javan et al., 2015);

d) Pearson's Correlation Coefficient, r (Moriasi et al., 2007; Javan et al., 2015);

e) Coefficient of Determination, R^2 (Moriasi et al., 2007; Jimeno-Sáez et al., 2018);

f) Nash-Sutcliffe Efficiency, E_{NS} (Nash and Sutcliffe, 1970; Moriasi et al., 2007; Javan et al., 2015; Jimeno-Sáez et al., 2018);

g) Percent of Bias, |PBIAS| (Moriasi et al., 2007; Jimeno-Sáez et al., 2018); and

h) Scatter Index, SI (Janssen and Komen, 1984; Moriasi et al., 2007).

2.3. Results and Discussion

Predicting recovery effectiveness (REN) for an ASR system operating in an unconfined aquifer would customarily require groundwater flow and solute transport simulations, followed by evaluation of results. To obviate the need for that process by potential ASR

implementers, REN-predictors were developed that require merely eight input values. The accuracy of the predictors is demonstrated below.

Simulations were carried out assuming an ASR well installed within an unconfined, homogenous, isotropic, freshwater, one-layer aquifer. It was also assumed, that when excess surface water is available, 61 days (two months) of steady injection into the ASR well occur, followed by 91 days (three months) of steady extraction from the same well. For six specified aquifer porosities and six distinct times after extraction begins, REN-prediction equations were developed. All such equations have the form of Equation 12, but weights and coefficients differ for each porosity and each extraction duration.

Tables 2.2 to 2.7 present the weights and coefficients for the equations predicting REN after 15, 30, 45, 61, 76, and 91 days (REN15, REN30, …, REN91). Tables 2.8 to 2.13 statistically report the accuracy of the REN-predictors. For all extraction durations and all porosities, R^2 values exceed 0.99. The root mean squared error (RMSE) of prediction usually increased with porosity and almost always increased with extraction duration.

Recalling that REN only ranges from 0.0 to 1.0 gm/gm, the equations accurately predict REN. For any porosity, the greatest RMSE for REN15 prediction is 0.004 gm/gm, or 0.4%. For any porosity, after 91 days of extraction, the greatest RMSE is 0.025 gm/gm, or 2.5% of a REN of 1.0 gm/gm.

Figures 2.3 to 2.6 compare simulated versus estimated REN values. In each figure, the x axis represents the simulated REN values. The y axis represents the estimated REN. Perfect estimation is represented by circles lying on the diagonal line. A point lying above

the diagonal shows overestimation, and a point lying below the diagonal shows underestimation.

- In Figure 2.3, for REN15 and 0.1 porosity, the greatest error, an underestimation, is about 0.02 gm/gm (difference between a 0.25 REN simulation and a 0.23 REN estimation). The greatest REN overestimation in Figure 2.3 is about 0.01 gm/gm.

- In Figure 2.4 (REN15, 0.6 porosity), the greatest REN underestimation is about 0.01 gm/gm. Above the diagonal line between Simulated REN15 values of 0.18 to 0.23, the string of symbols jutting out to the left of the main line represent 68 overestimations ranging from 0.01 to 0.03 gm/gm. As inputs, all the 68 simulations use the smallest injection or |extraction| rate (5.451 m³/d or 1 gpm), and a large initial saturated thickness (greater than or equal to 30 m or 98 ft).

- In Figure 2.5 (REN91, 0.1 porosity), the greatest underestimation is about 0.015 gm/gm. Above the diagonal line between Simulated REN91 of 0.64 to 0.85, the string of what appear to be approximately 16 symbols represent 43 overestimations ranging from about 0.10 to 0.16 gm/gm. As inputs, 36 of the 43 simulations use the smallest injection or extraction rate (5.451 m³/d or 1 gpm), the smallest hydraulic conductivity (4 m/d or 13 ft/d), and initial saturated thickness greater than or equal to 12 m. The other seven overestimations resulted from using the smallest initial saturated thickness, and injection rates equal to or exceeding 272.55 m³/d (50 gpm).

- In Figure 2.6 (REN91, 0.6 porosity), the greatest underestimation is about 15 gm/gm. Between Simulated REN91 of 0.3 to 0.72, the 23 symbols farthest above

the diagonal line represent 95 overestimations ranging from about 0.09 to 0.28 gm/gm. As inputs, most of the 95 simulations use the smallest injection or extraction rate (5.451 m^3/d or 1 gpm), and/or the minimum hydraulic conductivity. The rest of the 95 simulations use the minimum hydraulic conductivity and/or the minimum initial saturated thickness.

- In using the equations for the six tested porosities, the greatest errors occur when input combinations include the greatest porosity, end of extraction, and lowest hydraulic conductivity, initial saturated thickness and pumping rate (0.6 porosity, 91 days, 4 m/d, 8 m, 5.451 m^3/d).

For intermediate porosities not directly addressed by any of the developed polynomials, Tables 2.14 and 2.15 present observed and interpolated REN values for different situations. The Table 2.14 situation has a thicker aquifer, lower porosities, an order of magnitude steeper background hydraulic gradient, and smaller resulting REN values than the Table 2.15 situation. These two tables show that linear interpolation between polynomial-computed REN values estimates REN values well. The range of errors (simulated minus interpolated) is +0.203 to -0.006 percent (+0.002 to -0.00006 gm/gm) of a REN ranging from 0 to 1 gm/gm.

Table 2.2

Coefficients and weights to estimate REN15 (Max. zero-gradient capture zone = 6.25 m and Term 4 = -0.7)

Porosity	Coefficient							Weight		
	a	b	c	d	e	f	g	W_{DLV}	W_{CZR}	W_{CZPL}
0.1	37.622	-30.081	2.018	3.560	-1.289	0.324	0.197	12.528	-0.097	0.013
0.2	6.111	19.976	-21.006	7.152	-1.181	0.176	0.223	3.542	-0.061	0.002
0.3	-17.617	36.813	-23.911	6.773	-1.028	0.163	0.224	2.261	-0.060	0.002
0.4	-23.001	38.598	-22.370	6.150	-1.027	0.187	0.220	1.812	-0.059	0.002
0.5	-0.007	-0.067	0.270	-0.194	-0.201	0.273	0.169	4.600	-0.064	0.079
0.6	-0.0021	-0.0731	0.258	-0.184	-0.191	0.269	0.167	3.862	-0.0002	0.081

Table 2.3

Coefficients and weights to estimate REN30 (Max. zero-gradient capture zone = 8.84 m and Term 4 = -0.7)

Porosity	Coefficient							Weight		
	a	b	c	d	e	f	g	W_{DLV}	W_{CZR}	W_{CZPL}
0.1	-359.470	289.433	-74.819	7.396	-0.670	0.273	0.432	1.278	-0.020	0.001
0.2	-199.091	196.361	-62.623	9.300	-1.094	0.330	0.411	0.856	-0.031	0.001
0.3	-0.0306	0.0875	0.072	-0.317	-0.042	0.468	0.261	2.959	-0.073	0.117
0.4	-0.020	0.055	0.080	-0.274	-0.058	0.452	0.264	2.037	-0.013	0.121
0.5	-0.0116	0.0271	0.084	-0.228	-0.071	0.431	0.267	1.517	0.064	0.128
0.6	-0.0064	0.0119	0.077	-0.189	-0.074	0.409	0.269	1.249	0.108	0.138

Table 2.4

Coefficients and weights to estimate REN45 (Max. zero gradient capture zone = 10.82 m and Term 4 = -0.7)

Porosity	Coefficient							Weight		
	a	b	c	d	e	f	g	W_{DLV}	W_{CZR}	W_{CZPL}
0.1	-661.463	565.700	-126.066	2.208	0.514	0.460	0.587	0.558	-0.014	0.001
0.2	282.769	-40.008	-58.008	22.615	-2.506	0.492	0.511	0.590	-0.031	0.002
0.3	-0.0079	0.0378	0.006	-0.202	0.043	0.505	0.317	1.697	0.00004	0.175
0.4	-0.0067	0.0317	0.011	-0.189	0.031	0.496	0.321	1.218	-0.005	0.176
0.5	-0.0050	0.0233	0.018	-0.173	0.016	0.485	0.324	0.872	0.118	0.178
0.6	-0.0031	0.0139	0.022	-0.145	0.0006	0.463	0.329	0.679	0.182	0.189

Table 2.5

Coefficients and weights to estimate REN61 (Max. zero gradient capture zone = 12.60 m and Term 4 = -0.7)

Porosity	Coefficient							Weight		
	a	b	c	d	e	f	g	W_{DLV}	W_{CZR}	W_{CZPL}
0.1	-679.885	724.310	-175.744	-0.192	1.508	0.609	0.699	0.338	-0.012	0.001
0.2	-338.510	585.379	-172.051	2.669	1.396	0.677	0.656	0.219	-0.016	0.001
0.3	-0.0048	0.0268	0.0002	-0.175	0.063	0.546	0.361	1.102	-0.025	0.203
0.4	-0.00464	0.02611	0.0001	-0.173	0.065	0.544	0.358	0.814	0.039	0.200
0.5	-0.00415	0.02281	0.0053	-0.168	0.053	0.541	0.360	0.595	0.125	0.198
0.6	-0.00277	0.01529	0.0102	-0.145	0.036	0.519	0.365	0.461	0.194	0.208

Table 2.6

Coefficients and weights to estimate REN76 (Max. zero gradient capture zone = 14.06 m and Term 4 = -0.7)

Porosity	Coefficient							Weight		
	a	b	c	d	e	f	g	W_{DLV}	W_{CZR}	W_{CZPL}
0.1	780.367	-207.937	-77.931	34.354	-3.819	0.749	0.665	0.598	-0.028	0.002
0.2	978.920	54.868	-202.406	29.267	0.509	0.625	0.676	0.231	-0.018	0.001
0.3	-0.00846	0.04394	-0.00278	-0.239	0.093	0.639	0.382	0.821	-0.001	0.185
0.4	-0.00742	0.03935	-0.00164	-0.227	0.088	0.628	0.381	0.601	0.051	0.186
0.5	1.021	-2.137	1.173	-0.299	-0.267	1.044	0.410	0.304	0.112	0.058
0.6	-0.00431	0.02281	0.0115	-0.187	0.053	0.596	0.389	0.345	0.194	0.196

Table 2.7

Coefficients and weights to estimate REN91 (Max. zero gradient capture zone = 15.39 m and Term 4 = -0.7)

Porosity	Coefficient							Weight		
	a	b	c	d	e	f	g	W_{DLV}	W_{CZR}	W_{CZPL}
0.1	886.691	-168.223	-88.124	29.474	-3.758	1.014	0.676	0.567	-0.032	0.001
0.2	710.292	-238.203	-53.816	33.740	-4.390	0.862	0.649	0.309	-0.033	0.002
0.3	-0.01743	0.07862	0.002	-0.349	0.106	0.745	0.402	0.623	-0.004	0.161
0.4	-0.01458	0.06794	0.0027	-0.324	0.103	0.727	0.399	0.461	0.054	0.164
0.5	-0.0120	0.0558	0.0122	-0.303	0.084	0.713	0.402	0.341	0.141	0.166
0.6	-0.00824	0.03899	0.0192	-0.263	0.064	0.685	0.405	0.270	0.212	0.175

Table 2.8

Statistical comparisons of estimated versus simulated REN15 for six porosity (Po) values

Parameter	Po = 0.1	Po = 0.2	Po = 0.3	Po = 0.4	Po = 0.5	Po = 0.6	Interpretation Ranges
ME (gm/gm)	0.0001	0.0003	-0.0004	-0.0001	-0.0001	0.0006	$-\infty < ME < +\infty$; Perfect: 0
RMSE (gm/gm)	0.002	0.002	0.003	0.003	0.004	0.003	$0 \leq RMSE < +\infty$; Perfect: 0
PWRMSE (gm/gm)	0.002	0.002	0.003	0.003	0.003	0.003	$0 \leq PWRMSE < +\infty$; Perfect: 0
r	0.9998	0.9997	0.9994	0.9990	0.9989	0.9989	$-1 \leq r \leq 1$; Perfect: 1 or -1
R^2	0.9996	0.9994	0.9989	0.9980	0.9978	0.9979	$0 \leq R^2 \leq 1$; Perfect: 1
E_{NS}	0.9996	0.9994	0.9989	0.9980	0.9978	0.9978	$-\infty < E_{NS} \leq 1$; Perfect: 1
|PBIAS| (%)	0.09	0.17	0.24	0.08	0.06	0.31	|PBIAS| $\leq 25\%$ very good Perfect:
SI (%)	1.03	1.11	1.40	1.75	1.74	1.60	SI < 20%; Operational: SI < 60%

Table 2.9

Statistical comparisons of estimated versus simulated REN30 for six porosity (Po) values

Parameter	Po = 0.1	Po = 0.2	Po = 0.3	Po = 0.4	Po = 0.5	Po = 0.6	Interpretation Ranges
ME (gm/gm)	0.0004	-0.0003	-0.0010	-0.0006	0.0006	0.0010	$-\infty < ME < +\infty$; Perfect: 0
RMSE (gm/gm)	0.006	0.006	0.008	0.009	0.009	0.010	$0 \leq RMSE < +\infty$; Perfect: 0
PWRMSE (gm/gm)	0.006	0.007	0.008	0.009	0.009	0.010	$0 \leq PWRMSE < +\infty$; Perfect: 0
r	0.9996	0.9994	0.9991	0.9987	0.9985	0.9982	$-1 \leq r \leq 1$; Perfect: 1 or -1
R^2	0.9992	0.9988	0.9981	0.9975	0.9970	0.9964	$0 \leq R^2 \leq 1$; Perfect: 1
E_{NS}	0.9992	0.9988	0.9981	0.9975	0.9970	0.9964	$-\infty < E_{NS} \leq 1$; Perfect: 1
|PBIAS| (%)	0.15	0.12	0.31	0.19	0.17	0.30	|PBIAS| $\leq 25\%$ very good Perfect:
SI (%)	1.75	1.84	2.20	2.33	2.43	2.55	SI < 20%; Operational: SI < 60%

Table 2.10

Statistical comparisons of estimated versus simulated REN45 for six porosity (Po) values

Parameter	Po = 0.1	Po = 0.2	Po = 0.3	Po = 0.4	Po = 0.5	Po = 0.6	Interpretation Ranges
ME (gm/gm)	-0.0001	-0.0015	0.0031	0.0023	-0.0008	-0.0001	$-\infty < ME < +\infty$; Perfect: 0
RMSE (gm/gm)	0.011	0.015	0.013	0.013	0.014	0.015	$0 \leq RMSE < +\infty$; Perfect: 0
PWRMSE (gm/gm)	0.012	0.016	0.014	0.013	0.014	0.015	$0 \leq PWRMSE < +\infty$; Perfect: 0
r	0.9992	0.9986	0.9988	0.9988	0.9985	0.9982	$-1 \leq r \leq 1$; Perfect: 1 or -1
R^2	0.9984	0.9972	0.9977	0.9976	0.9969	0.9964	$0 \leq R^2 \leq 1$; Perfect: 1
E_{NS}	0.9984	0.9972	0.9975	0.9975	0.9969	0.9964	$-\infty < E_{NS} \leq 1$; Perfect: 1
|PBIAS| (%)	0.03	0.38	0.76	0.53	0.17	0.02	|PBIAS| $\leq 25\%$ very good Perfect:
SI (%)	2.56	3.06	2.63	2.50	2.70	2.81	SI < 20%; Operational: SI < 60%

Table 2.11

Statistical comparisons of estimated versus simulated REN61 for six porosity (Po) values

Parameter	Po = 0.1	Po = 0.2	Po = 0.3	Po = 0.4	Po = 0.5	Po = 0.6	Interpretation Ranges
ME (gm/gm)	0.0003	-0.0001	0.0016	-0.0007	-0.0009	-0.0008	$-\infty < ME < +\infty$; Perfect: 0
RMSE (gm/gm)	0.016	0.019	0.015	0.016	0.017	0.018	$0 \le RMSE < +\infty$; Perfect: 0
PWRMSE (gm/gm)	0.017	0.020	0.016	0.017	0.018	0.019	$0 \le PWRMSE < +\infty$; Perfect: 0
r	0.9990	0.9984	0.9990	0.9988	0.9985	0.9982	$-1 \le r \le 1$; Perfect: 1 or -1
R^2	0.9980	0.9969	0.9980	0.9976	0.9970	0.9964	$0 \le R^2 \le 1$; Perfect: 1
E_{NS}	0.9980	0.9969	0.9980	0.9976	0.9970	0.9964	$-\infty < E_{NS} \le 1$; Perfect: 1
|PBIAS| (%)	0.08	0.03	0.33	0.14	0.17	0.14	|PBIAS| $\le$ 25% very good Perfect:
SI (%)	2.96	3.33	2.48	2.61	2.82	2.95	SI < 20%; Operational: SI < 60%

Table 2.12

Statistical comparisons of estimated versus simulated REN76 for six porosity (Po) values

Parameter	Po = 0.1	Po = 0.2	Po = 0.3	Po = 0.4	Po = 0.5	Po = 0.6	Interpretation Ranges
ME (gm/gm)	-0.0005	-0.0001	0.0007	0.0012	0.0005	0.0007	$-\infty < ME < +\infty$; Perfect: 0
RMSE (gm/gm)	0.017	0.021	0.017	0.018	0.030	0.021	$0 \leq RMSE < +\infty$; Perfect: 0
PWRMSE (gm/gm)	0.019	0.022	0.018	0.019	0.031	0.022	$0 \leq PWRMSE < +\infty$; Perfect: 0
r	0.9990	0.9984	0.9988	0.9987	0.9960	0.9980	$-1 \leq r \leq 1$; Perfect: 1 or -1
R^2	0.9980	0.9969	0.9977	0.9973	0.9921	0.9961	$0 \leq R^2 \leq 1$; Perfect: 1
E_{NS}	0.9980	0.9969	0.9977	0.9973	0.9921	0.9961	$-\infty < E_{NS} \leq 1$; Perfect: 1
|PBIAS| (%)	0.11	0.01	0.13	0.22	0.09	0.12	$\|PBIAS\| \leq 25\%$ very good Perfect:
SI (%)	2.93	3.37	2.70	2.79	4.59	3.13	SI < 20%; Operational: SI < 60%

Table 2.13

Statistical comparisons of estimated versus simulated REN 91 for six porosity (Po) values

Parameter	Po = 0.1	Po = 0.2	Po = 0.3	Po = 0.4	Po = 0.5	Po = 0.6	Interpretation Ranges
ME (gm/gm)	0.0002	0.0003	0.0023	0.0009	0.0009	0.0022	$-\infty < ME < +\infty$; Perfect: 0
RMSE (gm/gm)	0.016	0.022	0.020	0.021	0.023	0.025	$0 \leq RMSE < +\infty$; Perfect: 0
PWRMSE (gm/gm)	0.019	0.024	0.022	0.022	0.024	0.025	$0 \leq PWRMSE < +\infty$; Perfect: 0
r	0.9991	0.9984	0.9986	0.9984	0.9980	0.9976	$-1 \leq r \leq 1$; Perfect: 1 or -1
R^2	0.9983	0.9968	0.9972	0.9967	0.9960	0.9951	$0 \leq R^2 \leq 1$; Perfect: 1
E_{NS}	0.9983	0.9968	0.9971	0.9967	0.9960	0.9951	$-\infty < E_{NS} \leq 1$; Perfect: 1
|PBIAS| (%)	0.05	0.07	0.42	0.16	0.15	0.36	$\|PBIAS\| \leq 25\%$ very good Perfect:
SI (%)	2.75	3.44	3.03	3.09	3.30	3.50	SI < 20%; Operational: SI < 60%

Table 2.14

Comparison of simulated versus interpolated estimated REN values for porosities of 0.22, 0.26, and 0.28 for a site having 0.005 background hydraulic gradient, 15 m/d hydraulic conductivity, 20 m³/d injection rate, 25 m initial saturated thickness, and 0.5 specific yield/porosity ratio

Type of obtaining REN	Porosity	REN15	REN30	REN45	REN61	REN76	REN91
simulated	0.22	0.05853	0.06637	0.06857	0.06937	0.06966	0.06978
estimated	0.22	0.05841	0.06632	0.06852	0.06932	0.06961	0.06973
simulated	0.26	0.06557	0.07493	0.07758	0.07857	0.07894	0.07911
estimated	0.26	0.06538	0.07485	0.07753	0.07852	0.07889	0.07905
simulated	0.28	0.06900	0.07917	0.08207	0.08315	0.08356	0.08375
estimated	0.28	0.06886	0.07912	0.08203	0.08312	0.08353	0.08372

Table 2.15

Comparison of simulated versus interpolated estimated REN values for porosities of 0.32, 0.36 and 0.38 at a site having 0.0005 background hydraulic gradient, 15 m/d hydraulic conductivity, 20 m³/d injection rate, 20 m initial saturated thickness, and 0.5 specific yield/porosity

Type of obtaining REN	Porosity	REN15	REN30	REN45	REN61	REN76	REN91
simulated	0.32	0.24569	0.48018	0.66458	0.79099	0.86364	0.91171
estimated	0.32	0.24575	0.47997	0.66420	0.79010	0.86248	0.91053
simulated	0.36	0.24602	0.48135	0.66794	0.79797	0.87205	0.92006
estimated	0.36	0.24584	0.48070	0.66698	0.79634	0.87002	0.91804
simulated	0.38	0.24605	0.48145	0.66897	0.80057	0.87522	0.92325
estimated	0.38	0.24588	0.48107	0.66837	0.79946	0.87379	0.92179

Figure 2.3

Comparison of estimated versus simulated REN15 for 0.1 porosity and 7750 unique combinations of other input parameters
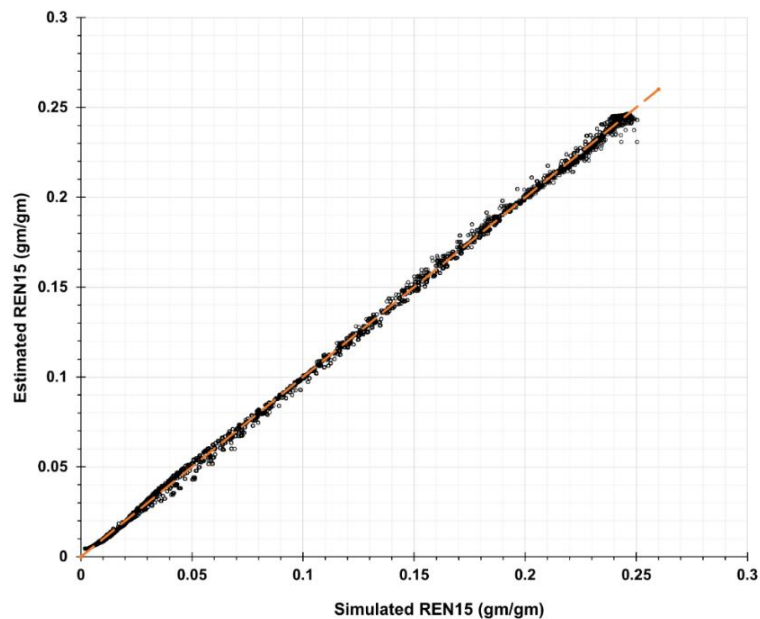
Figure 2.4

Comparison of estimated versus simulated REN15 for 0.6 porosity and 7790 unique combinations of other input parameters
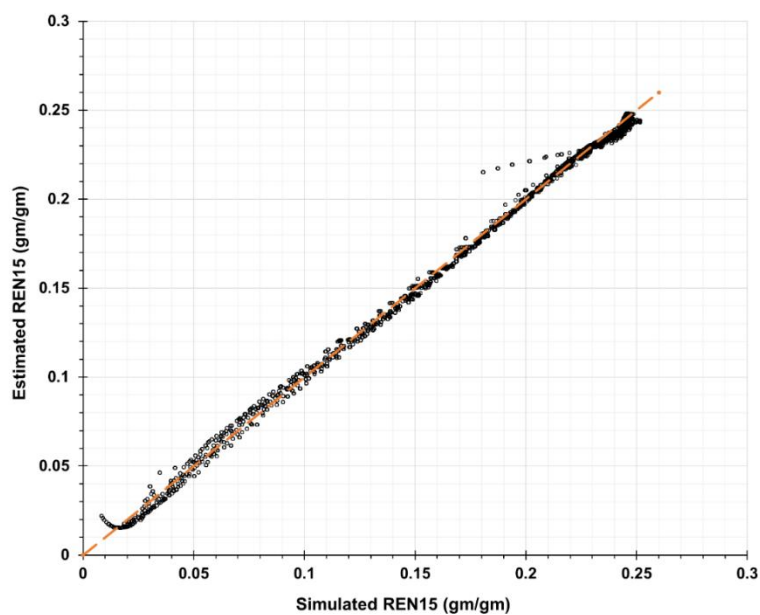
Figure 2.5

Comparison of estimated versus simulated REN91 for 0.1 porosity and 7750 unique combinations of other input parameters
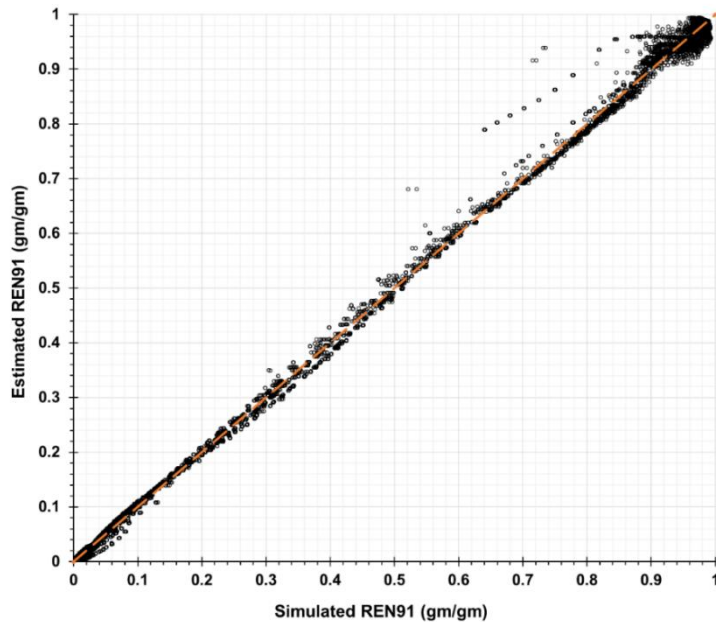
Figure 2.6

Comparison of estimated versus simulated REN91 for 0.6 porosity and 7790 unique combinations of other input parameters
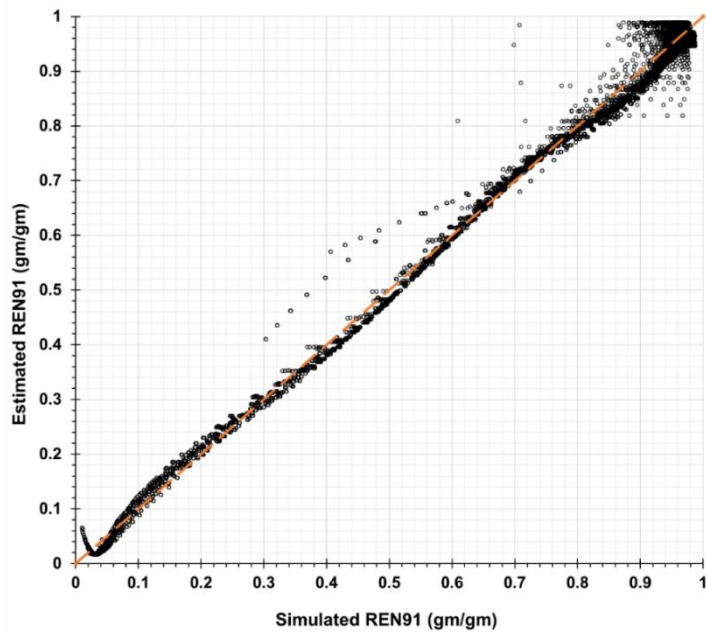
2.4. Conclusions

This study provides a rapid method to predict aquifer storage and recovery (ASR) well recovery effectiveness (REN). Here, REN is the proportion of the water molecules injected into an ASR well that subsequent extraction from the same well will recover after a specified extraction duration. For a conservative contaminant, REN is useful for predicting the concentration of the extracted water that consists of a mixture of injectate and natural background groundwater. The presented analytical porosity-specific polynomial estimators predict REN for one ASR well fully penetrating an assumed homogenous, isotropic, unconfined, one-layer aquifer about every 15 days of a 91-day extraction period. The presented equations are applicable for a wide range of parameter values. Ranges are aquifer hydraulic conductivity (4-20 m/d or 13.124-65.61 ft/d), porosity (0.1-0.6), ratio of specific yield/porosity (0.375-0.95), initial saturated thickness (8-46 m or 26.25-150.91 ft), background hydraulic gradient (0.00001-0.015), steady pumping rate of injection and extraction (5.451-327.06 m^3/d or 1-60 gpm). Statistics describing accuracy of equation-predicted REN values after 15 to 91 days of extraction, range from 0.002 to 0.025 for root mean square error (RMSE), from 0.9921 to 0.9996 for R^2, and 1.03 to 4.59% for scatter index (SI). The greatest errors in equation-predicted REN values occur when input parameters include the greatest porosity (0.6), and the lowest pumping rate (5.451 m^3/d or 1 gpm).

As shown statistically, the porosity-specific polynomial estimators allow a user to predict REN rapidly without having to prepare for and execute flow or solute transport simulations. For intermediate porosities not directly addressed by any of the developed polynomials, linear interpolation between polynomial-computed RENs estimates intermediate REN values well. The

generated expressions should make it simple and practical to evaluate ASR potential for a wide range of unconfined aquifer conditions.

Acknowledgments

References

Bakker, M. (2010). Radial Dupuit interface flow to assess the aquifer storage and recovery potential of saltwater aquifers. Hydrogeology J., 18, 107-115. https://doi.org/10.1007/s10040-009-0508-1

Bear, J. (1961). Some Experiments in Dispersion. Geophysical Research J., 66(8), 2455-2467. https://doi.org/10.1029/JZ066i008p02455

Bedient, P. B., Rifai, H. S., & Newell, C. J. (1999). Ground Water Contamination, Transport and Remediation. (2nd edn.). Prentice-Hall Inc.

Bockelmann, A., Zamfirescu, D., Ptak, T., Grathwohl, P., & Teutsch, G. (2003). Quantification of mass fluxes and natural attenuation rates at an industrial site with a limited monitoring network: a case study. Contaminant Hydrology J., 60(1–2), 97-121. https://doi.org/10.1016/S0169-7722(02)00060-8

Brown, C. J., Ward, J., & Mirecki, J. (2016). A Revised Brackish Water Aquifer Storage and Recovery (ASR) Site Selection Index for Water Resources Management. Water Resources Management J., 30, 2465–2481. https://doi.org/10.1007/s11269-016-1297-7

Cooper, H. H. Jr., & Jacob, C. E. (1946). A Generalized Graphical Method for Evaluating Formation Constants and Summarizing Well-Field History. Eos, Transactions American Geophysical Union J., 27(IV). https://doi.org/10.1029/TR027i004p00526

Daus, A. D., Frind, E. O., & Sudicky, E. A. (1985). Comparative error analysis in finite element formulations of the advection-dispersion equation. Advances in Water Resources J., 8(2), 86-95. http://dx.doi.org/10.1016/0309-1708(85)90005-3

Fetter, C. W. (1999). Contaminant Hydrogeology. (2nd edn). Prentice-Hall Inc.

Fitts, C. R. (1996). Uncertainty in deterministic groundwater transport models due to the assumption of macrodispersive mixing: evidence from the Cape Cod (Massachusetts, U.S.A.) and Borden (Ontario, Canada) tracer tests. Contaminant Hydrology J., 23, 69-84. https://doi.org/10.1016/0169-7722(95)00101-8

Fitts, C. R. (2002). Groundwater Science. Academic Press (An Imprint of Elsevier Science).

Forghani, A., & Peralta, R. C. (2018). Intelligent performance evaluation of aquifer storage and recovery systems in freshwater aquifers. Hydrology J., 563, 599-608. https://doi.org/10.1016/j.jhydrol.2018.06.042

Freeze, R. A., & Cherry, J. A. (1979). Groundwater. Englewood Cliffs, NJ., Prentice Hall Inc.

Gelhar, L. W., Welty, C., & Rehfeldt, K. R. (1992). A Critical Review of Data on Field-Scale Dispersion in Aquifers. Water Resources Research J., 28(7), 1955-1974. https://doi.org/10.1029/92WR00607

Gropp, W., Lusk, E., & Skjellum, A. (2014). Using MPI: Portable Parallel Programming with the Message-Passing Interface. (3rd edn.). MIT press.

Heath, R. C. (1983). Basic Ground-Water Hydrology. U. S. Geological Survey Water-Supply Paper 2220. https://doi.org/10.3133/wsp2220

Huisman, L. (1972). Groundwater Recovery. Winchester Press and the Macmillan Press.

Innovate Urban Transitions and Arid region Hydro-sustainability (iUTAH). (2012). https://iutahepscor.org/

Jacob, C. E. (1944). Notes on determining permeability by pumping tests under water table conditions, U. S. Geological Survey Open-file Report.

Janssen, P. A. E. M., & Komen, G. J. (1984). An Operational Coupled Hybrid Wave Prediction Model, Geophysical Research J., 89(C3), 3635-3654. https://doi.org/10.1029/JC089Ic03p03635

Javan, K., Fallah Haghgoo Lialestani, M. R., & Nejadhossein, M. (2015). A comparison of ANN and HSPF models for runoff simulation in Gharehsoo River watershed, Iran. Modeling Earth Systems and Environ J., 1(41). https://doi.org/10.1007/s40808-015-0042-1

Jimeno-Sáez, P., Senent-Aparicio, J., Pérez-Sánchez, J., & Pulido-Velazquez, D. (2018). A Comparison of SWAT and ANN Models for Daily Runoff Simulation in Different Climatic Zones of Peninsular Spain. MDPI Water J., 10(2), 192. https://doi.org/10.3390/w10020192

Ketabchi, H., & Ataie-Ashtiani, B. (2015). Assessment of a parallel evolutionary optimization approach for efficient management of coastal aquifers. Environmental Modelling and Software J., 74, 21–38. https://doi.org/10.1016/j.envsoft.2015.09.002

Kimbler, O. K., Kazmann, R. G., & Whitehead, W. R. (1975). Cyclic storage of freshwater in saline aquifers. Louisiana Water Resources Research Institute Bulletin # 10, Baton Rouge.

Lambert, P. M. (1995). Numerical Simulation of Ground-Water Flow in Basin-Fill Material in Salt Lake Valley, Utah. U. S. Geological Survey Technical Publication No. 110-B. https://pubs.er.usgs.gov/publication/70179464

Landmeyer, J. E. (1994). Description and application of capture zone delineation for a wellfield at Hilton Head Island, South Carolina. U. S. Geological Survey Water-Resources Investigations Report 94-4012. https://doi.org/10.3133/wri944012

Lowry, C. S., & Anderson, M. P. (2006). An Assessment of Aquifer Storage Recovery Using Ground Water Flow Models, Ground Water J., 44(5), 661-667. https://doi.org/10.1111/j.1745-6584.2006.00237.x

Lu, C., Du, P., Chen, Y., & Luo, J. (2011). Recovery efficiency of aquifer storage and recovery (ASR) with mass transfer limitation. Water Resources Research J., 47(8), 1-12. https://doi.org/10.1029/2011WR010605

McDonald, M. G., & Harbaugh, A. W. (1988). A modular three-dimensional finite-difference ground-water flow model. U. S. Geological Survey Report Techniques of Water-Resources Investigations 06-A1. https://doi.org/10.3133/twri06A1

Mentaschi, L., Besio, G., Cassola, F., & Mazzino, A. (2013). Problems in RMSE-based wave model validations. Ocean Modelling J., 72, 53-58. http://dx.doi.org/10.1016/j.ocemod.2013.08.003

Moriasi, D. N., Arnold, J. G., Van Liew, M. W., Bingner, R. L., Harmel, R. D., & Veith, T. L. (2007). Model Evaluation Guidelines for Systematic Quantification of Accuracy in Watershed Simulations. Soil and Water Division of American Society of Agricultural and Biological Engineers J., 50(3), 885-900. https://doi.org/10.13031/2013.23153

Nash, J. E., & Sutcliffe, J. V. (1970). River flow forecasting through conceptual models: Part 1, A discussion of principles. Hydrology J., 10(3), 282-290. https://doi.org/10.1016/0022-1694(70)90255-6

Neal, J. C., Fewtrell, T. J., Bates, P. D., & Wright, N. G. (2010). A comparison of three parallelization methods for 2D flood inundation models. Environmental Modelling and Software J., 25(4), 398-411. https://doi.org/10.1016/j.envsoft.2009.11.007

Neuman, S. P. (1975). Analysis of Pumping Test Data from Anisotropic Unconfined Aquifers Considering Delayed Gravity Response. Water Resources Research J., 11(2), 329-342. https://doi.org/10.1029/WR011i002p00329

Pavelic, P., Dillon, P. J., & Simmons, C. T. (2005). Multiscale Characterization of a Heterogeneous Aquifer Using an ASR Operation. Groundwater J., 44(2), 155-164. https://doi.org/10.1111/j.1745-6584.2005.00135.x

Ptak, T., Piepenbrink, M., & Martac, E. (2004). Tracer tests for the investigation of heterogeneous porous media and stochastic modelling of flow and transport—a review of some recent developments. Hydrology J., 294(1–3), 122-163. https://doi.org/10.1016/j.jhydrol.2004.01.020

Pyne, R. D. G. (1995). Groundwater Recharge and Wells: A Guide to Aquifer Storage Recovery. CRC Press.

R Core Team. (2019). R: A language and environment for statistical computing. http://www.R-project.org/

Schwartz, F. W., & Zhang, H. (2003). Fundamentals of Groundwater. John Wiley and Sons Inc.

Sloan, J. D. (2009). High Performance Linux Clusters: With OSCAR, Rocks, OpenMosix, and MPI, A Comprehensive Getting-Started Guide. O'Reilly Media.

Smith, W. B., Miller, G. R., & Sheng, Z. (2017). Assessing aquifer storage and recovery feasibility in the Gulf Coastal Plains of Texas. Hydrology J., 14, 92–108. https://doi.org/10.1016/j.ejrh.2017.10.007

Snir, M., Otto, S., Huss-Lederman, S., Walker, D., & Dongarra, J. (1996). MPI: The Complete Reference. The MIT Press.

U.S. EPA. (2019). On-line Tools for Site Assessment Calculation, U.S. Environmental Protection Agency. https://www3.epa.gov/ceampubl/learn2model/part-two/onsite/longdisp.html

U.S. EPA. (2008). A Systematic Approach for Evaluation of Capture Zones at Pump and Treat Systems. U.S. Environmental Protection Agency, Washington, DC, EPA/600/R-08/003.

Visser, A., Singleton, M. J., & Esser, B. K. (2014). Xenon Tracer Test at Woodland Aquifer Storage and Recovery Well. Lawrence Livermore National Laboratory, A report to West Yost Associates LLNL-TR-652313. https://www.osti.gov/servlets/purl/1162248

Ward, J. D., Simmons, C. T., & Dillon, P. J. (2008). Variable-density modelling of multiple-cycle aquifer storage and recovery (ASR): importance of anisotropy and layered heterogeneity in brackish aquifers. Hydrology J., 356(1–2), 93–105. https://doi.org/10.1016/j.jhydrol.2008.04.012

Ward, J. D., Simmons, C. T., Dillon, P. J., & Pavelic, P. (2009). Integrated assessment of lateral flow, density effects and dispersion in aquifer storage and recovery. Hydrology J., 370(1-4), 83–99. https://doi.org/10.1016/j.jhydrol.2009.02.055

Wilson, J. L., Conrad, S. H., Mason, W. R., Peplinski, W., & Hagan, E. (1990). Laboratory Investigation of Residual Liquid Organics. U. S. Environmental Protection Agency, 600/6-90/004.

Xu, M., & Eckstein, Y. (1995). Use of Weighted Least-Squares Method in Evaluation of the Relationship between Dispersivity and Field Scale. Ground Water J., 33(6), 905-908. https://doi.org/10.1111/j.1745-6584.1995.tb00035.x

Zheng, C., & Wang, P. P. (1999). MT3DMS: A Modular Three-Dimensional Multispecies Transport Model for Simulation of Advection, Dispersion, and Chemical Reactions of Contaminants in Groundwater Systems, Documentation and User's Guide. U.S. Army Engineer Research and Development Center Cataloging-in-Publication Data, Final Report, Contract Report SERDP-99-1.

CHAPTER 3

MANAGED AQUIFER STORAGE FOR EFFECTIVE RECOVERY (MASER) SOFTWARE

Abstract

From water supply and environmental protection perspectives, the MASER software simplifies designing and evaluating the suitability of well systems for aquifer storage and recovery (ASR) or aquifer recharge (AR). MASER evaluates preliminary ASR or AR well design for user criteria (well diameter, drawup/drawdown, etc.) and 61-day injection and ASR 91-day extraction. The design includes: a) absence or existence of a pre-existing groundwater right allows extracting the same or a greater volume that is injected; b) conservative contaminant concentration of (un)steadily injected stormwater/treated water/surface water differs from the concentration within native groundwater; and c) where delaying extraction temporarily after injection is desirable. MASER is also helpful where important goals are to maintain aquifer quality or to achieve an appropriate concentration in the extracted water. Applicable conservative contaminants include: chloride; sulfate, except within very reductive conditions; nitrate in the absence of a carbon source for denitrifying bacteria; and others.

For one fully penetrating well, MASER sequentially simulates: ASR or AR 61-day surface water injection into a homogenous, (an)isotropic, (un)confined aquifer; optional pumping hiatus; and ASR 91-day extraction (for uses such as secondary irrigation and others). At approximately 15-day intervals, MASER provides: i) simulated aquifer solute concentration maps; ii) estimated

and/or simulated iia) hydraulic drawup and drawdown; iib) values of REN; and iic) blended solute concentration of ASR-extracted water.

3.1. Introduction

3.1.1. Overview

MASER is designed to facilitate evaluation and use of: i) aquifer storage and recovery (ASR); and ii) aquifer recharge (AR) to increase groundwater availability and aid aquifer protection. When surface water is available, the considered ASR process involves injecting surface water through a vertical tube well into an aquifer. Subsequently, when surface water is no longer available, but water is needed, the same well extracts water that is a blend of the injected water (injectate) and native groundwater. Conservative contaminants such as chloride might exist within the injectate and/or the native groundwater. Reconnaissance ASR or AR well evaluation and design can involve estimating solute concentrations within ASR extracted water, and solute distribution and mass remaining within the aquifer. Both estimate types are interesting to water users and environmental protection specialists. Ideally, without treatment or further blending, the solute concentration in the extracted water is adequate for the intended water use, and enough injectate has been removed from the aquifer to satisfy aquifer protection goals. Evaluating such solute concentration or remaining mass involves groundwater flow and solute transport simulation.

The presented easy-to-use MASER software promotes initial evaluation of ASR or AR well suitability by land and natural resource developers, planners, and managers. The software provides more information than can be obtained from analytical equations, without requiring the development of a site-specific groundwater flow and solute transport simulation model. Although not negating the potential need for site-specific groundwater simulation modeling, MASER software uses hydrogeologic-site information to reasonably estimate time series of: aquifer head drawup and/or drawdown; solute concentrations in water being extracted from the aquifer; and solute remaining within the aquifer. MASER functionality is demonstrated for a Salt Lake Valley, Utah, location. Compared are values of recovery effectiveness--REN (i.e., the time-varying proportion of injectate that has been extracted) for situations involving unsteady versus steady injections. To demonstrate how to satisfy aquifer protection criteria concerning the amount of injected solute remaining within the aquifer (i.e., 1.00 - REN), another comparison is between extraction of the same volume as is injected, versus extracting more water than is injected. MASER demonstrations highlight the benefits of: 1) predicting movement of conservative (e.g., NO_3) contaminants (injectate and native groundwater) within the aquifer; 2) having a pre-existing groundwater right to permit extracting more water than the well injects during a season to obtain a desired proportion of injectate recovery; 3) presenting differences between injectate contaminant transport within the aquifer resulting from the extracting more than is injected; 4) injecting stormwater or other surface water to increase groundwater availability and improve groundwater quality; and 5) injecting steadily, versus unsteadily. The subsequent literature review highlights the

importance of providing software that addresses the above-mentioned water supply and environmental protection concerns.

3.1.2. Literature review

3.1.2.1. Water supply concern

Escalating withdrawals of ambient surface water and groundwater for domestic, industrial, and agricultural uses can harm water sustainability. Water resources management to increase water sustainability involves controlling movement to: a) increase beneficial use; and b) avoid damage to life and nature. The managed aquifer recharge (MAR) method helps achieve long-term water sustainability by using available stormwater runoff, treated wastewater, or other surface water (Alam et al., 2021). As a potentially relatively inexpensive way to improve water supply, MAR methods that inject water into an aquifer saturated zone are: a) aquifer recharge (AR) wells; b) aquifer storage and recovery (ASR) wells. Methods that introduce water into the vadose zone overlying a water table are: c) bank filtration via dry wells; and d) infiltration gallery (Dillon, 2005; Alam et al., 2021).

AR can be used to increase stored groundwater volume, or groundwater heads to prevent seawater intrusion and control land subsidence (Masciopinto, 2013). AR wells that inject stormwater can improve groundwater storage and surface water quality (Daus, 2019). For instance, AR wells inject stormwater runoff in

the Kingdom of Bahrain to prevent flooding problems in open and densely populated areas (Naik et al., 2017). Intentionally recharging urban aquifers helps manage stormwater runoff and increases groundwater storage (Datry et al., 2004; Page et al., 2015). ASR well systems both inject water into an aquifer and then extract groundwater when needed. ASR wells can provide water for irrigation, agriculture, industry, ecosystem restoration, and human consumption. ASR wells are especially useful where there is limited space, high population density, and increasing demand for groundwater (Daus, 2019; U.S. EPA, 2021). ASR can help provide water storage in regions that have periods of both drought and intense precipitation (Smith et al., 2017).

ASR or AR injectate can affect water quality within an aquifer, and of subsequently discharged water. The quality of naturally discharged or ASR-extracted water can affect the well-being of the receiving water users and ecosystem.

3.1.2.2.   Environmental protection concern

Water supplies are important for maintaining a healthy and safe environment for human beings and wildlife. Applying a managed aquifer recharge (MAR) method can cause groundwater improvement or deterioration based upon: a) the water itself; b) the applied MAR technique; and c) the interaction between the injectate and the aquifer materials (Luxem, 2017). As ASR injectate passes

through an aquifer, bacteria inactivation and retention can improve its quality (Page et al., 2015). In the Kingdom of Bahrain, the dilution of injected stormwater with groundwater reduced risks of aquifer contamination significantly (Naik et al., 2017). Datry et al. (2004) tested methods of recharging urban aquifers via stormwater infiltration systems. They recommended trying to minimize contact between inflowing stormwater and the organic sediments common in infiltration basins because organic sediments reduce the dissolved oxygen (DO) in cold winter stormwater that would otherwise re-oxygenate groundwater. I conclude, that by avoiding the sediments, ASR and AR injection systems can increase groundwater DO better than infiltration basins.

In Lebanon, aquifer recharge wells protect coastal groundwater and groundwater users by preventing seawater intrusion. Such barrier wells inject treated municipal wastewater mixed with surface water into aquifers (Masciopinto, 2013). Mixed stormwater runoff and groundwater via ASR or AR implementation could result in negative or positive impacts on aquifer because of variations of injectate quality. Prediction of the impacts can be modeled by flow and solute transport simulations (Luxem, 2017).

USEPA Underground Injection Control (UIC) programs address Class V ASR, AR and other injection wells in many states including California (U.S. EPA, 1999). In California, any treated wastewater ASR injectate must meet drinking water standards at the well. USEPA requires that Regional Water Quality Control Boards and the Department of Health Services establish ASR discharge

requirements and approve applications in the state. To aid application review, MASER predicts the ASR discharge or AR groundwater quality impacts for a selected site. MASER executes flow, MODFLOW (McDonald and Harbaugh, 1988), and solute transport, MT3DMS (Zheng and Wang, 1999) simulations and presents results within suitable outputs for users.

3.2.   Methods and Materials

3.2.1. Overview and assumptions

This section reports the assumptions and procedures used within MASER to provide preliminary predictions of aquifer head, and concentrations of a conservative contaminant within the groundwater ASR-extracted water. MASER can address situations in which water does or does not need treatment prior to ASR or AR injection into an aquifer. MASER allows user specification of the concentration (e.g., a conservative or non-conservative contaminant solute) existing either within the injectate or initially and uniformly distributed within the aquifer. For a non-conservative solute, user can provide inputs MT3DMS reaction package of MT3DMS when MASER allows.

MASER uses analytical equations and numerical finite difference simulators to predict groundwater head and concentration within the aquifer. Assumptions of both the employed analytical groundwater hydraulic equations and the numerical flow simulation model are:

- one ASR or AR well within quasi-infinite aquifer, without other nearby boundary conditions;

- homogeneous, (an)isotropic aquifer storativity and hydraulic conductivity;

- initially uniform aquifer thickness and hydraulic gradient; and

- horizontal groundwater flow (i.e., one-layer aquifer by default).

Input of site hydrogeologic and design parameters precedes execution of predictive equations and simulations.

3.2.2. MASER input parameters, modeled system, and predictors

MASER employs data of quality similar to that required by analytical equations. Consecutively, the MASER user first provides inputs that describe the aquifer: metric or US units; simulation Run Name; unconfined or confined aquifer; initial aquifer (background) hydraulic gradient; and either hydraulic conductivity and initial (original) aquifer saturated thickness, or aquifer transmissivity. Then the user provides the aquifer porosity, and specific yield or storage coefficient. If available and relevant, the user can provide the concentrations of a conservative contaminant within the injection water and within the native groundwater. MASER produces and employs flow and solute transport simulator input files based upon metric units (length in meters, time in days, and mass in grams), and produces output files based upon user-specified units (metric or US units) in the

graphic user interface. Before simulation, MASER allows the user to convert from a conservative to a non-conservative contaminant if desired (Note, MASER allows user provides inputs of reaction package of MT3DMS to simulate a non-conservative contaminant).

Then the user inputs: a) an assumed ASR or AR well diameter that is less than or equal to 91.44 cm (36 inch); b) the maximum increase in head just outside the well casing considered acceptable resulting from ASR or AR well injection; c) the maximum decrease in head resulting from ASR well extraction considered acceptable; d) the assumed rate of steady injection (or a time series of unsteady injection rates); e) the ratio of total extraction volume divided by total injection volume; and f) the time duration between the end of injection and the beginning of extraction.

As a preliminary check on the assumed well diameter, MASER uses the above inputs and analytical equations (Theis, 1935; Jacob, 1944; Copper and Jacob, 1946) and superposition in time, to predict head changes resulting from ASR or AR. It compares those predictions with the head change acceptability criteria to guide the user concerning a possible need to increase the well diameter.

With the user-specified values, MASER prepares the inputs for one of two auto-selected grids of a 20 km x 20 km (or a 1.2 km x 1.2 km); a) one-layer MODFLOW2005 groundwater flow simulation model; and b) a one-layer MT3DMS groundwater solute transport model. MASER selects the grid to use based upon the user-input well diameter. Cell sizes range from the 100 m x 100 m (or 10 m x

10 m) cells at the model grid periphery to the 2.5 m x 2.5 m (or 0.5 m x 0.5 m) cell located in the grid center. The central cell contains a fully penetrating screened well of the specified diameter and modeled using the multi-node well (MNW2) package. Initial elevations slope uniformly from the right-most model column 231 (or 129) to the left-most model column 1. All initial elevations and heads are uniform for a specific column.

The vertical datum of the models is assumedly 0.0 m and is located at the aquifer base at the downstream end in column 1. To satisfy input hydraulic gradient and saturated thickness values, MASER computes aquifer base and top elevations that increase uniformly to the upstream-most specified head of column 231 (or 129). No-flow conditions represent the lateral boundaries of the model area (Figures 3.1 and 3.2).

Figure 3.1

MODFLOW2005-MT3DMS model study area for ASR or AR well in MASER, top view (not to scale)
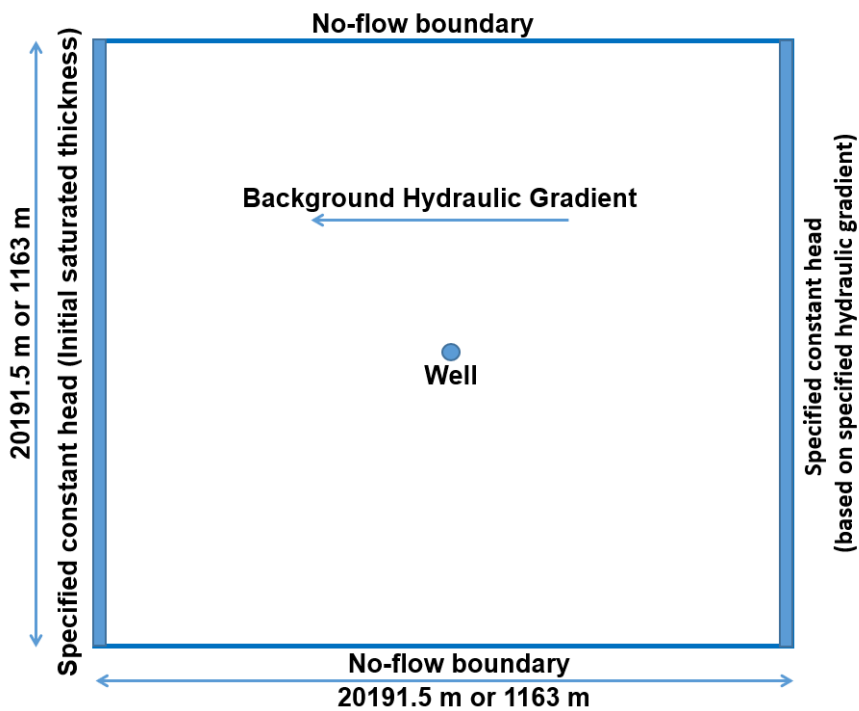
Figure 3.2

MODFLOW2005-MT3DMS model study area for ASR or AR well in MASER, side view (not to scale)
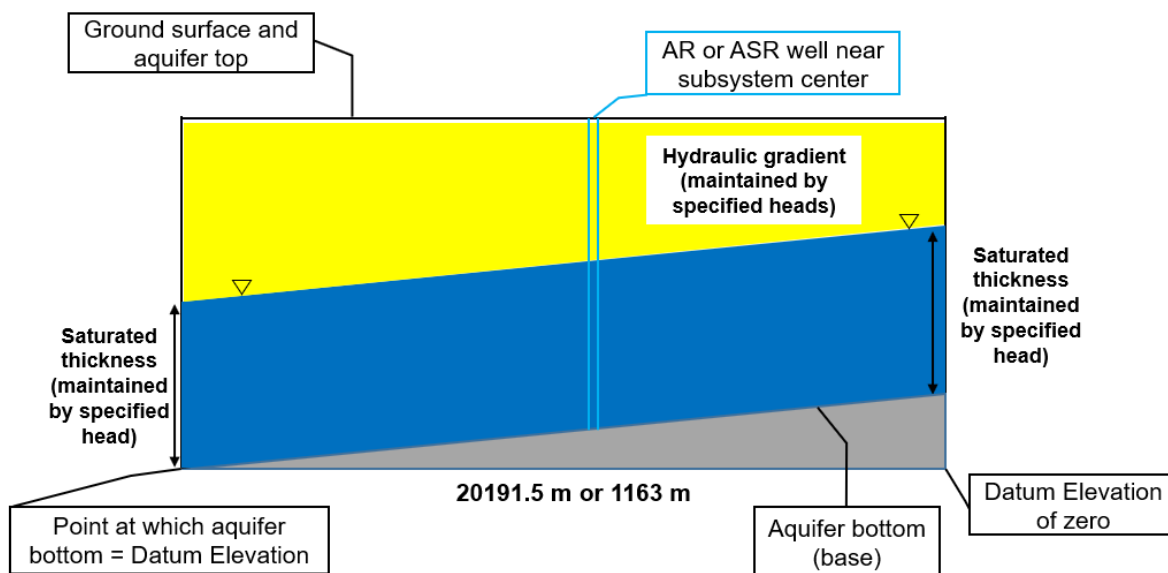
For REN (recovery effectiveness) estimation, MASER uses the developed surrogate estimators within defined ranges: a) unconfined aquifer; b) initial aquifer (background) hydraulic gradient of 0.00001-0.015; c) horizontal hydraulic conductivity of 4-20 m/d (13.124-65.61 ft/d); d) initial saturated thickness of 8-46 m (26.25-150.91 ft); e) porosity of 0.1-0.6; f) specific yield of 0.0375-0.57; g) steady injection rate of 5.451-327.06 m^3/d (0.0022-0.132 cfs or 1-60 gpm); h) steady injection rate equals to extraction rate (extraction-injection volume ratio of 1.49 to 1.5); and i) well diameter of 15.24 cm (6 inch). For developing the estimators, grid size of 1163 m by 1163 m was used. For flow and solute transport simulations, MASER uses the grid (1163 m by 1163 m) when selected-site information is within the defined ranges. Otherwise, it selects the grid of 20191.5 m by 20191.5 m.

For solute transport simulation, MT3DMS, MASER estimates longitudinal dispersivity via analytical equations found in an EPA on-line tool (2019) that incorporates work by Wilson et al. (1990), Gelhar et al. (1992), and Xu and Eckstein (1995):

$$\text{If} \quad L_p \leq 1 \text{ m:} \qquad \alpha_L = 0.1 \times L_p \tag{1a}$$

$$\text{If} \quad L_p > 1 \text{ m:} \quad \alpha_L = 0.83 \times \left[\log_{10} L_p\right]^{2.414} \tag{1b}$$

where L_p = advective plume length (m) = (v × injection duration), v = linear pore velocity (m/d) = (K × i/n), K = horizontal hydraulic conductivity (m/d), i = aquifer

initial (background) hydraulic gradient, n = porosity, and α_L = longitudinal dispersivity (m).

Also, the Courant number (C) is an input parameter of the MT3DMS advective process to decrease oscillations, improve accuracy, and decrease numerical dispersion when advection dominates dispersion. The number equals $(v \times \Delta t)/\Delta x$, where v = linear pore velocity, Δx = the grid cell dimension at the well location of 2.5 m or 8.20 ft (or 0.5 m or 1.64 ft), and Δt is maximum desirable time step size (Daus et al., 1985).

To determine the simulation time step size in days, suitable for the preferred spatial discretization, the grid Peclet number, P, as equaling 2C (Daus et al., 1985) is estimated. By assuming that P also equals $(\Delta x/\alpha_L)$, one can compute the maximum time step size desirable for use during injection.

The first estimation of the total number of time steps needed for the injection era was the integer result of dividing the total injection duration by the time step size. Those steps are partitioned equally into each injection stress period. Then two more steps per period are added to increase the likelihood of successful simulation. The injection stress period has varied time step durations. To avoid excessive processing time, the extraction period has a single time step (using even 300 time steps for extraction increases REN less than 0.005). Note, after calculating the number of time steps, for a Courant number greater than one, MASER applies one for the number in the MT3DMS advective input file (Zheng and Wang, 1999).

MASER provides input files of MODFLOW2005 and MT3DMS based upon: a) 11 (no storage time) or 12 (including storage time that is one stress period between the end of injection and the beginning of extraction) half-month stress periods for steady injection and extraction; or b) 68 (no storage time) or 69 (including storage time that is one stress period between the injection and the extraction) daily stress periods for unsteady injection, and half-month stress periods for steady extraction. Thus, Period 1 simulates steady-state background heads. Transient periods 2-5 (or 2-62) employ steady (or unsteady) injection, and periods 6-11 (or 63-68) without storage time, or period 6 for storage time, and half-month stress periods 7-12 (or period 63 for storage time, and half-month stress periods 64-69) simulate extraction. Both flow and solute transport models also use identical numbers of time steps per period, and that number can differ with period. The MODFLOW2005 PCG solver uses a 0.01 m head change criterion, and a 0.01 m residual convergence criterion. To simulate advection and dispersion, MT3DMS employs the total variation diminishing (TVD) package and the generalized conjugate gradient (GCG) solver. MT3DMS obtains the mass of injected solute, and the mass of solute recovered from the ASR well. Recovery effectiveness (REN) equals the extracted mass of the injectate divided by the total injected mass. MASER computes recovery effectiveness (REN) values for every half-month extraction. They are REN values after 15, 30, 45, 61, 76 and 91 days of extraction (REN15, REN30, REN45, REN61, REN76 and REN91, respectively) from the IN-OUT mass results of MNW2 in list file of MT3DMS. The software allows the user to

import a reaction package for a non-conservative contaminant for MT3DMS. Then

the user needs to add the name of reaction-package input file in name file of

MT3DMS if the non-conservative contaminant is applied.

The MASER graphic user interface simulates and/or predicts the water quality of

the ASR or AR system in the aquifer, and of the ASR extracted water using REN

values and Equations 2a-c.

$$P(IW, te) = \frac{REN(te) \times V_{inj}}{Q \times te} \qquad (2a)$$

$$P(NGW, te) = 1 - P(IW, te) \qquad (2b)$$

$$BC(te) = [C_{IW} \times P(IW, te)] + [C_{NGW} \times P(NGW, te)] \qquad (2c)$$

where te is time (i.e., days) after extraction begins; $P(IW, te)$ is portion of injected

water in te days (15...,91 days of extraction); REN(te) is REN in te days (REN15 to

REN91); V_{inj} is total injection volume; Q is steady pumping extraction rate;

$P(NGW, te)$ is the portion of native groundwater in te days (15...,91 days of

extraction); BC(te) is average of blended concentration of extracted water in te

days (15...,91 days of extraction); C_{IW} is concentration (i.e., a particular

conservative constituent) of injected water; and C_{NGW} is concentration (i.e., a

particular conservative constituent) of native groundwater.

MASER provides the benefits of: a) allowing the user to predict

drawup/groundwater mound height of AR or ASR injection, and AR or ASR impact

on groundwater quality and ASR extracted water quality rapidly without having to

prepare input files for flow and solute transport simulations; and b) illustrate responses of flow and solute transport simulations. Note, MASER was tested to apply inputs in MODFLOW2005-MT3DMS simulators correctly.

3.2.3. MASER graphic user interface

The Managed Aquifer Storage for Effective Recovery (MASER) software is written in the Python programming language and published at HydroShare website along with its user guide (Masoudiashtiani and Peralta, 2022). MASER employs site-specific user input with pre-prepared groundwater flow (MODFLOW2005) and solute transport (MT3DMS version 5.30) simulators under the Windows 10 operating system. It rapidly predicts AR/ASR injection impacts in aquifer, and ASR extracted water quality. The software includes one main window that requires input of Site information and selection of a Design Option (Fig. 3.3). Site information includes hydrogeologic-site properties having an option for adding concentrations of injected water and native groundwater. If the option is not used, MASER employs an imaginary 100-ppm concentration in the injected water to simplify simulated and/or predicted REN values. For Design options, MASER allows the user to: a) select the ASR or AR well diameter of less than or equal to 91.44 cm (36 inch); b) select steady or unsteady injection (an input file including 61 daily varying injection rates needs to be provided); and c) optionally include simulation

of concentration changes occurring during a storage time (period without extraction) between the end of injection and the beginning of extraction.

The MASER interface (Fig. 3.3) contains buttons of: a) "Predict drawup & drawdown suitability" to import all user-input values, and report head-change predictions; b) "Run surrogate REN estimators" to predict REN values if the user-input values are within the defined range specified in sub-section 3.2.2; c) "Run flow & transport simulators" to provide input files for flow and solute transport simulators and execute them; and d) "Display & Save outputs" to show: i) bar charts of REN-simulation and/or REN-prediction values, and save the prediction and simulation results in text files; and ii) Row-Column (RC) maps from the end of injection through the end of extraction if optional water qualities (concentrations) for ASR or AR applied.

Figure 3.3

A partial screenshot of the MASER main window

Illustrating MASER applications helps model an ASR or AR system rapidly. The illustration shows the use of MASER features to execute the system, and to present results easily.

3.2.4. Illustration of MASER applications

3.2.4.1.   Selected-site information

Figure 3.4 shows parts of Salt Lake City and Salt Lake County in Utah, USA. The assumed ASR or AR well location is within a 15.271-acre residential city block (Site 5). The site is located to the northeast of the confluence of the westward flowing Red Butte Creek with the northward flowing Jordan River. It is: a) bounded on the north and south by Fremont and Lucy Avenues, respectively; b) almost bisected from north to south by Jeremy Street; and c) bounded to the west and east by South 900 W and South 800 W, respectively.

The hydrogeologic information for Site 5 properties of the underlying shallow unconfined aquifer (Lambert, 1995a) includes: a) horizontal hydraulic conductivity of 18.17 m/d (59.61 ft/d); b) initial aquifer (background) hydraulic gradient of 0.0029; c) porosity of 0.3; d) specific yield of 0.15; and e) initial (original) saturated thickness of 10.23 m (33.56 ft). The potential water resources for injection are stormwater runoff in Site 5, and/or diversion from Red Butte Creek (RBC). In this study, WinSLAMM software (PV and Associates, 2013) helped simulate daily varying stormwater runoff (i.e., assumed unsteady

injection water) of Site 5 during April through May. Included properties for the

simulation are: a) silty soil, and ground cover consisting of nearly flat roofs

(2.238 acres, 14.6%); b) sidewalk (2.421 acres, 15.8%); c) streets of intermediate

texture (2.741 acres, 17.9%); d) small landscaping (3.935 acres, 25.7%); and e)

undeveloped area (3.936 acres, 25.7%). The daily April-May precipitation data

of 1986-2016 (31 years) from the Salt Lake City (SLC) international airport

weather station that is 5.91 km (3.67 miles) away was used (Fig. 3.4). Rain

distinguished from snow by the Static Temperature method and a 1 ℃ (33.8 ℉)

threshold temperature (Kienzle, 2008) to simulate the runoff. To substitute for

any missing precipitation data, the SLC Triad Center station that is 3.38 km (2.1

miles) away from Site 5 was applied (Fig. 3.4).

Figure 3.4

*Residential area (Site 5), and weather stations at international airport and Triad
Center in Salt Lake County, Utah, USA*
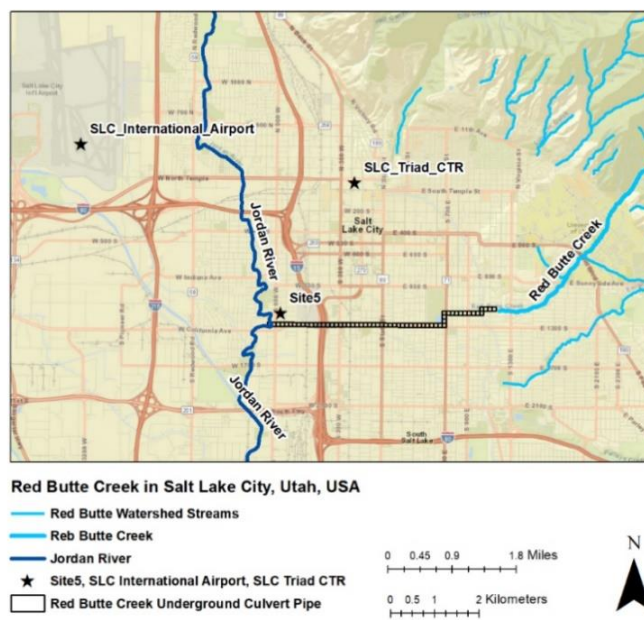
To simulate a stormwater injection situation, the runoff volume during a particular day would be injected into the aquifer at a steady rate during that day. To simulate a surface water situation, water would be diverted from RBC at an assumed steady rate and injected into the aquifer at the same rate.

For Site 5, the ASR extracted water can irrigate turf based upon a defined irrigation schedule (Kopp et. al, 2013). An application efficiency (E_a) of 70% was used for sprinkler irrigation systems in a moderate climate (Savva and Frenken, 2001) during June through August. Here, provided demonstrations show applications of MASER features to simulate an ASR or AR system for the situations.

3.2.4.2.   Demonstrations

The following demonstrations (Demos) result in understanding of MASER beneficial use for ASR or AR designs. Demos apply the selected-site information and presented characteristics in Table 3.1 to disclose the MASER applications.

Table 3.1

Characteristics of demonstrations (Demos)

	I	II	III	IV	V	VI	VII
Demo	Number of MODFLOW-MT3DMS simulations	Injection volume in Julian Day of 61-day inj. period	Total 61-day injection vol.	Extraction vol. in each of 91 days	Total 91-day extraction vol.	Type(s) of Water Quality	Goal(s)
1a	1	Steady. Each day's injection volume = {(total injection vol.) / 61 days}	Total injection volume = Site 5 total runoff volume $\leq$ Total runoff vol. of 90% of April-May PDF*	Steady. Daily extraction volume = (Total injection vol. / 91 days)	Total extraction vol. = Total injection vol.	Assumed 10-ppm nitrate concentration for injectate	Present recovery of statistically derived steady injection & NO_3 transport in aquifer
1b	1	"	"	"	"	TDS case-study, 387-ppm injectate & 1500-ppm native groundwater	Present time series of blended TDS concentration of extracted water
1c	1	"	"	"	Total extraction vol. = 5.4 × total injection vol.; achieves 80% recovery	"	Present time series of blended TDS concentration of extracted water
1d	2	"	"	Steady. Daily extraction volume = 0	Total extraction vol. = 0	"	Present increase of groundwater volume, improvement of its quality, and assume 60 and 365 days for storage times
2.1-2.31	31	Unsteady. For 61-day simulations for each of 31 years, the injection volume of each day in year is: Injection volume = Site 5 runoff of day in year.	Total injection volume = sum of Column II daily injection volumes in year	Steady. Daily extraction volume for year = (Total injection vol. for year / 91 days)	Total extract. vol. = Total injection vol.	Assumed 100-ppm TDS injectate	Present recovery of unsteady stormwater injection by steady extraction
3.1-3.31	31	Steady injection volume in year = {(Demo 1 total injection volume) / 61 days}	"	"	"	"	Present recovery of steady injection of diverted surface water by steady extraction

*- From the Probability Density Function (PDF) of total April-May runoff, the volume that is equaled or exceeded during 90% of the April-May periods. The PDF results from rainfall-runoff simulations of 31 years (1986-2016).

In Table 3.1, the characteristics of Demos 1a-d show the applied 90%-probability runoff volume for steady injected water can be diverted from RBC during April and May for ASR or AR at Site 5. As the proposed RBC diversion for ASR or AR steady injection, Demos 2 and 3 evaluate whether steady or unsteady injection results in extracting a predictable portion of the injectate.

In short, the presented Demos address the: a) water quality; b) available extra surface water for steady injection; c) desired injectate recovery based upon pre-existing groundwater extraction; d) quantity and quality of groundwater improvement; and e) steady versus unsteady injection are the desired purposes/goals of ASR or AR designs.

3.2.4.3. Purposes of selected demonstrations

The provided demonstrations (Demos) can guide users to apply MASER for the desired goal(s). Here, for the selected site, Demos in Table 3.1 highlight MASER features to achieve the following five goals.

1. Design and evaluate an ASR well that steadily injects diverted ambient surface water for two months (61 days) and extracts an equivalent total volume during the subsequent three months (91 days). Demo 1a assumes 10 ppm conservative contaminant (e.g., NO_3) in injectate and 0 ppm in native groundwater. It shows the results of spatial distribution of

the injected contaminant. Demo 1b quantifies the blending of injected water and native groundwater of different salinities to achieve adequate quality of extracted water. It assumes 387 and 1500-ppm TDS in injectate (Red Butte Creek water) and native groundwater, respectively (Salt Lake County, 2016);

2. Quantify the pre-existing groundwater right needed to obtain a desired (i.e., 80 percent) injectate recovery (Demo 1c);

3. Contrast the injectate contaminant spread within the aquifer resulting from extracting the same volume as is injected (Demo 1b) versus extracting enough to recover 80% of the injectate (Demo 1c);

4. Use steady AR to increase groundwater volume within the aquifer and improve its quality if it is extracted after 60 days, and a year (365 days) within aquifer storage (Demo 1d); and

5. Determine which ASR injection type (unsteady or steady) can provide greater confidence in extracting a predictable portion of the injectate (Demos 2 and 3).

Defining the desired goals for Demos at the selected site illustrates MASER applications to increase sustainable groundwater availability and water supply for use. MASER provides different types of output files to present the results of the Demos. The discussion of the results can indicate much about achieving the goals for ASR or AR at the site.

3.3.   Results and Discussion

Evaluating responses of any aquifer storage and recovery (ASR), and aquifer recharge (AR) is required for water use and the environment (i.e., aquifer). To access the responses easily for evaluation, the developed (MASER) software provides features to simulate a single-well ASR or AR. The well is within a quasi-infinite, one-layer, and unconfined or confined aquifer. The provided demonstrations (Demos) 1 to 3 illustrate how MASER features can design and evaluate responses of flow (MODFLOW2005) and solute transport (MT3DMS) simulations for the desired goals.

Here, for the selected site (Site 5), water-volume use of stormwater runoff during the wet months (April and May) can provide ASR or AR injection water. To quantify the volume, the April-May runoff volume of every year from 1986 to 2016 (31 years) at Site 5 was simulated by WinSLAMM software. Figure 3.5 shows the annual volumes that were used for estimating the historical 90%-probability volume statistically.

Figure 3.5

Total April-May runoff volumes of the 31 years in Site 5 simulated by WinSLAMM software
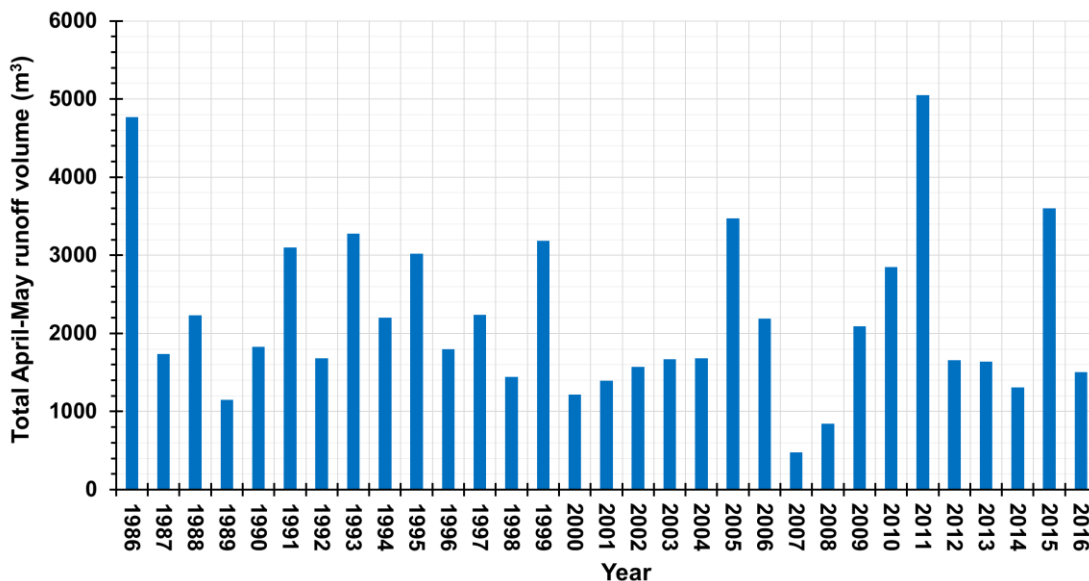
The 90%-probability runoff volume (happening water volume) during the wet months (April and May) of the 31 years (Fig. 3.5) equals 1047.46 m³ (230409 gallons). Assumed pre-existing groundwater 91-day extraction volume is the same as the 61-day injection for ASR. The ASR extracted water volume can irrigate 1896.71 m² (0.47 acre) of turf in Site 5 based on the turf irrigation schedule (Kopp et. al, 2013; Savva and Frenken, 2001) during June through August (dry months, 91 days). Thus, the ASR design aids water supply during the dry months for the turf irrigation.

Here, Demos 1a-d inject the happening water volume into aquifer steadily diverted by surface water (Red Butte Creek, RBC) nearby. Demos 1a-c include different extraction and water quality characteristics (Table 3.1) concerning the desired goals. Signifying the beneficial use of RBC water steadily for ASR or AR

injection equaling the unsteady runoff volume for each of 31 years appears in the

goals of Demos 2 and 3. Acknowledged that a tributary can divert daily varying

stormwater runoff (unsteady inflow) from Site 5 into RBC in exchange for steady

RBC outflow into the ASR or AR during the wet months.

Demo 1a injects an average steady rate (the happening water volume diverted

from RBC) of 0.1987 l/s (15.85 gpm). For the steady injection, MASER evaluates

80% of injected NO_3 contaminant remained in aquifer after 91-day extraction with

the highest aquifer concentration of 9 ppm (Table 3.2). Figure 3.6 illustrates NO_3-

contaminant transport in the aquifer that is 41.5 m (136.15 ft) long in the flow

direction, and 18 m (59.04 ft) wide from the well.

Figure 3.6

MASER image for total concentration in aquifer (assumed 10-ppm injectate and 0-ppm native groundwater include the same contaminant) after 91-day extraction; ASR well located at (X=0, Y=0)
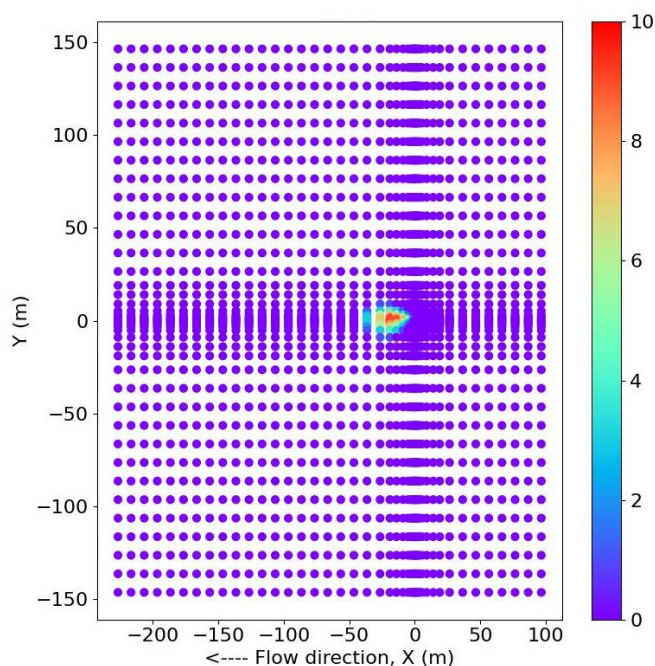
Demo 1b includes the same injected volume and rate as Demo 1a but uses reported total dissolved solid (TDS) of injectate, RBC, and native groundwater of 387 and 1500 ppm (Salt Lake County, 2016; Lambert, 1995b) for ASR at Site 5. As expected, the same injected-contaminant percent remained in the aquifer. However, the simulated highest TDS in the aquifer, and maximum average TDS of extraction during the last 15-day extraction period are about 1609 ppm after 91 days of extraction and 1488 ppm, respectively (Table 3.2). A MASER bar chart shows REN values from 15 to 91 days of extraction (Fig. 3.7), and the increasing injectate recovery is insignificant after 61 days.

Table 3.2

Selected results of demonstrations; native groundwater and Red Butte Creek have 1500 and 387 ppm (Lambert, 1995; Salt Lake County, 2016); stormwater has 72 ppm (Pitt et al., 2004)

Demo	Number of MODFLOW2005-MT3DMS simulations	Description	Total Inj. Vol.	(Ext. Vol.) / (Inj. Vol.) (-)	Period of max. avg. extraction conc. (-)	Inj. Solute in aquifer after 91 days (%)
			Avg. flowrate	Irrigated area	Period conc. (ppm)	Highest aq. Conc. after 91 days (ppm)
1a	1	*Steady injection*, assumed 10 ppm nitrate of water from stream. Compare extraction conc.	1047.46 m³ or 276709.7 gal	1.0	Stress period 2, (through day 15);	80.0%
			0.1987 l/s or 15.85 gpm	1896.7 m² (0.47 acre)	7	9
1b	1	*Steady injection,* 387 ppm water from stream; Compare extraction conc.	"	"	Stress period 11, (days 77-91);	80.0%
			"	"	1488	1609
1c	1	Like 1b, but get REN >=0.8	"	5.4	Stress period 11, (days 77-91);	14.9%
			"	10240.69 m² (or 2.53 acre)	1468	1643
1d	2	*Steady injection*, 387 ppm water from stream; a) 60 days for storage time; b) 365 days for storage time	"	0	NA	NA
			"	0	0	NA
2.1-2.31	31	Injecting values of daily varying runoff for 31 seasons to compare REN	478.23 to 5048.26 m³	1.0	….	….
			0.42 l/s or 6.58 gpm	865.92 to 9141.17 m² (0.21 to 2.26 ac.)	….	….
3.1-3.31	31	*Steady injection* of the same annual volumes as Demo 2. Compare REN.	"	"	….	….
			"	"	….	….

Note. Demos 1a-d use Red Butte Creek water. Demos 2 and 3 compare REN only (no quality).

Figure 3.7

REN values after 15 to 91 days of extraction for Demos 1a-b
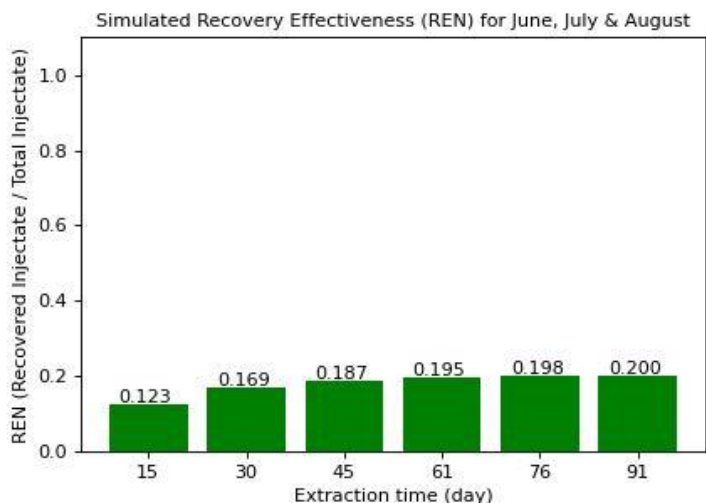
Demo 1c is to quantify the pre-existing groundwater right for the 80% recovery of the injectate. MASER shows the right for extraction is about 4.4 times the injection (happening water) volume (total extraction volume equals 5.4 times total injection volume). The extraction rate (the extraction volume divided by extraction days) causes the shrinkage of the injectate transport. The shrinkage is about 10 m (32.81 ft) long in the flow direction, and 6 m (19.68 ft) wide from the ASR well, compared with Demo 1b. The Demo 1c extraction volume can irrigate 10240.69 m^2 (or 2.53 acre) of turf in Site 5 (Table 3.2). Also, the extracted TDS is less than the turfgrass limit of 1920 ppm (Carrow and Duncan, 1998; Peacock et al., 2012).

As mentioned above in Table 3.2, the stormwater (72 ppm), and diverted surface water, RBC, (387 ppm) contain no negative impacts on the 1500-ppm shallow unconfined aquifer if injected. Thus, AR can help increase aquifer protection by injecting the surface water into the aquifer. For Demo 1d, storage times of 60 and

365 days after injection were applied to evaluate injectate transport in the aquifer.

MASER simulates the total concentration less than 1500 ppm at the AR well

location after 60 days of storage time. The injectate was transported 51 m (167.32

ft) long in the flow direction, and 34 m (111.55 ft) wide from the AR well. Thus,

extracting the injectate within 60 days after the injection is possible due to the

existing injectate at the well location (Fig. 3.8).

Figure 3.8

MASER image for total concentration in aquifer (assumed 378-ppm injectate and 1500-ppm native groundwater include the same contaminant), 151 days after injection ceases (60 days of storage); AR well located at (X=0, Y=0)
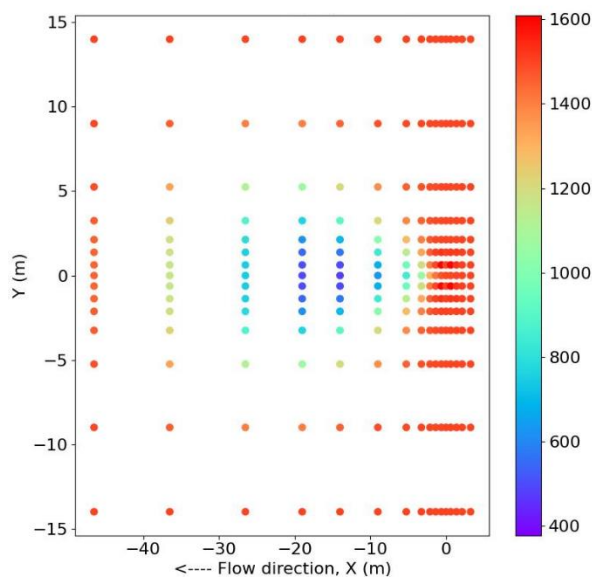
Simulation of applying a 365-day storage time for Demo 1d shows the injectate

located in 45 (147.64) to 109 m (357.61 ft) long in the flow direction from the AR

well. Thus, for injectate recovery, an extraction well within the 45 to 109 m long

in the flow direction from the AR well is needed after a year (Fig. 3.9).

Figure 3.9

MASER image for AR showing total concentration in aquifer (assumed 378-ppm injectate and 1500-ppm native groundwater include the same contaminant), 426 days after injection ceases (365 days of storage); AR well located at (X=0, Y=0)
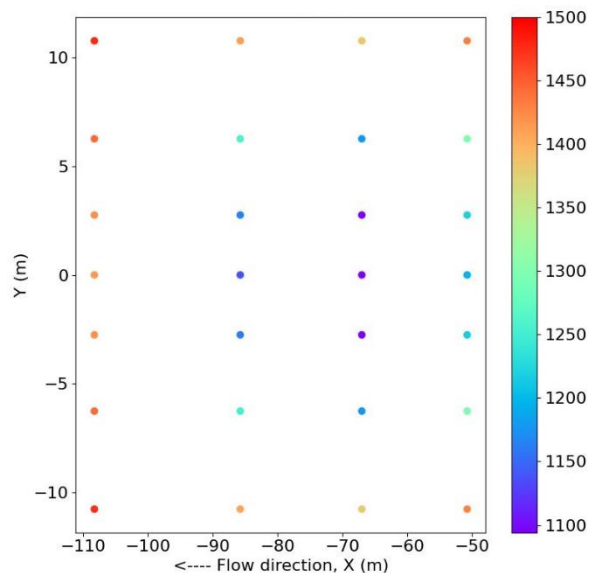
Demos 2 and 3 explore which type of ASR injection can result in predictive recovery (REN) during extraction. For these Demos, the 100-ppm imaginary conservative contaminant for injectate of ASR was applied to evaluate impacts of unsteady versus steady injection on injectate recovery during extraction.

Demo 2 injects the daily varying stormwater runoff (unsteady injection) during April and May (61 days) in each of 31 years and extracts the injection volume during the dry months (91 days) steadily. Figure 3.10 shows that even though one year might have a greater total injection volume than a second year, the REN resulting from the first year might not be greater than that of the second year.

Figure 3.10

REN (gm/gm) values of every half month during extraction for Demo 2; continuous (steady) extraction rate equals the injection volume divided by 91 days for each 31 years. Extraction volume equals the injection volume.
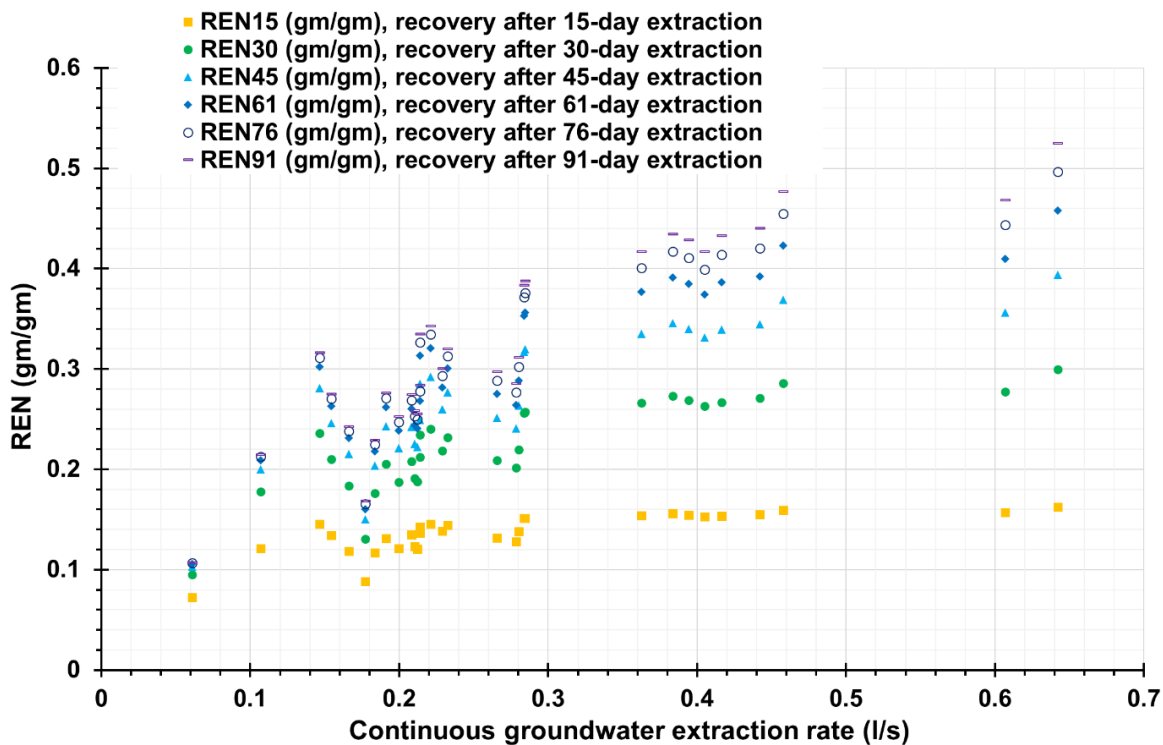
For Demo 3, the runoff volume in each of 31 years is divided by number of injection days (61 days) was calculated to provide the daily steady injection rate of ASR. As steady injection, the increasing rate of the continuous groundwater (steady) extraction results in increasing REN values (Fig. 3.11). Thus, steady injection can provide greater confidence in extracting a predictable portion of the injectate.

Figure 3.11

REN (gm/gm) values of every half month during extraction for Demo 3; continuous (steady) extraction rate equals the injection volume divided by 91 days for each 31 years. Extraction volume equals the injection volume.
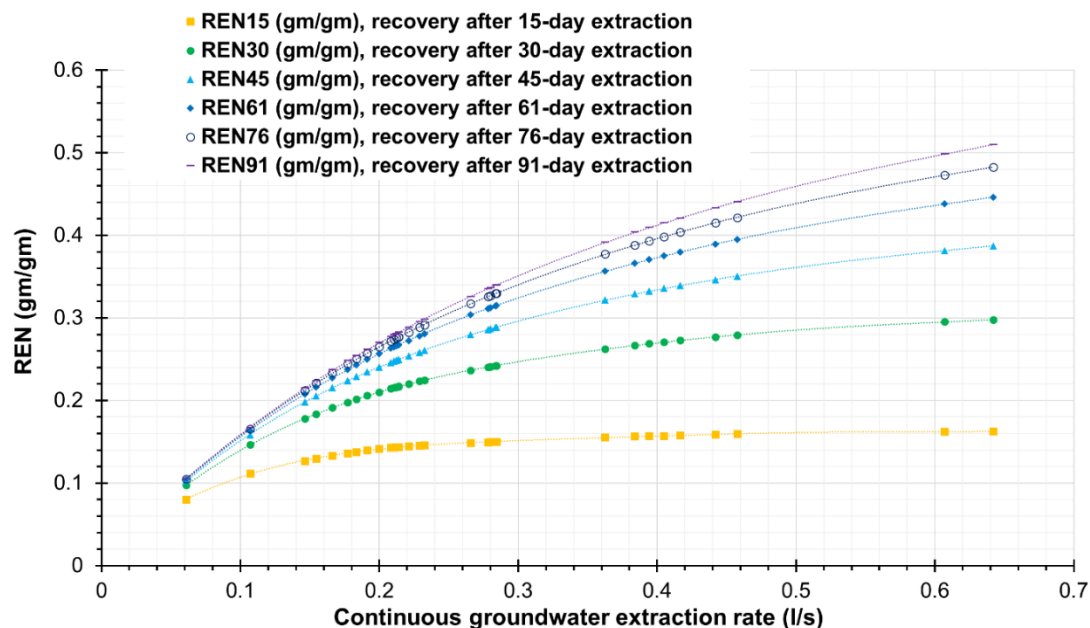
When comparing RENs resulting from steady versus unsteady injection of the same total volume, the unsteady could achieve a higher or lower predicted REN than the steady. For example, simulated injection volumes for 1987 and 2001 are 1392.81, and 1738.17 m^3, respectively. For 1987, predicted REN values of the steady and unsteady injections are 0.288 and 0.342, respectively. For 2001, respective REN values are 0.248 for steady injection and 0.168 for unsteady injection.

Results of Demos indicate MASER features can conduct simple ASR or AR system for the desired goals. MASER facilitates evaluating and designing ASR and AR systems for injecting available water unsteadily, or steadily whatever source. The evaluations can help water managers predict whether an ASR or AR system

improve quantity and quality of water supply in aquifer, and for uses (e.g., secondary irrigation) or not.

3.4.   Conclusions

Aquifer storage and recovery (ASR) and aquifer recharge (AR) systems improve the sustainable availability of groundwater and aquifer protection. The user-friendly Managed Aquifer Storage for Effective Recovery (MASER) software aids reconnaissance level design and evaluation of a single-well ASR or AR system for user-selected sites. One MASER option invokes prediction of REN. Alternatively, for flow-transport modeling in other situations, MASER applies groundwater flow (MODFLOW2005) and solute transport (MT3DMS version 5.30) simulators under the Windows 10 operating system. Addressable site features include: a) aquifer type (confined and unconfined); b) concentrations of injected water and native groundwater; c) injection type (steady and unsteady); d) extraction and injection volumes (ratio is zero for AR and is based upon pre-existing groundwater right for ASR); e) storage time between the end of injection and the beginning of ASR extraction; f) 61 days of injection; and g) 91 days of extraction. MASER provides estimated and/or simulated hydraulic drawup and drawdown, REN, and estimated and/or simulated blended solute concentration of ASR-extracted water, about every 15 days. MASER also provides simulated aquifer solute concentration maps.

Two discussed groups of MASER simulations employ precipitation data for Salt Lake Valley (SLV), and shallow unconfined aquifer hydrogeologic data underlying a Salt Lake City (SLC) block (native groundwater has 1500-ppm TDS). Three demonstrated ASR and AR

simulations (Demos 1b-d) assume 61 days of steady injection of 387 ppm diverted stream

flow and 91 days of ASR steady extraction (the total arbitrary injection volume equals the

90%-probability April-May precipitation runoff volume of 1986-2016 years from the SLC

block). Demos differ in extraction rate and total extraction volume. In the below Group A

Demos, Demo ii), and Demos i-ii) are compared with Demo i), and Demo iii) respectively.

Group A Demos details are:

    i)   assuming a total extraction volume equaling the injection volume, the extracted water can irrigate 1896.71 m^2 (0.47 acre) of turf with a blended TDS of 1277 ppm, and 91-day extraction recovers 20% of injectate (i.e., REN is 0.2) and leaves a reduced-TDS plume (41.5 m or 136.15 ft long in the flow direction and 9 m or 29.52 ft wide);

    ii)   assuming a goal of 80% injectate recovery requires and involves extracting 5.4 times the total injection volume (i.e., requires having a pre-existing groundwater extraction right 4.4 times the injection volume), allows irrigating 5.4 times as much turf, increases the blended TDS by 57 ppm, shrinks the reduced-TDS plume length by 10 m (32.81 ft) and width by 6 m (19.68 ft), and achieves a REN of 0.8 at end of 91-day extraction;

    iii)   assuming steady AR injection, 60-day (maximum storage time if the extraction of the injectate at the well desired) transport of the injectate in the flow direction after injection, and no extraction

increases the length of the reduced-TDS plume by 37 m (121.39 ft)

and the width by 16 m (52.49 ft).

Group B ASR simulations without considering water quality show how, depending upon the injection time-series, injecting a specific volume unsteadily versus steadily can either increase or decrease REN. Two types of Group B simulations were performed for each year of 1986-2016. One type simulated 61 days of injection of estimated daily runoff from the specified SLC block. The other type simulated steady injection at a rate equaling 1/61 of the total April-May runoff from the block of that year. Both simulation types extracted steadily for 91 days to remove a volume equal to the total injection. Results show: a) when comparing unsteady injection simulations, the unsteady injection time series has more impact on REN than the total injection volume--a year having greater total injection volume might not yield a higher REN; b) when comparing steady injection simulations, the greater the total injection volume, the greater the resulting REN; and c) when comparing results from steady versus unsteady injection of the same total volume, the unsteady could achieve either a higher or lower predicted REN than the steady. For example, simulated injection volumes for 1987 and 2001 are 1392.81, and 1738.17 m^3, respectively. For 1987, predicted REN values of the steady and unsteady injections are 0.288 and 0.342, respectively. For 2001, respective REN values are 0.248 for steady injection and 0.168 for unsteady injection. In general, steady injection is more likely to cause a predictable REN but might not cause a higher REN than unsteady injection.

In summary, MASER facilitates evaluation and design of systems for injecting available water unsteadily, or steadily whatever source via ASR or AR. Unless stormwater runoff is

augmented or stored sufficiently to allow steady injection, the group B simulations compare RENs of transient stormwater runoff versus steady diversion of water such as surface water or recyclable water.

Acknowledgments

References

Alam, S., Borthakur, A., Ravi S., Gebremichael, M., & Mohanty, S. K. (2021). Managed aquifer recharge implementation criteria to achieve water sustainability. Science of The Total Environment, 768, 144992. https://doi.org/10.1016/j.scitotenv.2021.144992

Carrow, R. N., & Duncan, R. R. (1998). Salt-Affected Turfgrass Sites: Assessment and Management. Ann Arbor Press, Chelsea, MI.

Cooper, H. H. Jr., & Jacob, C. E. (1946). A Generalized Graphical Method for Evaluating Formation Constants and Summarizing Well-Field History. Eos, Transaction American Geophysical Union J., 27(IV). https://doi.org/10.1029/TR027i004p00526

Datry, T., Malard, F., & Gibert J. (2004). Dynamics of solutes and dissolved oxygen in shallow urban groundwater below a stormwater infiltration basin. Science of The Total Environment, 329, 215–229. https://doi.org/10.1016/j.scitotenv.2004.02.022

Daus, A., & GSI Environmental Inc. (2019). Aquifer Storage and Recovery. Improving Water Supply Security in the Caribbean Opportunities and Challenges. Inter-American Development Bank, Water and Sanitation Division. Discussion paper No. IDB-DP-00712.

Daus, A. D., Frind, E. O., & Sudicky, E. A. (1985). Comparative error analysis in finite element formulations of the advection-dispersion equation. Advances in Water Resources, 8(2), 86-95. http://dx.doi.org/10.1016/0309-1708(85)90005-3

Dillon, P. (2005). Future management of aquifer recharge. Hydrogeology Journal, 13, 313–316. https://doi.org/10.1007/s10040-004-0413-6

Gelhar, L. W., Welty, C., & Rehfeldt, K. R. (1992). A Critical Review of Data on Field-Scale Dispersion in Aquifers. Water Resources Research, 28(7), 1955-1974. https://doi.org/10.1029/92WR00607

Jacob, C. E. (1944). Notes on determining permeability by pumping tests under water table conditions. U. S. Geological Survey Open-file Report.

Kienzle, S. W. (2008). A new temperature-based method to separate rain and snow. Hydrological

Processes, John Wiley and Sons. Ltd., 22, 5067-5085. https://doi.org/10.1002/hyp.7131

Kopp, K., Allen, N., & Wagner, K. (2013). Simple Sprinkler Performance Testing for Salt Lake

County. Utah St. Univ. Coop. Ext. Svc.

https://digitalcommons.usu.edu/extension_curall/339

Lambert, P. M. (1995a). Numerical Simulation of Ground-Water Flow in Basin-Fill Material in Salt

Lake Valley, Utah. U. S. Geological Survey Technical Publication No. 110-B.

https://pubs.er.usgs.gov/publication/70179464

Lambert, P. M. (1995b). Particle-Tracking Analysis of Time-Related Capture Zones for Selected

Public-Supply Wells in Salt Lake Valley, Utah. U. S. Geological Survey Technical Publication

No. 110-C. https://pubs.er.usgs.gov/publication/70179465

Luxem, K. (2017). Managed Aquifer Recharge. A tool to replenish aquifers and increase

underground water storage. American Geosciences Institute (AGI), Factsheet 2017-006,

This work is licensed under a Creative Commons BY-NC-ND 4.0 license.

https://www.americangeosciences.org/geoscience-currents/managed-aquifer-recharge

Masciopinto, C. (2013). Management of aquifer recharge in Lebanon by removing seawater

intrusion from coastal aquifers. Journal of Environmental Management, 130, 306-312.

http://dx.doi.org/10.1016/j.jenvman.2013.08.021

Masoudiashtiani, S., & Peralta, R. C. (2022). Managed Aquifer Storage for Effective Recovery

(MASER) software. HydroShare.

http://www.hydroshare.org/resource/3186303590a846e484f4c67d1a336511

McDonald, M. G., & Harbaugh, A. W. (1988). A modular three-dimensional finite-difference ground-water flow model. U. S. Geological Survey Report Techniques of Water-Resources Investigations 06-A1. https://doi.org/10.3133/twri06A1

Naik, P. K., Mojica, M., Ahmed, F., & Al-Mannai, S. (2017). Storm water injection in Bahrain: pilot studies. Arab J. Geosci, 10, 452. https://doi.org/10.1007/s12517-017-3232-5

Page, D. W., Vanderzalm, J. L., Barry, K. E., Torkzaban, S., Gonzalez, D., & Dillon, P. J. (2015). E. coli and turbidity attenuation during urban stormwater recycling via Aquifer Storage and Recovery in a brackish limestone aquifer. Ecological Engineering, 84, 427–434. http://dx.doi.org/10.1016/j.ecoleng.2015.09.023

Peacock, C., Miller, G., & Martin, M. (2012). Irrigation Water Quality Problems. NC State Extension Publications, AG-759. https://content.ces.ncsu.edu/irrigation-water-quality-problems#

Pitt, R., Maestre, A., & Morquecho, R. (2004). The National Stormwater Quality Database (NSQD, version 1.1). World Water and Environmental Resources Congress, Salt Lake City, UT, ASCE. http://rpitt.eng.ua.edu/Research/ms4/Paper/Mainms4paper.html

PV and Associates, LLC. (2013). WinSLAMM Model Algorithms. http://www.winslamm.com

Salt Lake County, Utah. (2016). Salt Lake County Water Quality Annual Report. Watershed Planning and Restoration Program. https://slco.org/globalassets/1-site-files/watershed/2016-slco-water-quality-report.pdf

Savva, A. P., & Frenken, K. (2001). Irrigation Development: A Multifaceted Process: Social, Economic, Engineering, Agronomic, Health and Environmental Issues to be Considered in a Feasibility Study. Water Resources Development and Management Officers FAO Sub-Regional Office for East and Southern Africa in collaboration with Simon MADYIWA,

Irrigation Engineer Consultant Kennedy MUDIMA, National Irrigation Programme Officer, Zimbabwe Tove LILJA, Associate Professional Officer, FAO-SAFR, Volume I, Module 1.

Smith, W. B., Miller, G. R., & Sheng, Z. (2017). Assessing aquifer storage and recovery feasibility in the Gulf Coastal Plains of Texas. Journal of Hydrology, Regional Studies, 14, 92–108. https://doi.org/10.1016/j.ejrh.2017.10.007

Theis, C. V. (1935). The Relation between the Lowering of Piezometric Surface and the Rate and the Duration of Discharge of Well Using Groundwater Storage. Eos, Transactions American Geophysical Union J., 16, 519-524. https://doi.org/10.1029/TR016i002p00519

U.S. Environmental Protection Agency (U.S. EPA). (1999). The Class V Underground Injection Control Study, Volume 21, Aquifer Recharge and Aquifer Storage and Recovery Wells. Office of Ground Water and Drinking Water, 4601, EPA/816-R-99-014u. https://www.epa.gov/uic/class-v-underground-injection-control-study

U.S. Environmental Protection Agency (U.S. EPA). (2019). EPA On-line Tools for Site Assessment Calculation.

https://www3.epa.gov/ceampubl/learn2model/part-two/onsite/longdisp.html

U.S. Environmental Protection Agency (U.S. EPA). (2021). Underground Injection Control, Aquifer Recharge, and Aquifer Storage and Recovery. https://www.epa.gov/uic/aquifer-recharge-and-aquifer-storage-and-recovery

Wilson, J. L., Conrad, S. H., Mason, W. R., Peplinski, W., & Hagan E. (1990). Laboratory Investigation of Residual Liquid Organics. United States Environmental Protection Agency, EPA.600/6-90/004.

Xu, M., & Eckstein, Y. (1995). Use of Weighted Least-Squares Method in Evaluation of the

Relationship between Dispersivity and Field Scale. Ground Water, 33(6), 905-908.

https://doi.org/10.1111/j.1745-6584.1995.tb00035.x

Zheng, C., & Wang, P. P. (1999). MT3DMS: A Modular Three-Dimensional Multispecies Transport

Model for Simulation of Advection, Dispersion, and Chemical Reactions of Contaminants in

Groundwater Systems, Documentation and User's Guide. U.S. Army Engineer Research and

Development Center Cataloging-in-Publication Data, Final Report, Contract Report SERDP-

99-1.

CHAPTER 4

MODELING GROUNDWATER AND SURFACE WATER WITHIN RED BUTTE WATERSHED IN UTAH

Abstract

This study focuses on groundwater-surface water interactions within the Red Butte (RB) watershed, a part of Salt Lake Valley (SLV) of Utah, USA. The modeled area (HyperRBC) includes the entire SLC 1300 South Drainage Basin and receives all Red Butte Creek flow. For the interactions simulation, the employed MODFLOW2005 transient model deriving from an existing numerical model includes: a) newly refined groundwater discretization (cell size of 308 ft by 308 ft within seven aquifer layers) for a portion of SLV; b) relevant and updated boundary conditions and input data; and c) a Streamflow-Routing (SFR) package for representing the RBC flow. The SFR includes: i) assumed RBC domain values; ii) inflows into RBC; and iii) outflows from RBC to calibrate values of vertical hydraulic conductivity (ranged from 0.0045 to 12.26 ft/d) of the streambed. After calibration of the conductivity values, HyperRBC was used to predict unconfined aquifer storage changes due to a hypothetical GI implementation of grass swales to reduce stormwater runoff. Assumed was a total of 54.30 ac-ft GI aquifer recharge from April through June of 2016 within a 704-acre area located east of the Jordan River. The simulation predicted that by the end of a year: a) about three percent of the GI recharge remained within the unconfined aquifer in the HyperRBC area; b) 66.6% of the recharge flowed north into the continuation of the unconfined aquifer as groundwater; and c) 30.3% (11.7%, 1.3%, and 17.3%) discharged to surface waters (the JR, RBC, and connected drain to the JR respectively).

In summary, such water-supply modeling tools can guide management efforts in increasing groundwater availability for later use.

4.1. Literature review

4.1.1. Green infrastructure impacts on water resources

Green infrastructure (GI) embodies nature-based approaches to help address challenges of climate and environmental change, and food security (Caparrós-Martínez et al., 2020). Environmental change such as green-space reduction in urbanized areas could result in adverse impacts on ecosystems, and human health. GI in areas can provide ecosystem services including healthy environment, runoff reduction, and temperature management in areas (Tzoulas et al., 2007; Naumann et al., 2011). Use of GI (e.g., bioretention and bioswale) for stormwater management in urbanized areas might result in reducing and/or delaying salt loading to surface waters; however, it might allow solute (e.g., salt) to percolate through groundwater (Burgis et al., 2020). Methods for evaluating impacts of GI infiltration on shallow groundwater environments are (Zhang and Chui, 2019): a) laboratory monitoring; b) in-situ monitoring; c) numerical models being more efficient; and d) remote sensing. The infiltration would result in: i) recharging aquifer and improving sustainable groundwater availability; and ii) changing stream-aquifer seepages and their water qualities in time. Applying numerical simulations helps quantify the infiltration flowing into an aquifer, and then seeping through surface water nearby.

4.1.2. Quantifying groundwater and surface water interaction

Numerical simulation of stream-aquifer seepages can quantify impacts of applied GI recharge on water supplies. One of common three-dimensional numerical groundwater flow simulators, MODFLOW (McDonald and Harbaugh, 1988) including several surface-water features such as: a) river, RIV; b) stream, STR (Prudic, 1989); and c) Streamflow-Routing, SFR (Prudic et al., 2004; Niswonger and Prudic, 2005) can execute a groundwater-surface water model (Ou et al., 2013). The newest feature, SFR, has been applied for: 1) seepage simulation between streams and aquifers to study subsidence (Schmid et al., 2014); 2) evaluation of best management practices (BMPs) to reduce adverse environmental impacts of inefficient irrigation practices in the alluvial Lower Arkansas River Basin of Colorado (Shultz et al., 2018; Rohmat et al., 2019); and 3) simulation of surface water delivery for irrigation in Sagehen Creek watershed, California (Niswonger, 2020).

Herein, a sub-system numerical model (HyperRBC) within MODFLOW2005 was developed to simulate stream-aquifer interaction in the Red Butte (RB) watershed of Salt Lake Valley (SLV) in Utah. The model represents Red Butte Creek (RBC), and a part of the Jordan River (JR) by SFR, and RIV packages respectively. However, the USGS MODFLOW model presented RBC via recharge and drain packages (Lambert, 1995). The SFR and RIV in the developed model simulate changes of groundwater-surface water seepages resulting from percolated grass-swale recharge through the RB shallow unconfined aquifer. Also, the simulation quantifies the magnitude of the recharge stored in the aquifer.

4.2. Modeling grass swale impacts on groundwater and surface water within Red Butte watershed

4.2.1. USGS Salt Lake Valley (SLV) numerical groundwater model

4.2.1.1. SLV groundwater model

The SLV groundwater model (Lambert, 1995) represents the shallow unconfined aquifer (Layer 1) and the underlying shallow semi-confining layer, Layer 2 (Figures 4.1 and 4.2). Those two layers have spatially varying thicknesses. The SLV model uses model Layers 3-7 to represent the principal aquifer. Layer 3 (i.e., principal aquifer) covers the largest horizontal area (Figures 4.1 and 4.2). Layers 3 to 5 are each 150 ft. thick. Layer 6 is 200 ft. thick and Layer 7 ranges in thickness from 200 ft. to more than 1500 ft. The model has 94 rows, 62 columns, and a cell size of 1848 ft. by 1848 ft. After calibrating the model for assumed steady-state conditions, Lambert (1995) used simulated steady-state heads as the initial conditions for transient simulations. He performed transient calibration to 1969-91 heads using annual time periods and data. Thus, the Lambert's model needs to be updated for any recent research project such as the EPA-STAR Grant# 83582401 project.

Figure 4.1

Layers of Salt Lake Valley groundwater model (Thiros et al., 2010)
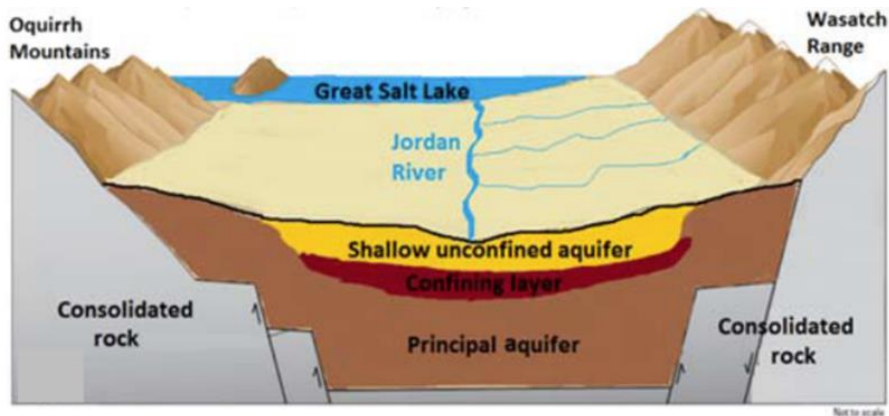
Figure 4.2

Layers 1 and 3 of Salt Lake Valley groundwater model (blue arrow shows Red Butte sub watershed)
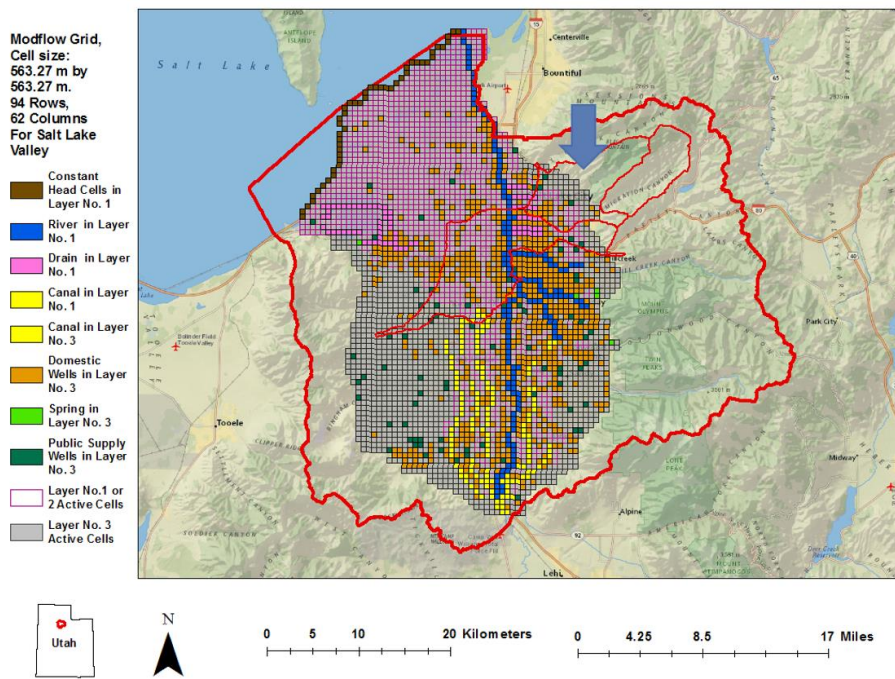
4.2.1.2. Updated model boundary conditions

Lambert (1995) provided numerical groundwater transient model of 1969 through 1991 using annual time periods and data for the entire SLV. Here,

purposes of the EPA-STAR Grant# 83582401 project are to quantify groundwater and surface water interaction within Red Butte watershed of SLV during 2009 through 2016. Thus, updating of the boundary conditions data for the EPA-STAR project was needed to develop a sub-system numerical model. In a previous study, Forghani and Peralta (2018) applied the Lambert model cell size and parameters but used monthly time periods when simulating hydrologic conditions from 1993 to 2014. Comparison of simulated and observed heads showed their model was acceptably accurate.

For the EPA-STAR project, the same procedure of updated boundary conditions data was applied to obtain the monthly data for the 2009-2016 duration. Here, the updated SLV numerical groundwater model uses the monthly data to simulate from 2009 to the end of 2016 (96 monthly stress periods). The model uses the same 1848 by 1848 ft^2 discretization as Lambert's model and assumed input values to represent the water levels in rivers and streams. But the original and updated SLV numerical models presented RBC via the MODFLOW recharge and drain packages. Thus, for RBC representation accurately, a new definition and discretization were required to include the headwaters of, inflows into, and outflows from RBC distribution network. To simulate RBC network, a sub-system numerical model within Red Butte watershed was developed to use the newest stream (Streamflow-Routing, SFR) package within MODFLOW2005.

4.2.2. Red Butte Creek (RBC) distribution network within Red Butte watershed of SLV

4.2.2.1.   RBC

Figure 4.1 visualizes RBC as one of the streams flowing westward from the Wasatch Range to the Jordan River. Near the Wasatch Front, RBC flows through and recharges the principal SLV water supply aquifer where it is unconfined. This aquifer is semiconfined near the center of the valley, where it discharges to an overlying shallow unconfined aquifer.

RBC was surveyed from the outlet of Red Butte Reservoir (RBR), the first RBC reach, through the Jordan River (JR), the last RBC, for the EPA-STAR project. The survey showed all RBC components being: a) headwaters (RBR outlet); b) inflows into RBC; c) outflows from RBC; and d) streamflow monitoring stations within the Red Butte watershed of SLV (Fig. 4.3). The provided diagram resulting from the survey helped model the RBC network within the watershed. The following subsections explain roles of the RBC components for the model.

Figure 4.3

Diagram of Red Butte Creek distribution network (not to scale)
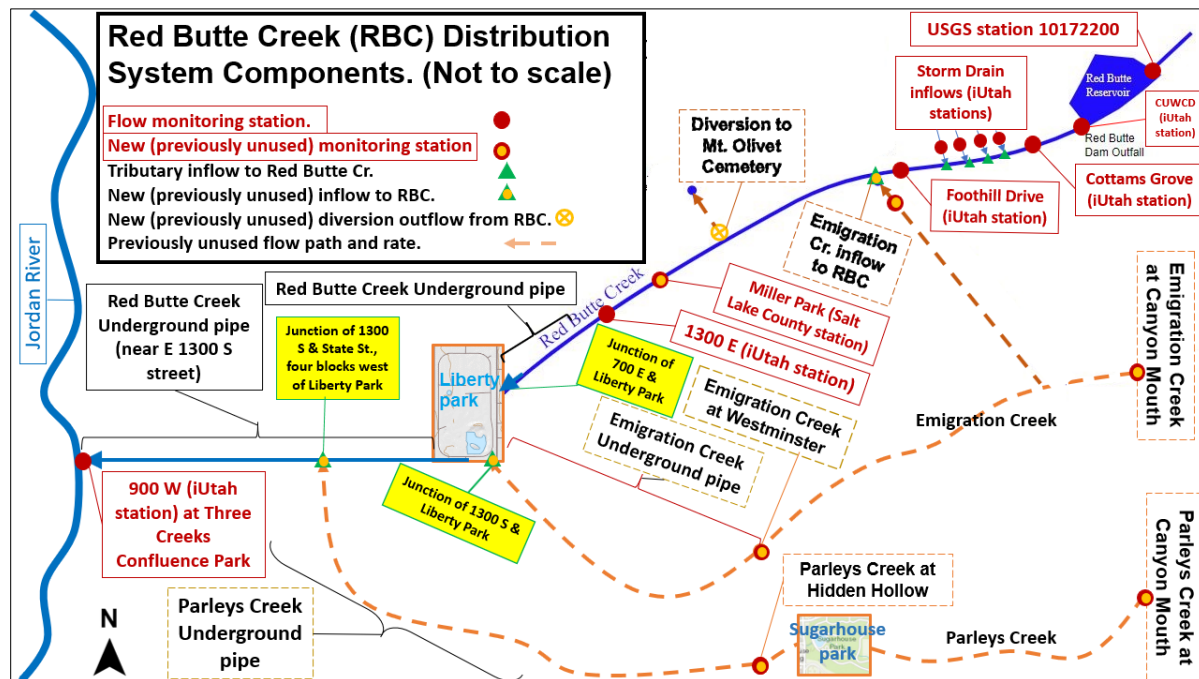
4.2.2.2.   Headwaters of RBC

First, the RBC network starts from RBR outlet (Fig. 4.3) that discharges managed RBR water as headwaters into the first RBC reach. At the RBR outlet, the iUTAH (2012) streamflow monitoring station (named as CUMCD) measures the RBR discharge (Fig. 4.3). The RBR provides a high magnitude of RBC water in time. But the RBC network gains surface water via its tributary inflows spatially and temporally.

4.2.2.3.   Tributary inflows into RBC

Second, apart from the headwaters, the network gains surface water from seven tributary inflows (Fig. 4.3) that include: a) four storm drains between Cottams Grove and Foothill Drive; b) two from Emigration Creek shortly after Foothill Drive and at Liberty Park; and c) the last from Parleys Creek at the junction of 1300 S and State streets. Each increases RBC streamflow in reference to varying runoff resulting from precipitation changes in time. However, diversion outflows deliver RBC surface water to users, or discharge it into the Jordan River (JR) of SLV.

4.2.2.4.   Diversion outflows from RBC

Third, RBC streamflow is distributed by two diversion outflows (Fig. 4.3) that are: 1) RBC outflow into Mount Olivet Cemetery (Utah Division of Water Rights, 2008) for water use during April through October; and 2) RBC discharge into the Jordan River (JR) permanently at the confluence area of RBC and the JR at 900 W. Observing and monitoring the RBC outflows can aid in managing RBC water balance for environmental protection purposes and ensure compliance with water rights regulations. This helps to gain insights into the overall water usage and availability.

4.2.2.5.   RBC streamflow monitoring stations

Fourth, six stations measure RBC streamflow (iUTAH, 2012; Salt Lake County, 2004) that helped the following calibration process. Figure 4.3 shows the stations as: 1) CUMCD at RBR outlet; 2) Cottams Grove; 3) Foothill Drive; 4) Miller Park; 5) 1300 E; and 6) 900 W. Evaluation of the streamflow shows that seepages between the aquifer and RBC result in changes of the streamflow spatially and temporally. Thus, to quantify the changes, a sub-system numerical model was developed within the Red Butte watershed of SLV.

4.2.3. Sub-system numerical groundwater (HyperRBC) model for Red Butte watershed in Utah

4.2.3.1.   HyperRBC study area and period

The EPA-STAR Grant# 83582401 project focuses on quantifying groundwater and surface water interactions within the Red Butte watershed of SLV from 2009 through 2016. The study area of the project involves the 1300 South Drainage Basin that receives RBC flow in SLV (Fig. 4.4).

The spatial discretization of the original SLV numerical groundwater model is too large for quantifying the interactions. Thus, constructing a sub-system numerical groundwater model (HyperRBC) that includes a finer discretization was required. Hydraulically, HyperRBC simulates RBC streamflow, stream-aquifer seepage, and groundwater flow. At its upstream end, the HyperRBC model uses discharge from RBR (i.e., headwater) inflow into RBC. From that location,

HyperRBC simulates flows and seepages downstream to and including a part of the Jordan River (Fig. 4.4).

Figure 4.4

HyperRBC groundwater model grid (Layer no. 3) and hatched RBC underground culvert pipe, superimposed over USGS Salt Lake Valley groundwater model grid.
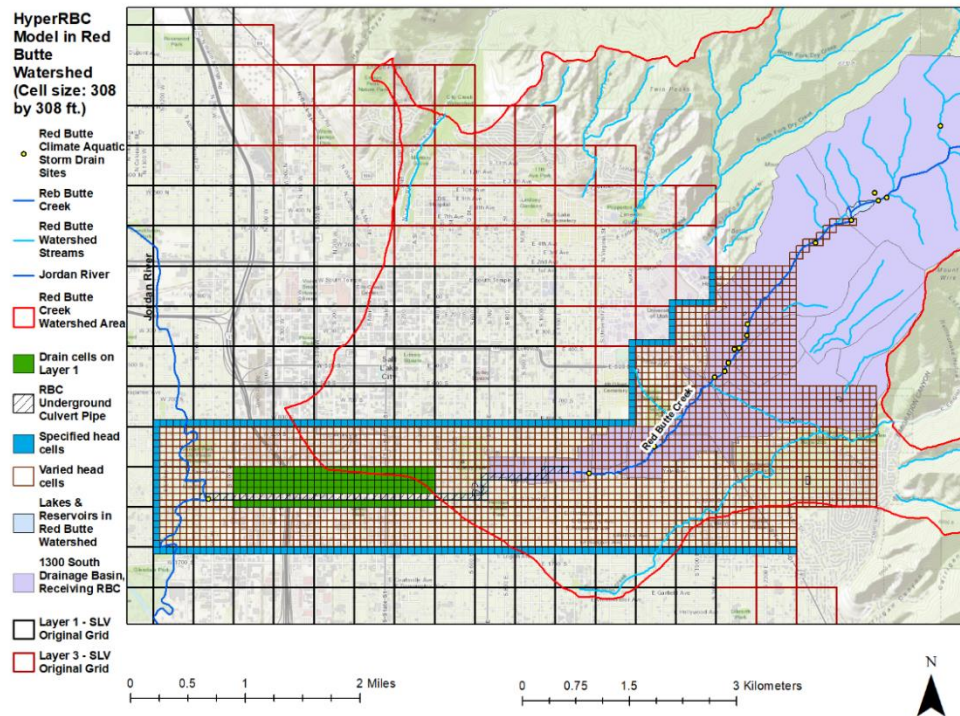
In general terms, developing the HyperRBC model involves: 1) designating a subsystem of the SLV MODFLOW groundwater flow model calibrated by the USGS (Lambert, 1995); 2) selecting a refined spatial discretization (cell size of 308 ft by 308 ft within seven aquifer layers) to increase model accuracy; 3) conceptualizing and implementing the addition of RBC features to the groundwater subsystem model; 4) obtaining available physical system data to describe the coupled aquifer and stream system; 5) identifying available and relevant boundary condition data;

and 6) calibrating the streambed vertical hydraulic conductivity values was required to simulate stream-aquifer seepages.

4.2.3.2.   Developing HyperRBC model

4.2.3.2.1.   Refined version of SLV (SLV308) numerical groundwater model

In Subsection 4.2.1.2, the updated SLV model uses the same 1848 by 1848 ft^2 discretization as Lambert's (1995) model. Because groundwater pumping data cannot be obtained with finer temporal discretization than monthly, the model used monthly discretization for most groundwater boundary conditions. However, to represent groundwater-surface water interactions with appropriate accuracy, it needed a finer spatial discretization for the model.

A refined version of the updated SLV groundwater model that has a uniform 308 ft cell side length was provided to achieve sufficient accuracy. Other than discretization, this Salt Lake Valley 308 (SLV308) groundwater model uses all the same aquifer parameter values as the original SLV groundwater model (Lambert, 1995). Six times 308 feet equals the 1848 ft side length of the original SLV MODFLOW model cells. Thirty-six of the 308 ft x 308 ft cells cover the same area as one original model cell.

SLV308 was tested to simulate the same quasi-steady-state situation as Lambert (1995) used for the SLV model. Both models simulated the water table to be above the ground surface. However, the SLV308 ponding did not occur in the part of the study area where impacts of grass swale implementation were tested on aquifer storage and stream-aquifer seepage. The simulated ponding occurred mainly in areas of high ground surface slope. SLV308 had additional ponding mainly because, although its ground surface elevations are the same as the original SLV model, SLV308 computes water table heads for each 308 x 308 cell. Hence the simulated ponding occurred most within the uphill side of SLV cell locations. The SLV308 model performed transient monthly simulations of 2009-2016 Salt Lake Valley conditions. Ultimately, it assigned transient SLV308 head values to be the time-varying specified head values in designated HyperRBC boundary specified head cells (Fig. 4.4). The defined components of RBC (Fig. 4.3) helped represent RBC network within the sub-system numerical model by using SFR package of MODFLOW2005.

4.2.3.2.2.   RBC representation via MODFLOW2005 Streamflow-Routing (SFR) package within HyperRBC model

Properly simulating RBC streamflow requires inclusion of known headwater inflows. To provide those, HyperRBC was extended from the

Salt Lake Valley (SLV) to the northeast that surrounded by boundary specified head cells within each aquifer layer (Fig. 4.4). The most northeastern HyperRBC cell encompasses the location of the outflow from RBR. That discharge is the headwater or beginning point of modeling RBC flow. All 16 of the additional northeastern cells lie in aquifer Layer 3 (Fig. 4.4). To improve the accuracy of heads and seepages computed for model simulations, a developed HyperRBC study area and model includes: a) a refined spatial discretization (cell size of 308 ft by 308 ft) within seven aquifer layers; and b) an extended area further to the south and east (i.e., the entire Salt Lake County 1300 South drainage basin) that receives RBC flow (Fig. 4.4).

Of the three rows of large USGS model cells positioned from east to west in Figure 4.4, the center row represents drain cells in the USGS model. In that model, the drain cells provide a means for shallow groundwater to leave the aquifer. Instead of using drain cells, HyperRBC uses stream cells representing RBC to discharge groundwater from the aquifer. Figures 4.4 and 4.5 show those stream cells located approximately in the center row of the USGS model grid.

Figure 4.5

HyperRBC groundwater model grid, uppermost aquifer layer specified head cells, and Parts 1-4 of RBC cells having Streamflow-Routing (SFR) reaches.
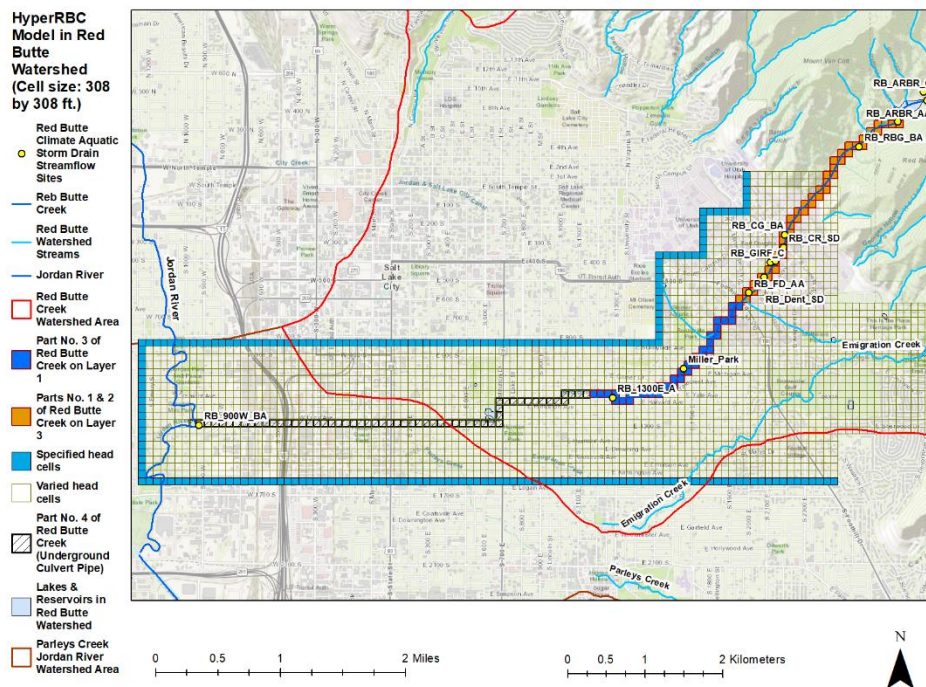
As in the USGS model (Lambert, 1995), simulated groundwater heads are above the assumed ground surface around Miller Park and Liberty Park. Around Liberty Park, water near the ground surface would contribute to the 80-acre Liberty Park Pond (Fig. 4.3). Around the Miller Park Bird Refuge and Nature Park, such water would be lost via evapotranspiration. Table 4.1 describes features of the model's 142 stream segments (and 142 stream reaches). One segment-reach represents the diversion from RBC toward Mount Olivet Cemetery. HyperRBC represents the 7.44 miles (11.97 km) of RBC from the RBR discharge location, downstream to and including the point of discharge to the Jordan River. HyperRBC represents

RBC as a rectangular channel having widths (Table 1, Column M). Column D of Table 1, and Figures 4.6a-b refer to Parts 1-4 of the modeled RBC watershed. The Parts differ in data availability, material through which the stream flows, and type of stream conduit. From the RBC headwaters location downstream to the point of RBC discharge to the Jordan River, the Parts differ as follows: 1) RBC is within aquifer model Layer 3 from RBR outflow downstream to the edge of initial USGS SLV groundwater model; 2) RBC is within aquifer model Layer 3; 3) RBC is within aquifer model Layer 1; and 4) RBC flow is within a leaky subsurface pipeline within aquifer model Layer 1 (Fig. 4.7). The 3.44 mi subsurface pipeline conveys RBC, Emigration Creek, and Parleys Creek water from Liberty Park to the Jordan River.

Table 4.1

Stream segment information for RBC within HyperRBC model; assumed streambed of 0.4 ft for entire RBC;

A	B	C	D	E	F	G	H	I	J	K	L	M
Flow or Streamflow Measurement Station modeled in HyperRBC	Modflow Segment / Reach No.	Convey-ance type	Part No.	Label	(L_R_C) of most downstream HyperRBC cell; Number of cells	Length (m)	Distance from downstream end (km)	Distance from upstream (km)	Up-stream Elev. (m)	Down-stream Elev. (m)	Manning n	Bottom Width (m)
Headwater (inflow from RBR)	1	Str.					11.969	0.000				
			1	RB_RBR_CUVCD	3_12_105; 1	57.74	11.912	0.058	1642.63	1634.67	0.1	0.6
	2-9	Str.	1		3_15_100; 8	579.80	11.332	0.638	1634.67	1609.98	0.1	0.6
	10	Str.	1	RB_RBG_BA	3_15_99; 1	105.54	11.226	0.743	1609.98	1576.33	0.1	0.6
	11-16	Str.	1		3_18_96; 5	450.49	10.776	1.194	1576.33	1572.59	0.1	0.6
	17-31	Str.	2		3_27_90; 14	1305.17	9.471	2.499	1572.59	1503.79	0.1	0.6
Cottom Grove SMS	32	Str.	2	RB_CG_BA	3_27_89; 1	69.33	9.401	2.568	1503.79	1501.61	0.1	0.6
	33	Str.	2		3_28_89; 1	94.35	9.307	2.662	1501.61	1496.34	0.09	5
Connor Road SD inflow	34	Str.	2	RB_CR_SD	3_29_89; 1	96.71	9.210	2.759	1496.34	1486.71	0.09	5
	35-36	Str.	2		3_30_88; 2	117.74	9.093	2.877	1486.71	1481.37	0.09	5
GIRF SD inflow	37	Str.	2	RB_GIRF_SD	3_31_88; 1	112.18	8.980	2.989	1481.37	1473.85	0.09	5
	38-40	Str.	2		3_33_87; 3	212.77	8.768	3.202	1473.85	1468.63	0.09	5
Fort Douglas SD inflow	41	Str.	2	RB_FortD_SD	3_33_86; 1	76.80	8.691	3.279	1468.63	1465.81	0.09	5
Dentistry SD inflow	42	Str.	2	RB_Dent_SD	3_34_86; 1	103.98	8.587	3.383	1465.81	1460.35	0.09	5
	43-44	Str.	2		3_35_85; 2	169.02	8.418	3.552	1460.35	1455.61	0.09	5
Foothill Drive SMS	45	Str.	2	RB_FD_AA	3_35_84; 1	59.39	8.358	3.611	1455.61	1453.99	0.09	5
Tributary 1: Mount Olivet Ditch inflow; spring inflow	46	Str.	2		3_36_84; 1	82.84	8.276	3.694	1453.99	1451.95	0.09	3
spring inflow	47	Str.	2		3_36_83; 1	49.77	8.226	3.744	1451.95	1449.31	0.09	3
	48-56	Str.	3		1_41_79; 8	721.06	7.505	4.465	1449.31	1425.90	0.09	3
Diversion 1: Mount Olivet Cemetery	57	Str.	3	Mount Olivet Cemetery	1_41_79;		7.505	4.465				
	58-65	Str.	3		1_46_76; 7	631.68	6.873	5.096	1425.90	1399.22	0.05	3
Miller Park SMS (near 1600 E)	66	Str.	3		1_46_75; 1	104.38	6.769	5.201	1399.22	1396.13	0.05	3
	67-79	Str.	3		1_50_66; 12	932.02	5.837	6.133	1396.13	1358.22	0.03	3.5
1300 E SMS	80	Str.	3	RB_1300E_A	1_49_66; 1	46.85	5.790	6.180	1358.22	1356.14	0.03	3.5
	81-83	Str.	3		1_49_63; 3	251.00	5.539	6.431	1356.14	1339.61	0.011	3.5
	84	UnP.	4		1_49_62; 1	93.88	5.445	6.524	1339.61	1335.16	0.011	3.5
	85-98	UnP.	4		1_51_50; 14	1314.30	4.131	7.839	1335.16	1298.66	0.011	3.5
Tributary 2: Emigration Creek inflow	99	UnP.	4	LibertyLake_in	1_52_50; 1	93.88	4.037	7.933	1298.66	1298.61	0.011	3.5
	100	UnP.	4		1_53_50; 1	93.88	3.943	8.027	1298.61	1298.46	0.07	50
	101	UnP.	4	LibertyLake_out (187 m from inlet)	1_53_49	93.88	3.849	8.120	1298.46	1297.46	0.07	50
	102-114	UnP.	4		1_53_36; 13	1220.42	2.629	9.341	1297.46	1289.86	0.011	3.5
Tributary 3: Parleys Creek inflow	115	UnP.	4	1.41 km from Liberty Park	1_53_35; 1	93.88	2.535	9.435	1289.86	1289.26	0.011	3.5
	116-140	UnP.	4		1_53_10; 25	2346.96	0.188	11.782	1289.26	1285.04	0.011	3.5
900 W SMS	141	UnP.	4	RB_900W_BA (3.8 km from Liberty outlet)	1_53_9; 1	93.88	0.094	11.876	1285.04	1285.00	0.011	3.5
Diversion 2: RBC into Jordan river (Three Creeks Confluence Park)	142	Str.	4		1_53_8; 1	93.88	0.00	11.969	1285.00	1284.97	0.011	3.5

Abbreviations: RB=Red Butte Creek; RBR=Red Butte Reservoir; SMS=Streamflow Measurement Station;   Total length (m)   11,969
Str.=stream; SD=storm drain; UnP = underground pipe;   Total length (km)   11.97
Cr.=creek.   Total length (miles)   7.44

Figure 4.6

Portions of RBC modeled in HyperRBC from the headwaters downstream to discharge to Jordan River. a. Highlighting Parts 1 to 3 as: (Part 1) streambed within HyperRBC aquifer model Layer 3 from Red Butte Reservoir outflow to edge of initial USGS Salt Lake Valley groundwater model; (Part 2) in streambed within aquifer model Layer 3; (Part 3) in streambed within aquifer model Layer 1. b. Full extent of Red Butte Creek Part 4 where RBC flow is within a leaky subsurface pipeline within aquifer model Layer 1.

a.
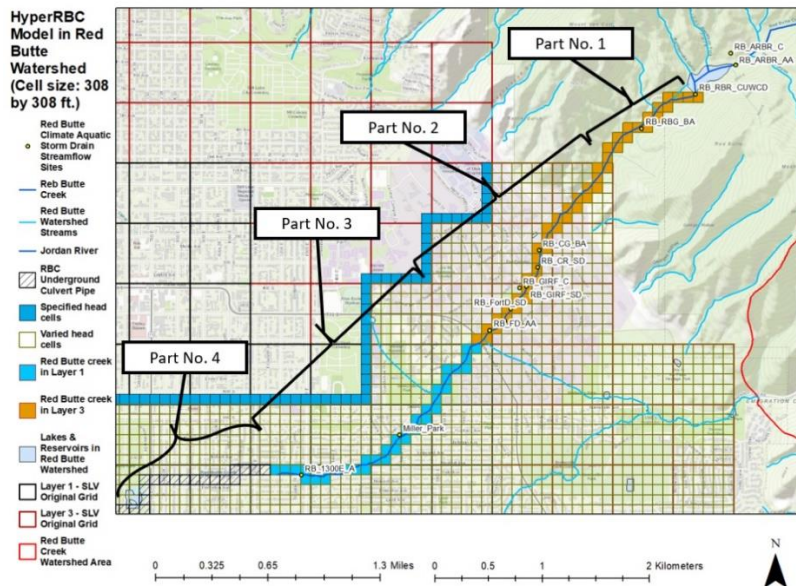
b.
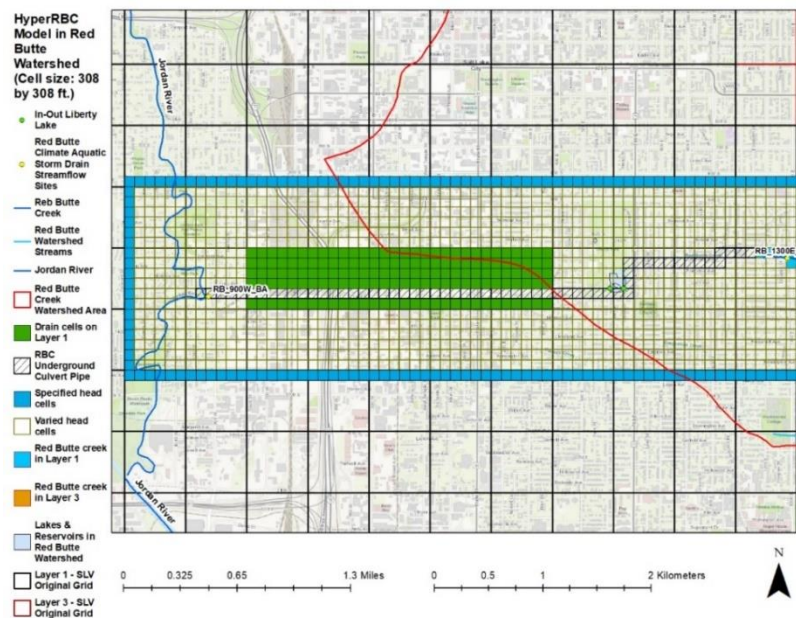
Figure 4.7

Red Butte Creek cells, drain cells and Jordan River cells within Layer no. 1 of HyperRBC model
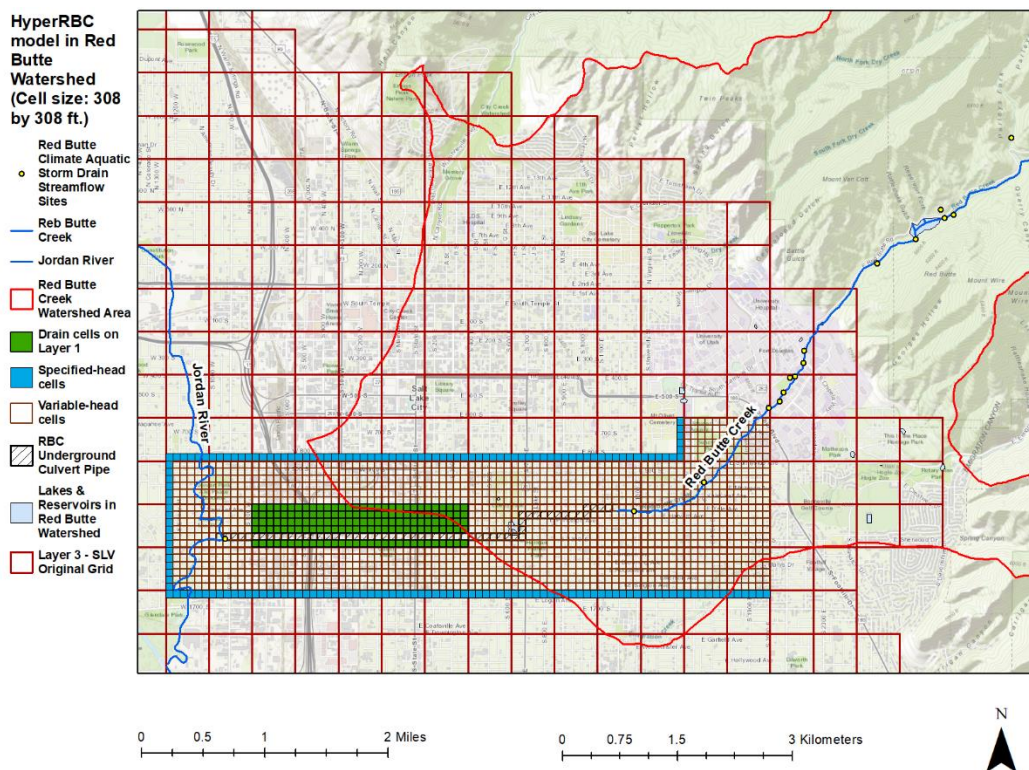
MODFLOW2005 SFR package represents RBC within HyperRBC. The SFR package simulates steady or transient stream flows, heads, and stream-aquifer seepage. The seepage rate in each cell depends upon the aquifer head, stream stage, stream bottom elevation, and the vertical hydraulic conductivity of the streambed. Here, SFR used the Manning equation to simulate surface water flow. The aquifer heads come from a simultaneous solution of the MODFLOW2005 groundwater flow equations.

To simulate stream-aquifer seepages, SFR requires values of the vertical hydraulic conductivity of the streambed along RBC. These need a

calibration process to estimate. The process requires values of each RBC component for SFR in the HyperRBC model, both spatially and temporally.

4.2.3.2.3. Available and estimated data for RBC components

Some data of the RBC inflows and outflows has been measured spatially and temporally. For data needed, the available downstream flow divided by upstream flow as the proportion was defined to help estimate such flows. Also, simulating stream-aquifer seepage uses values of such flows and the vertical hydraulic conductivity of the streambed along RBC. Here, the calibration process can help estimate the values of the conductivities. To execute the process, the required RBC components are:

- one headwater (RBR outflow);

- one diversion (Mt. Olivet Cemetery);

- seven tributaries (four storm drains, Mt. Olivet Ditch conveying Emigration Creek water, Emigration Creek at Liberty Park, Parleys Creek at the junction of 1300 S and State St.);

- five locations, where, during the calibration, stream flows of HyperRBC are matched to observed values (Cottams Grove, Foothill Drive, Miller Park, 1300 East, and 900 West).

Although the locations of the additional flows are known, the actual flowrate values are not. For the above data locations, Figure 4.8

summarizes those periods for which daily or monthly flow rates are available. Because not all locations have data for May and June 2016, tributary and diversion values were estimated for those periods. For example, Emigration Creek inflow rates to RBC via Mount Olivet Ditch are available only for 2014. Thus, 2014 proportions were used to estimate 2016 inflows to RBC. For instance, $SFP_{MOD,m} = (Q_{MOD,m}/Q_{CMEC,m})$: where m = month 1, 2,...,12; $SFP_{MOD,m}$ = Streamflow Proportion at Mount Olivet Ditch for month m; $Q_{MOD,m}$ = Mount Olivet Ditch discharge into RBC during month m of 2014; and $Q_{CMEC,m}$ = streamflow at Canyon Mouth of Emigration Creek in month m of 2014. The $SFP_{MOD,m}$ values for June through September 2014 are 0.0102, 0.0035, 0.0527, and 0.0296 respectively. Those proportions were used to estimate 2016 inflows into Red Butte Creek via Mount Olivet Ditch for calibration. Table 4.2, and Tables B.2 to B.9 in Appendix B show these proportions and other values used to estimate diversion outflow from RBC and tributary inflows into RBC in May and June 2016.

Figure 4.8

Station monitoring flow within, toward, and from Red Butte Creek and flow data available online as of Oct. 6, 2020.

1) **Monitoring stations within streams**
   - ✓ Red Butte Creek:
     1) **USGS 10172200** (**inflow into Red Butte Reservoir**), 2009-2020 data is on-line;
     2) **CUWCD** (**outflow from Red Butte Reservoir into RBC**, iUtah station), no data on-line, but previously available and downloaded was data of 2014-2017;
     3) **Cottams Grove** (iUtah station), 2013-2019 data is on-line;
     4) **Foothill Drive** (iUtah station), 2013-2019 data is on-line;
     5) **Miller Park** (around 1600 E, Salt Lake County station), 2009-2019 data is on-line;
     6) **1300 E** (iUtah station): no data on-line; but previously available was data of May 15-16 and June 13-14, 2016;
     7) **900 W** located at **Three Creeks Confluence park** (iUtah station), no data on-line, but previously available and downloaded was data of 2015-2017;
   - ✓ Emigration Creek:
     1) **Emigration Creek** at **Canyon mouth** (Salt Lake County website), 2009-2020 data is on-line;
     2) **Emigration Creek** at **Westminster** (Salt Lake County website), 2018-2020 data is on-line;
   - ✓ Parleys Creek:
     1) **Parleys Creek** at **Canyon mouth** (Salt Lake County website), 2009-2020 data is on-line;
     2) **Parleys Creek** at **Hidden Hollow** (Salt Lake County website), 2019-2020 data is on-line;
2) **Downstream flows into or** toward Red Butte Creek:
   - ✓ **Four storm drains** to RBC (Conner Road, GIRF, Fort Douglas & Dentistry in iUtah website), no data on-line, but previously available and downloaded was data of 2015-2017;
   - ✓ **Emigration Creek** enters RBC via **Mount Olivet Ditch** (by Foothill Drive), 2014 data is on-line;
   - ✓ **Emigration Creek at Westminster** (flows by underground pipe into RBC at **Liberty Park),** 2018-2020 data is on-line;
   - ✓ **Parleys Creek** at **Hidden Hollow** (flows by underground pipe into RBC about **four blocks west of Liberty Park),** 2019-2020 data is on-line;
3) **Diversions from Red Butte Creek:**
   - ✓ RBC discharges toward Mount Olivet Cemetery (Utah Water Rights website),2014 data on-line.

Table 4.2

Diversion (Div) from RBC, and stream flow proportions used to estimate tributary inflows into RBC

For month m, Diversion to Mount Olivet Cemetery (MO), Tributary to RBC, or the proportion of flow x, that flow y equals (SFP$_{y,x,m}$); or(cfs)	Month m	Jan. 1	Feb. 2	Mar. 3	Apr. 4	May 5	Jun. 6	Jul. 7	Aug. 8	Sep. 9	Oct. 10	Nov. 11	Dec. 12
Div$_{MO,m}$ (cfs)		0	0	0	1.36	1.27	0.52	0.28	0.58	0.74	0.19	0	0
SFP$_{ORBR,IRBR,m}$	Min.	1.20	0.76	0.39	0.84	0.80	0.78	0.81	0.86	0.83	0.40	0.46	0.43
SFP$_{ORBR,IRBR,m}$	Avg.	1.25	1.02	0.91	0.91	0.89	0.90	0.97	1.16	0.95	0.73	0.77	0.70
SFP$_{ORBR,IRBR,m}$	Max.	1.30	1.18	1.17	0.97	0.97	0.97	1.10	1.41	1.16	0.93	1.08	1.02
SFP$_{MOD,CMEC,m}$	-	0	0	0	0	0	0.0102	0.0035	0.0527	0.0296	0	0	0
SFP$_{WM,CMEC,m}$	Min.	2.88	4.18	1.36	1.04	1.27	1.22	0.31	0	0	6.77	4.12	3.19
SFP$_{WM,CMEC,m}$	Avg.	4.73	4.72	1.87	1.12	1.34	1.71	1.87	4.85	7.97	23.65	5.48	3.80
SFP$_{WM,CMEC,m}$	Max.	6.59	5.27	2.37	1.21	1.4	2.2	3.43	12.63	15.93	40.54	6.85	4.41
SFP$_{HH,CMPC,m}$	Min.	0.58	0.62	0.43	1.16	0.48	0.85	0.71	0.21	0.23	0.22	0.31	0.42
SFP$_{HH,CMPC,m}$	Avg.	0.58	0.62	0.43	1.16	0.48	0.85	0.78	0.46	0.33	0.22	0.31	0.42
SFP$_{HH,CMPC,m}$	Max.	0.58	0.62	0.43	1.16	0.48	0.85	0.85	0.71	0.43	0.22	0.31	0.42

Notes. ORBR = Outflow from Red Butte Reservoir; IRBR = Inflow into Red Butte Reservoir (Table B.1 in Appendix B); MO = diversion to Mount Olivet Cemetery; MOD = flow in Mount Olivet Ditch; CMEC = flow at Canyon Mouth of Emigration Canyon; WM = flow at Westminster; HH = flow at Hidden Hollow; CMPC = flow at Canyon Mouth of Parleys Canyon.

Computed SFP values were used to prepare the assumed tributary May and June 2016 inflows shown in columns 4a and 5a of Table 4.3. Columns 4a and 5a also show assumed inflow from previously undocumented springs above Foothill Drive and assumed diversion rates. Columns 4b and 5b show the measured stream flows. If confidence was high in the values derived from Table 4.2, during HyperRBC calibration all the measured flowrates in Columns 4b and 5b of Table 4.3 would have matched. Unfortunately, downstream of Foothill Drive, the assumed inflows via Mt.

Olivet Ditch and groundwater springs, and diversion to Mount Olivet
Cemetery prevented reasonable results. Hence, below Foothill Drive, only
June stream flows were used when calibrating the RBC streambed vertical
hydraulic conductivity within the HyperRBC model.

Table 4.3

RBC flow monitoring locations used to calibrate vertical hydraulic conductivity values of the RBC streambed

(1)	(2)	(3)	(4a)	(4b)	(5a)	(5b)	(6)
Streamflow Monitoring station	Distance down-stream from Red Butte Reservoir (ft.)	Headwater, tributary, inflow, or diversion name	May 15-16, 2016 inflow (+) to or outflow (-) from RBC (cfs)	May 15-16, 2016 measured streamflow (cfs)	June 13-14, 2016 inflow (+) to or outflow (-) from RBC (cfs)	June 13-14, 2016 measured streamflow (cfs)	Considerations for flow estimates
Headwater (outflow from Red Butte Reservoir)	0.00	Headwater (outflow from Red Butte Reservoir)	4.374	4.374	1.799	1.799	
Cottams Grove	8,425.43			3.495		1.151	
		Conner Road Storm Drain	0.373		0.442		
		GIRF Storm Drain	0.005		0.016		
		Fort Douglas Storm Drain	0.020		0.017		
		Dentisty Storm Drain	0.092		0.157		
		Assumed groundwater springs	0.850		0.060		Partitioned between 2 reaches above Foothill Drive
Foothill Drive	11,847.17			4.438		1.700	
		Mount Olivet Ditch	0.000		0.045		SFP for May and June = 0 & 0.0102 respectively; Canyon-Mouth streamflow on June 13-14, 2016 = 4.41 cfs; Thus, Mount Olivet Ditch inflow = 0.0102 × 4.41 = 0.045 cfs
		Groundwater springs	0.371		0.706		Partitioned between two reaches below Foothill Drive
		Mount Olivet Cemetery Diversion	-1.270		-0.520		Monthly Mean values of May (1.27 cfs) and June (0.52 cfs) in 2014
Miller Park (near 1600 E)	17,062.82			0.015		1.175	
1300 E	20,274.35			0.627		1.339	
		Emigration Creek at Liberty Park	10.61		7.54		Min., Avg. & Max. of SFP for May = 1.27, 1.34 & 1.4 and for June = 1.22, 1.71 & 2.2; Canyon-Mouth streamflow on May 15-16, 2016 = 7.92 cfs, and on June 13-14, 2016 = 4.41 cfs; Thus, Westminster streamflow = = (1.27 or 1.34 or 1.4) × 7.92 = 10.05 or 10.61 or 11.08 cfs in May, and (1.22 or 1.71 or 2.2) × 4.41 = 5.38 or 7.54 or 9.7 cfs in June.
		Parleys Creek at Junction of 1300 S & State St., four blocks west of Liberty park	3.06		4.22		SFP for May & June = 0.48 & 0.85 (Min., Avg. & Min. of SFP are equal); Canyon-Mouth streamflow on May 13-14 and June 13-14, 2016 = 6.37 & 4.97 cfs; Thus, Hidden Hollow streamflow = 0.48 × 6.37 = 3.06 cfs in May, & 0.85 × 4.97 = 4.22 cfs in June
900 W	38,961.84			14.294		12.397	

Notes. Except for spring flow, Columns 4a,b and 5a,b do not include stream-aquifer seepage.
RBC=Red Butte Creek. Assumed RBC streambed thickness = 0.4 ft.
Vertical hydraulic conductivity of streambed is calibrated using numerical groundwater flow model (MODFLOW 2005),
and parameter estimation software (PEST 17.1).

4.2.3.3. Calibration of vertical hydraulic conductivity of RBC streambed within SFR

Calibration of the vertical hydraulic conductivity of RBC streambed used: a) HyperRBC's MODFLOW2005-SFR model; b) parallel processing; and c) the parameter estimation software (PEST 17.1).

Executed steps for the calibration process were: a) the use of monthly average values of boundary conditions data in the HyperRBC 2009-2016 model; b) the use of periods of May 15-16 and June 13-14 of 2016 for matching the RBC measured streamflow with the RBC simulated (Table 4.3); c) the use of two short-time (i.e., two days) HyperRBC transient models: HyperRBC May 15-16 that includes a transient stress period, and HyperRBC June 13-14 that has a transient stress period as well; and d) the use of a developed parallel processing code of C# programming language after preliminary PEST trials to: d1) provide hundreds input-file sets for PEST and MODFLOW2005; d2) calculate statistical indices such as mean error (ME), root mean square error (RMSE), correlation coefficient (r), R^2 measure of fit, and scatter index (SI); and d3) provide suitable output files containing selected optimal calibration results.

For the Cottams Grove (CG) and Foothill Drive (FD) monitoring locations, two models (HyperRBC 15-16 May and 13-14 June) were used simultaneously to calibrate one set of vertical hydraulic conductivity ($K_{vertical}$) streambed values. In other words, calibration automatically adjusted the streambed $K_{vertical}$ values to

cause simulated MODFLOW2005-SFR steady-state RBC streamflow values to simultaneously match the observed average RBC flows of 15-16 May 2016 and of 13-14 June 2016 at CG, and FD. Because data downstream of FD for May 2016 were not available, observed May stream flows downstream of FD were not used in the calibration effort. Below FD (at Miller Park, 1300 East and 900 West), simulated and observed 13-14 June 2016 values were used for model calibration (Figures 4.6a-b).

In Table 4.4, Column 3 repeats the target June RBC flowrates that calibration tried to match. Column 5 shows the number of stream reaches (segments) between streamflow monitoring locations. Vertical streambed hydraulic conductivity was allowed to vary with segment location as the underlying horizontal aquifer hydraulic conductivity varied. Column 4 shows that between two adjacent RBC monitoring locations, one to four different vertical streambed conductivity values were used. Column 4 reports the calibrated vertical streambed conductivities that provided the least error in simulated stream flows. The highest 12.26 (ft/d) vertical streambed conductivity occurred in locations where the aquifer horizontal conductivity was 33.29 ft/d.

Table 4.4

Observed and Simulated RBC streamflow, and streambed vertical hydraulic conductivity values at the five monitoring locations

(1)	(2)	(3)	(4)	(5)	(6)
Observed & Simulated streamflow values	Distance from Red Butte Reservoir (upstream) in ft.	Observed Streamflow in cfs at Monitoring locations of iUtah & Salt Lake County	Calibrated vertical hydraulic conductivity (K_v)* of Streambed (ft/d)	Number of Reaches	Simulated Streamflow in cfs
Date / Monitoring Locations		Avg. of June 13-14, 2016			June, 2016
Headwater	0	1.799	2.608, 1.036, & 6.635	32	1.799
Cottams Grove	8425.43	1.151			1.305
Foothill Drive	11847.17	1.700	0.992, & 0.050	13	1.725
Miller Park (around 1600 E)	17062.82	1.175	12.260, & 0.027	20	1.175
1300 E	20274.35	1.339	0.018	14	1.339
900 W	38961.84	12.397	0.2725, 4.215, 0.00528, & 0.0045	61	12.397

*- *Note.* Table B.10 in Appendix B shows the K_v values of RBC segments/reaches.

Table 4.5 shows the results of comparing measured stream flows with flows computed by calibrated HyperRBC. The first two rows of Table 4.5 report statistics for May and June 2016 together for just one station. Because of missing May data, the third row reports only June statistics for the three other monitoring locations. The bottom row reports the June 2016 statistics of flows at all five RBC locations, from CG through 900 West. These values, -0.036 cfs Mean Error (ME), 0.070 cfs Root Mean Square Error (RMSE), and 0.9998 R^2, are the most complete calibration statistics used in subsequent HyperRBC model.

Table 4.5

Statistical indices of calibrated HyperRBC-computed flows compared with measured May and June 2016 flows

Statistical index \ Streamflow station	Mean Error, ME (cfs)	Root Mean Squared Error, RMSE (cfs)	R^2	Data used simultaneously for calibration
Cottams Grove	-0.023	0.133	1.000	May & June, 2016
Cottams Grove to Foothill Drive	-0.012	0.095	0.9977	May & June, 2016
Cottams Grove to Miller Park	-0.060	0.090	0.9303	June, 2016
Cottams Grove to 1300 E	-0.045	0.078	0.9154	June, 2016
Cottams Grove to 900 West	-0.036	0.070	0.9998	June, 2016

Here, the calibration process shows values of the RBC vertical hydraulic conductivities that are applicable for monthly RBC simulation in the HyperRBC 2009-2016 numerical model. The purposes of preparing the HyperRBC model are to investigate groundwater and surface water interactions. For the investigation, impacts of applied grass swale infiltration that percolates and reaches the shallow water table were evaluated. The impacts include time series monthly changes in stored groundwater, and aquifer seepage to the Jordan River (JR), and to the JR and RBC simultaneously.

4.2.4. Grass swale impacts on SLV groundwater and surface water

4.2.4.1. Infiltration and percolation from grass swale into SLV groundwater

Infiltrating and percolating rainfall from applied grass swale that includes a density of 120 ft/ac into aquifer of a residential area, Site 5 (Chapter-3 area;

Zhang and Peralta, 2019) can affect the SLV groundwater and surface water interactions. For groundwater recharge, WinSLAMM software (PV and Associates, 2015) helped simulate 2016 April-June runoff values (injection water) resulting from rainfall and the grass-swale application. Then, the calculated proportion of the grass-swale infiltration from the Zhang and Peralta's (2019) study helped estimate the infiltration rates during April through June of 2016 (Table 4.6).

Table 4.6

Runoff and infiltration volumes of 120-ft/ac grass swale during April through June of 2016 in Site 5

Date (Month, Year)	Rainfall (inch)	Site-5 area in acre	Site-5 area in ft^2	Volume of rainfall for Site 5 in ft³	Volume of infiltration for Site 5 in ft³	Proportion of Infiltration for Site 5	Volume of runoff for Site 5 in ft³	Proportion of runoff for Site 5
April, 2016	1.4	15.271	665204.76	77607.19	21437.68	0.276	27931.63	0.360
May, 2016	1.65	15.271	665204.76	91465.62	24770.14	0.271	31158.18	0.341
June, 2016	0.54	15.271	665204.76	29934.20	5205.44	0.174	7345.27	0.245
Total	3.59							

To enable grass swale simulation, changes to HyperRBC, included: a) extending the HyperRBC boundary conditions of December 2016 (except for the SFR boundary conditions) to the end of March 2017; and b) adding the Table 4.7 rates of aquifer recharge to the 323 cells shown in Figure 4.9 (17 rows x 19 columns or a 704-acre area), around RBC and east of the Jordan River. Note, the selected area did not include any recharge in the USGS SLV (Lambert, 1995) and HyperRBC groundwater numerical models.

Table 4.7

Runoff and infiltration rates of 120-ft/ac grass swale during April through June of 2016 in Site 5

Date (Month, Year)	Rainfall (inch)	Infiltration rate in ft/s	Infiltration rate in ft/d	Runoff rate in ft/s	Runoff rate in ft/d
April, 2016	1.4	1.243E-08	0.001074	1.62E-08	0.001400
May, 2016	1.65	1.39E-08	0.001201	1.807E-08	0.001561
June, 2016	0.54	3.019E-09	0.000261	4.26E-09	0.000368

Figure 4.9

The 323 selected cells (shaded area) for the grass swale recharge into Layer no. 1 (top layer) of HyperRBC during April-June 2016
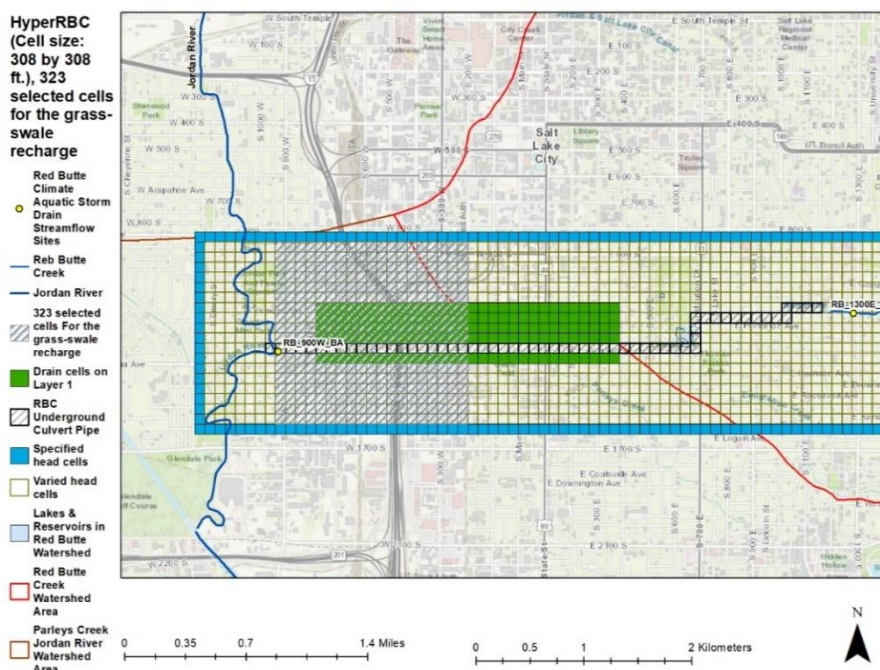
The grass swale recharge into the aquifer can change: a) stored groundwater; b) aquifer seepage to the JR; or c) aquifer seepage to the JR and RBC simultaneously.

For quantifying time-series changes of induced aquifer storage and seepage into the JR only, the HyperRBC model simulated the recharge in absence of RBC (SFR package).

4.2.4.2.   Seepage between SLV aquifer, and the Jordan River

Simulating seepages between the SLV aquifer and the JR did not need to include RBC (SFR package) in the HyperRBC model. The simulation required: a) extending the HyperRBC to the end of March 2017; and b) adding the Table 4.7 rates as the aquifer recharge to the selected area. HyperRBC simulated: i) changes of cumulative volumes (Fig. 4.10); and ii) total volumes by the end of March 2017 (Table 4.8), and flow rates (Fig. 4.11) during April 2016 through March 2017. Figures 4.10 and 4.11 present the stored volume and flowrate of the recharge in the unconfined aquifer by negative magnitudes. The 54.30 ac-ft recharge increased about 11.9% of seepage volume from SLV aquifer to the JR within a year directly. However, the aquifer stored 3.0% of the recharge within a year (Table 4.8). Obviously, a high percentage of the recharge flowed north into the continuation of the unconfined aquifer as groundwater (Table 4.8). That results from the south-north groundwater flow path following the groundwater hydraulic gradient in SLV (Lambert, 1995).

Figure 4.10

Simulated cumulative changes of seepage volumes to drain, to Jordan River, and aquifer storage volume of Layer 1 between the HyperRBC model with and without the grass swale.
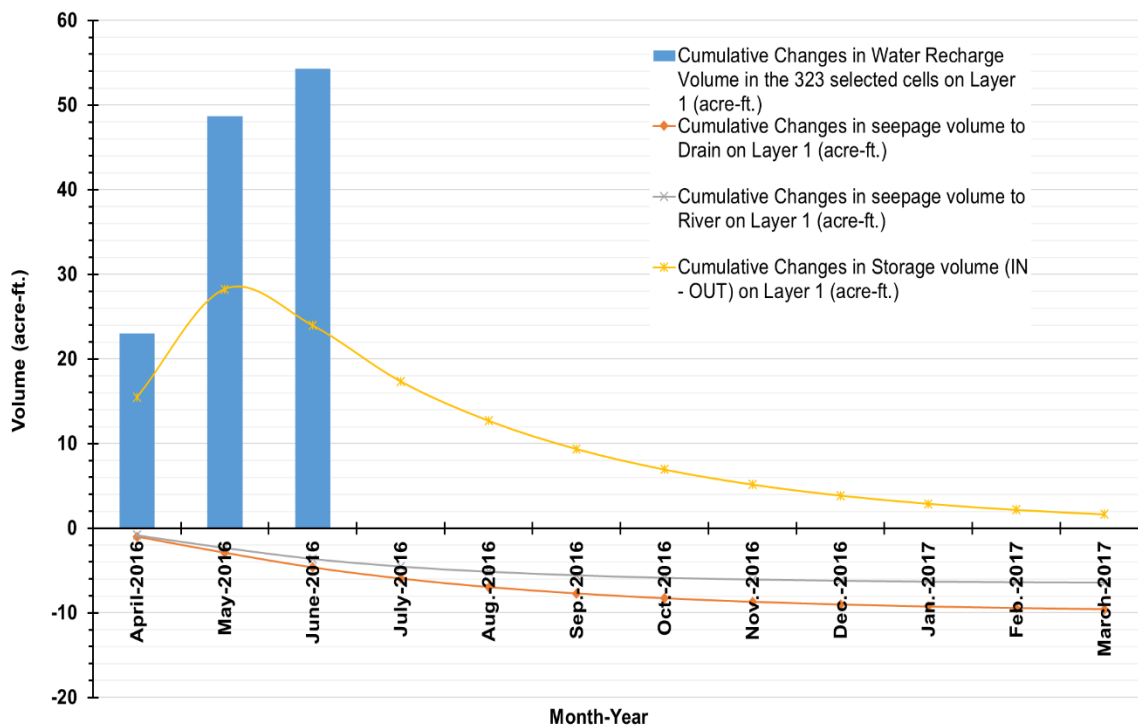
Table 4.8

Simulated total volumetric changes by end of March 2017 between the HyperRBC model with and without the grass swale

Simulated total volumetric changes	Simulated recharge	Volume (acre-ft.)	% of total recharge change	Water resource volume (acre-ft.)	% of total water resource recharge change
Applied recharge to regional unconfined aquifer		54.30	100.0%	54.30	100.0%
Groundwater	stored in regional unconfined aquifer	1.64	3.0%	38.19	70.3%
	departed from modeled area	36.55	67.3%		
Surface waters	flowed through River	6.44	11.9%	16.02	29.5%
	flowed through Drain that is connected to River	9.58	17.6%		

Note. negligible difference in volume and percent between total simulated recharge changes and the applied recharge into the aquifer results from numerical error in the model.

Figure 4.11

Simulated changes in water recharge, seepage, and storage rates on Layer 1 between the HyperRBC model with and without the grass swale
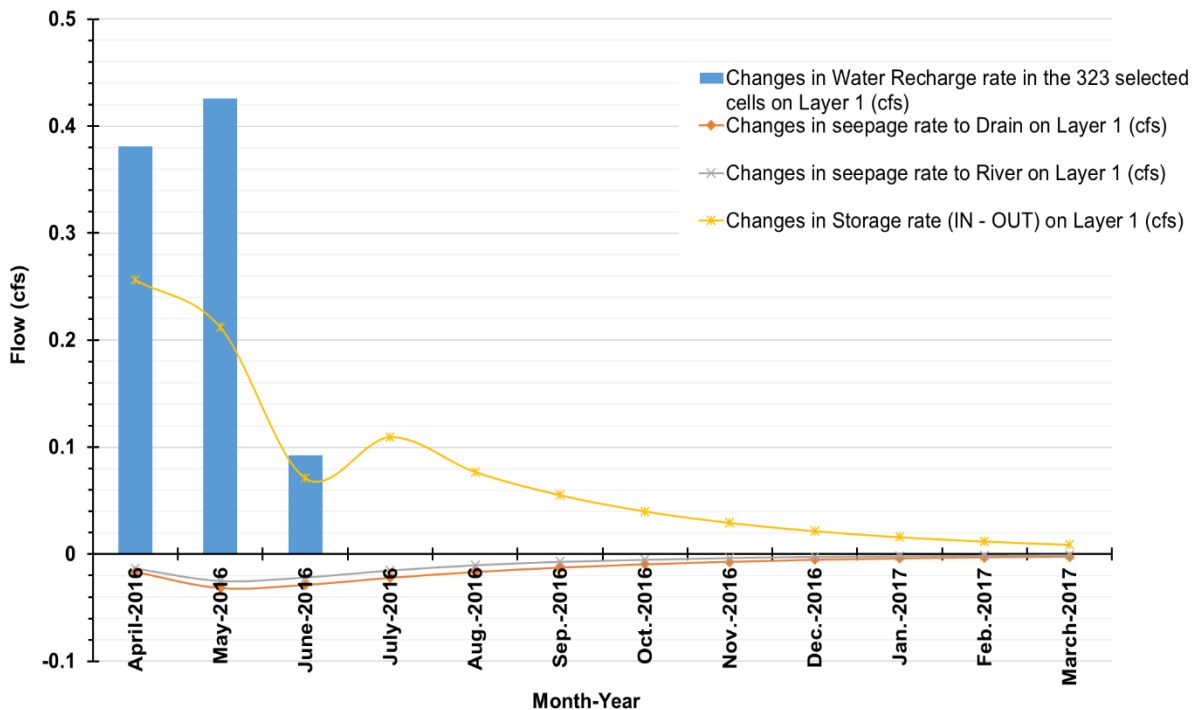
Simulation of RBC seepage changes resulting from the recharge needs SFR implement in the HyperRBC model. The simulation can show the time-series changes of induced aquifer storage, and seepages into both surface waters nearby (RBC, and the JR).

4.2.4.3.   Seepage between SLV aquifer, RBC, and the JR

The HyperRBC model quantifies impacts of the grass swale recharge (54.30 ac-ft) on groundwater and boundary conditions nearby. The recharge changes seepages between the SLV aquifer and other boundary conditions such as RBC

and the JR. Here, RBC gains 1.3% of the recharge volume within the HyperRBC

model simulation. The 1.3% is about 0.69 ac-ft (Fig. 4.12, and Table 4.9) that

results from RBC seepage rates from 0.0011 to 0.0002 cfs (Fig. 4.13) within a

year. The high percentage of the recharge flowed north into the continuation of

the unconfined aquifer as groundwater (Table 4.9) following the groundwater

hydraulic gradient in SLV (Lambert, 1995).

Figure 4.12

*Simulated cumulative changes of seepage volumes to stream of Layers 1 and 3, to drain, Jordan
River, and aquifer storage volume of Layer 1, between the HyperRBC model with and without the
grass swale*
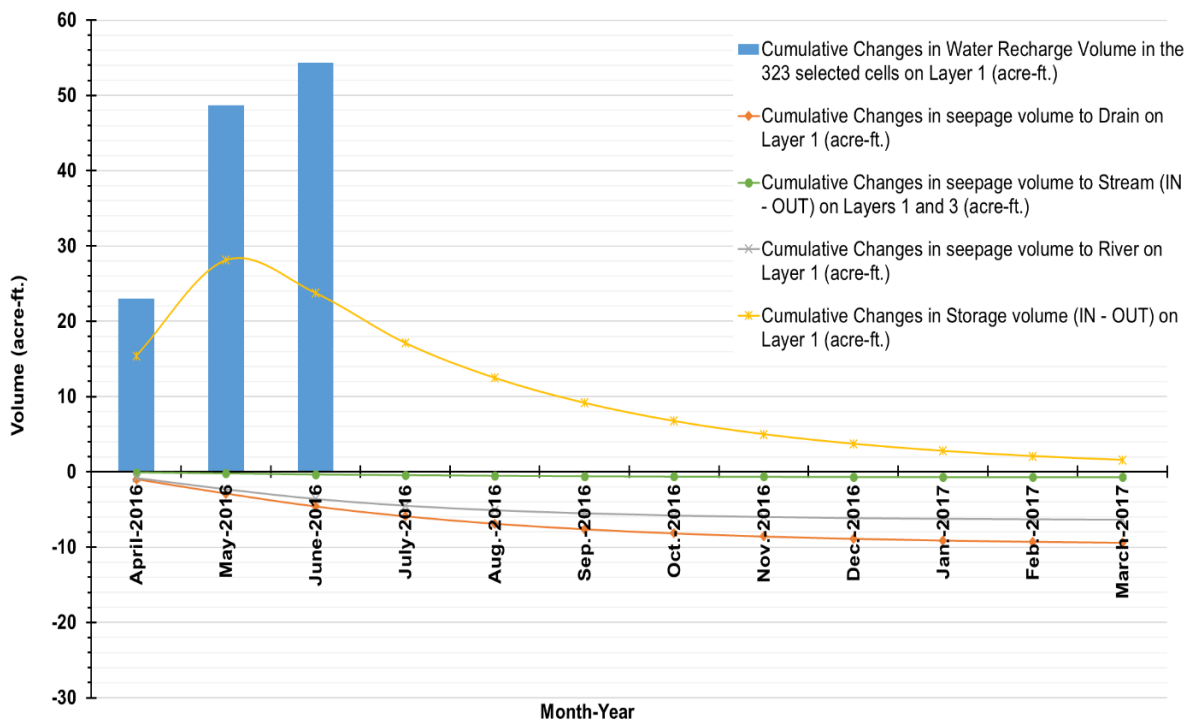
Table 4.9

Simulated total volumetric changes by end of March 2017 between the HyperRBC model with and without the grass swale

Simulated total volumetric changes	Simulated recharge	Volume (acre-ft.)	% of total recharge change	Water resource volume (acre-ft.)	% of total water resource recharge change
Applied recharge to regional unconfined aquifer		54.30	100.0%	54.30	100.0%
Groundwater	stored in regional unconfined aquifer	1.57	2.9%	37.75	69.5%
	departed from modeled area	36.18	66.6%		
Surface waters	flowed through Stream	0.69	1.3%	16.45	30.3%
	flowed through River	6.36	11.7%		
	flowed through Drain that is connected to River	9.40	17.3%		

Note. negligible difference in volume and percent between total simulated recharge changes and the applied recharge into the aquifer results from numerical error in the model.

Figure 4.13

Simulated changes in water recharge, seepage, and storage rates between the HyperRBC model with and without the grass swale
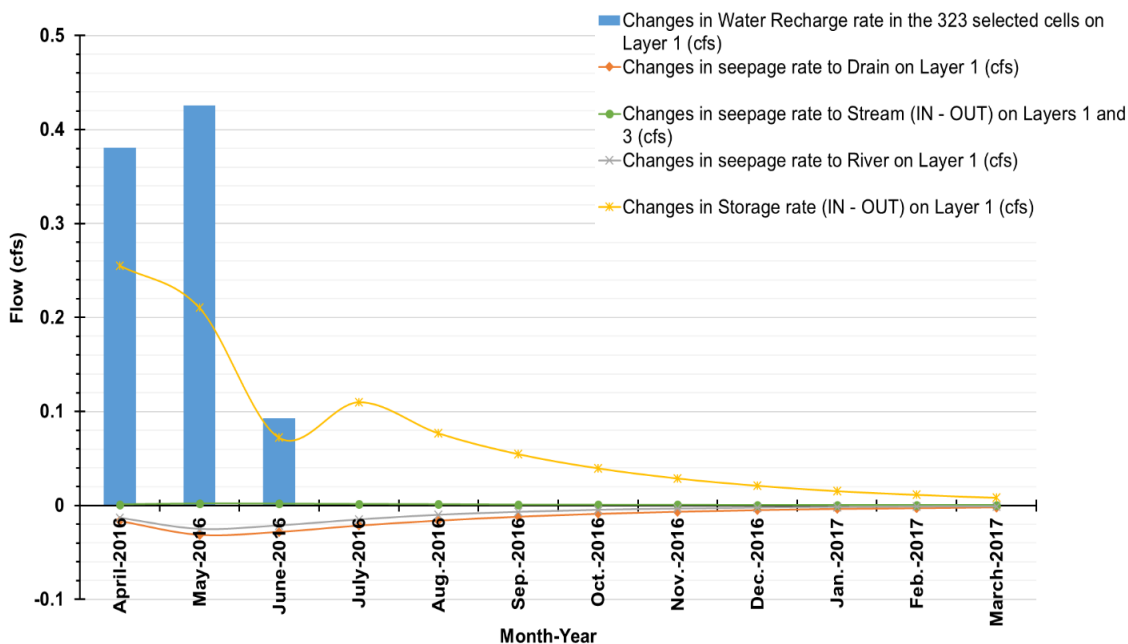
4.3.   Conclusions

Seepage-change simulation between groundwater and surface water can help manage water supply for use. Herein, a MODFLOW2005 stream-aquifer implementation is for the Salt Lake County 1300 South Drainage Basin in Utah. That derived from the existing Salt Lake Valley (SLV) multilayer groundwater model including only the Red Butte watershed. The HyperRBC sub-system model differs from the valley-wide model by using: a) a refined discretization (cell size of 308 ft by 308 ft within seven aquifer layers); and b) the Streamflow-Routing (SFR) package to simulate Red Butte Creek (RBC) flow from 2009 to 2016 monthly. The SFR includes: i) assumed RBC domain values; ii) inflows into RBC; and iii) outflows from RBC to calibrate values of vertical hydraulic conductivity (ranged from 0.0045 to 12.26 ft/d) of the streambed. HyperRBC was used to predict unconfined aquifer storage changes. They result from a hypothetical green-infrastructure (GI) implementation of grass swales to reduce stormwater runoff. Assumed was 54.30 ac-ft GI recharge in the aquifer from April to June of 2016 within a 704-acre area east of the Jordan river (JR). Simulation predicted that by the end of a year: a) about three percent of the recharge remained within the unconfined aquifer in the HyperRBC area; b) 66.6% of the recharge flowed north into the continuation of the unconfined aquifer as groundwater following the groundwater hydraulic gradient in SLV; and c) 30.3% discharged to surface waters (11.7% to the JR, 1.3% to RBC, and 17.3% to a drain connected to the JR).

In short, groundwater and surface water modeling can guide water planner efforts in increasing groundwater availability for later use.

Acknowledgments

References

Burgis, C. R., Hayes, G. M., Henderson, D. A., Zhang, W., & Smith, J. A. (2020). Green stormwater infrastructure redirects deicing salt from surface water to groundwater. Science of The Total Environment, 729, 138736. https://doi.org/10.1016/j.scitotenv.2020.138736

Caparrós-Martínez, J. L., Milán-García, J., Rueda-López, N., & de Pablo-Valenciano, J. (2020). Green Infrastructure and Water: An Analysis of Global Research. MDPI Water J., 12(6), 1760. https://doi.org/10.3390/w12061760

Forghani, A., & Peralta, R. C. (2018). Intelligent performance evaluation of aquifer storage and recovery systems in freshwater aquifers. Journal of Hydrology, 563, 599-608. https://doi.org/10.1016/j.jhydrol.2018.06.042

Gabor, R. S., Hall, S. J., Eiriksson, D. P., Jameel, Y., Millington, M., Stout, T., Barnes, M. L., Gelderloos, A., Tennant, H., Bowen, G., Neilson, B. T., & Brooks, P. D. (2017). Persistent Urban Influence on Surface Water Quality via Impacted Groundwater. Environ. Sci. Technol., 51(17), 9477–9487. https://doi.org/10.1021/acs.est.7b00271

Innovate Urban Transitions and Arid region Hydro-sustainability (iUTAH). (2012). https://iutahepscor.org/

Lambert, P. M. (1995). Numerical Simulation of Ground-Water Flow in Basin-Fill Material in Salt Lake Valley, Utah. U. S. Geological Survey Technical Publication No. 110-B. https://pubs.er.usgs.gov/publication/70179464

McDonald, M. G., & Harbaugh, A. W. (1988). A modular three-dimensional finite-difference ground-water flow model. U. S. Geological Survey Report Techniques of Water-Resources Investigations 06-A1. https://doi.org/10.3133/twri06A1

Naumann, S., Davis, M., Kaphengst, T., Pieterse, M., & Rayment, M. (2011). Design, implementation and cost elements of Green Infrastructure projects. Final Report to the European Commission, DG Environment, Contract no. 070307/2010/577182/ETU/F.1, Ecologic institute and GHK Consulting.

http://ec.europa.eu/environment/enveco/biodiversity/pdf/GI_DICE_FinalReport.pdf

Niswonger, R. G. (2020). An Agricultural Water Use Package for MODFLOW and GSFLOW. Environmental Modelling and Software, 125, 104617. https://doi.org/10.1016/j.envsoft.2019.104617

Niswonger, R. G., & Prudic, D. E. (2005). Documentation of the Streamflow-Routing (SFR2) package to include unsaturated flow beneath streams—A modification to SFR1. U. S. Geological Survey Techniques and Methods 6-A13. https://doi.org/10.3133/tm6A13

Ou, G., Chen, X., Kilic, A., Bartelt-Hunt, S., Li, Y., & Samal, A. (2013). Development of a cross-section based streamflow routing package for MODFLOW. Environmental Modelling and Software, 50, 132-143. https://doi.org/10.1016/j.envsoft.2013.09.012

Prudic, D. E. (1989). Documentation of a Computer Program to Simulate Stream-aquifer Relations Using a Modular, Finite-difference, Ground-water Flow Model. U.S. Geological Survey Technical Report 88-729. https://doi.org/10.3133/ofr88729

Prudic, D. E., Konikow, L. F., & Banta, E. R. (2004). A New Stream Flow-routing (SFR1) Package to Simulate Stream-aquifer Interaction with MODFLOW-2000. U.S. Geological Survey Technical Report 2004-1042. https://doi.org/10.3133/ofr20041042

PV and Associates. (2015). WinSLAMM Version 10.2 User's Guide. Tuscaloosa, AL. http://winslamm.com/docs/01%20WinSLAMM%20v%2010.2%20User%27s%20Guide%20-%20Introduction.pdf

Rohmat, F. I. W., Labadie., J. W., & Gates, T. K. (2019). Deep learning for compute-efficient modeling of BMP impacts on stream-aquifer exchange and water law compliance in an irrigated river basin. Environmental Modelling and Software, 122, 104529. https://doi.org/10.1016/j.envsoft.2019.104529

Salt Lake County. (2004). https://rain-flow.slco.org/

Schmid, W., Hanson, R. T., Leake, S. A., Hughes, J. D., & Niswonger, R. G. (2014). Feedback of land subsidence on the movement and conjunctive use of water resources. Environmental Modelling and Software, 62, 253-270. https://doi.org/10.1016/j.envsoft.2014.08.006

Shultz, C. D., Gates, T. K., & Bailey, R. T. (2018). Evaluating best management practices to lower selenium and nitrate in groundwater and streams in an irrigated river valley using a calibrated fate and reactive transport model. Journal of Hydrology, 566, 299–312. https://doi.org/10.1016/j.jhydrol.2018.09.005

Thiros, A., Bexfield, L. M., Anning, D. W., & Huntington, J. M. (2010). Conceptual Understanding and Groundwater Quality of Selected Basin-Fill Aquifers in the Southwestern United States. U.S. Geological Survey Professional Paper 1781. https://pubs.usgs.gov/pp/1781/

Tzoulas, K., Korpela, K., Venn, S., Tli-Pelkonen, V., Kazmierczek, A., Niemmela, J., & James, P. (2007). Promoting ecosystem and human health in urban areas using Green Infrastructure: A literature review. Landscape and Urban Planning, 81(3), 167-178. https://doi.org/10.1016/j.landurbplan.2007.02.001

Utah Division of Water Rights. (2008). https://waterrights.utah.gov/

Zhang, J., & Peralta, R. C. (2019). Estimating infiltration increase and runoff reduction due to green infrastructure. Journal of Water and Climate Change, 10(2), 237–242. https://doi.org/10.2166/wcc.2018.354

Zhang, K., & Chui, T. F. M. (2019). A review on implementing infiltration-based green infrastructure in shallow groundwater environments: Challenges, approaches, and progress. Journal of Hydrology, 579, 124089. https://doi.org/10.1016/j.jhydrol.2019.124089

CHAPTER 5

CONCLUDING REMARKS

5.1. Summary

Groundwater availability can be increased via aquifer storage and recovery (ASR), aquifer recharge (AR), and green-infrastructure (GI) recharge systems. This study predicts simulated impacts of applying these three recharge techniques to a shallow unconfined aquifer with/without simulated surface waters.

First developed, for an ASR well at which extraction from an unconfined aquifer begins when injection ceases, were porosity-specific polynomial equations that predict injectate recovery effectiveness (REN). REN is the time-varying proportion of total injectate that has been extracted. Presented estimators are suitable for specific ranges of inputs: a) aquifer hydraulic conductivity of 4-20 m/d (13.124-65.61 ft/d); b) specific yield of 0.0375-0.57; c) initial saturated thickness of 8-46 m (26.25-150.91 ft); d) initial aquifer hydraulic gradient of 0.00001-0.015; e) porosity of 0.1-0.6; and f) steady rates of injection (61 days) and extraction (during a 91-day period of high demand) of 5.451-327.06 m^3/d (1-60 gpm). Estimator-predicted REN values (after 15 to 91 days of extraction) are accurate--ranging from 0.002 to 0.025 gm/gm for root mean square error (RMSE), from 0.9921 to 0.9996 for R^2, and from 1.03 to 4.59% for scatter index (SI). Presented estimators help a user to predict REN rapidly, avoiding the necessity of preparing for and executing flow or solute

transport simulations. A developed graphic user interface facilitates using the estimators and evaluating ASR and AR designs.

Second, the easy-to-use Managed Storage for Effective Recovery (MASER) software aids reconnaissance level design and evaluation of a single-well ASR or AR system for user-selected sites. One MASER option invokes the above-mentioned REN estimators. For other situations, MASER semi-automatically applies groundwater flow (MODFLOW2005) and solute transport (MT3DMS version 5.30) simulators under the Windows 10 operating system. Addressable site features include: a) aquifer type (confined and unconfined); b) concentrations of injected water and native groundwater; c) injection type (steady and unsteady); d) ratio of extraction and injection volumes (ratio is zero for AR and is based upon pre-existing groundwater right for ASR); e) storage time between the end of injection and the beginning of ASR extraction; f) 61 days of injection; and g) 91 days of extraction. MASER provides estimated and/or simulated values of hydraulic drawup and drawdown, REN, and blended solute concentration of ASR-extracted water. MASER also provides simulated aquifer solute concentration maps.

Two discussed groups of MASER simulations employ precipitation data for Salt Lake Valley (SLV), and shallow unconfined aquifer hydrogeologic data underlying a Salt Lake City (SLC) block (native groundwater has 1500-ppm TDS). Three demonstrated ASR and AR simulations (Demos 1b-d) assume 61 days of steady injection of 387 ppm diverted stream flow and 91 days of steady extraction (the total arbitrary injection volume equals the 90%-probability April-May precipitation runoff volume of 1986-2016 years from the SLC block). Demos differ in extraction rate and total extraction volume. In the below Group A Demos,

Demo ii), and Demos i-ii) are compared with Demo i), and Demo iii) respectively. Group A Demos details are:

i)   assuming a total extraction volume equaling the injection volume, the extracted water can irrigate 1896.71 m^2 (0.47 acre) of turf with a blended TDS of 1277 ppm, and 91-day extraction recovers 20% of injectate (i.e., REN is 0.2) and leaves a reduced-TDS plume (41.5 m or 136.15 ft long in the flow direction and 9 m or 29.52 ft wide);

ii) assuming a goal of 80% injectate recovery requires and involves extracting 5.4 times the total injection volume (i.e., requires having a pre-existing groundwater extraction right 4.4 times the injection volume), allows irrigating 5.4 times as much turf, increases the blended TDS by 57 ppm, shrinks the reduced-TDS plume length by 10 m (32.81 ft) and width by 6 m (19.68 ft), and achieves a REN of 0.8 at end of 91-day extraction;

iii) assuming steady AR injection, 60-day (maximum storage time if the extraction of the injectate at the well desired) transport of the injectate in the flow direction after injection, and no extraction increases the length of the reduced-TDS plume by 37 m (121.39 ft) and the width by 16 m (52.49 ft).

Group B ASR simulations without considering water quality show how depending upon the injection time-series, injecting a specific volume unsteadily versus steadily can either increase or decrease REN. Two types of Group B simulations were performed for each

year of 1986-2016. One type simulated 61 days of injection of estimated daily runoff from the specified SLC block. The other type simulated steady injection at a rate equaling 1/61 of the total April-May runoff from the block of that year. Both simulation types extracted steadily for 91 days to remove a volume equal to the total injection. Results show: a) when comparing unsteady injection simulations, the unsteady injection time series has more impact on REN than the total injection volume--a year having greater total injection volume might not yield a higher REN; b) when comparing steady injection simulations, the greater the total injection volume, the greater the resulting REN; and c) when comparing results from steady versus unsteady injection of the same total volume, the unsteady could achieve either a higher or lower predicted REN than the steady. For example, simulated injection volumes for 1987 and 2001 are 1392.81, and 1738.17 m^3, respectively. For 1987, predicted REN values of the steady and unsteady injections are 0.288 and 0.342, respectively. For 2001, respective REN values are 0.248 for steady injection and 0.168 for unsteady injection. In general, steady injection is more likely to cause a predictable REN but might not cause a higher REN than unsteady injection. In essence, MASER facilitates evaluation and design of systems for injecting available water unsteadily, or steadily whatever source via ASR or AR. Unless stormwater runoff is augmented or stored sufficiently to allow steady injection, the group B simulations compare RENs of transient stormwater runoff versus steady diversion of water such as surface water or recyclable water.

A third tool, to predict GI recharge impacts on groundwater and surface waters in the Salt Lake County 1300 South Drainage Basin in Utah, is a MODFLOW2005 stream-aquifer

simulation model. GI can increase the proportion of precipitation that percolates into an aquifer and can improve the timing and volume of available groundwater and/or surface water. Derived from a Salt Lake Valley-wide multilayer groundwater model, the presented sub-system model includes only the Red Butte watershed. This HyperRBC sub-system model uses: a) a refined discretization (cell size of 308 ft by 308 ft within seven aquifer layers); and b) the Streamflow-Routing (SFR) package to simulate Red Butte Creek (RBC) flow. The SFR includes: i) assumed RBC domain values; ii) inflows into RBC; and iii) outflows from RBC to calibrate values of the RBC vertical hydraulic conductivity (ranged from 0.0045 to 12.26 ft/d) of the streambed. HyperRBC simulated the results of a hypothetical GI implementation of grass swales to increase groundwater storage. Assumed was 54.30 ac-ft GI recharge into the aquifer from April to June of 2016 within a 704-acre area east of the Jordan river (JR). Simulation predicted that by the end of a year: a) about three percent of the GI recharge remained within the unconfined aquifer in the HyperRBC area; b) 66.6% of the recharge flowed the general SLV groundwater hydraulic gradient northward into the continuation of the unconfined aquifer; and c) 30.3% discharged to surface waters (11.7% to the JR, 1.3% to RBC, and 17.3% to a drain connected to the JR).

In conclusion, the provided water supply modeling tools can guide water planning and management efforts in increasing groundwater availability for later use.

APPENDICES

Appendix A. Statistical indices

Table A.1

Statistical indices

Parameter	Formula*	Range	Applied by
Mean Error (ME)	$\dfrac{1}{n}\sum_{i=1}^{n}(O_i - S_i)$	$-\infty < ME < +\infty$; Perfect: 0	Javan et al. (2015)
Root Mean Square Error (RMSE)	$\sqrt{\dfrac{1}{n}\sum_{i=1}^{n}(O_i - S_i)^2}$	$0 \leq RMSE < +\infty$; Perfect: 0	Mentaschi et al. (2013); Javan et al. (2015); Jimeno-Sáez et al. (2018)
Peak Weighted Root Mean Square Error (PWRMSE)	$\sqrt{\dfrac{1}{n}\sum_{i=1}^{n}(O_i - S_i)^2 \times \left(\dfrac{O_i + \overline{O}}{\overline{2O}}\right)}$	$0 \leq PWRMSE < +\infty$; Perfect: 0	Javan et al. (2015)
Pearson's Correlation Coefficient (r)	$\dfrac{\sum_{i=1}^{n}(O_i - \overline{O}) \times (S_i - \overline{S})}{\sqrt{\sum_{i=1}^{n}(O_i - \overline{O})^2 \times \sum_{i=1}^{n}(S_i - \overline{S})^2}}$	$-1 \leq r \leq 1$; Perfect: 1 or -1	Moriasi et al. (2007); Javan et al. (2015)
Coefficient of Determination (R²)	$\dfrac{[\sum_{i=1}^{n}(O_i - \overline{O}) \times (S_i - \overline{S})]^2}{\sum_{i=1}^{n}(O_i - \overline{O})^2 \times \sum_{i=1}^{n}(S_i - \overline{S})^2}$	$0 \leq R^2 \leq 1$; Perfect: 1	Moriasi et al. (2007); Jimeno-Sáez et al. (2018)
Nash-Sutcliffe Efficiency (NSE or E_{NS})	$1 - \dfrac{\sum_{i=1}^{n}(O_i - S_i)^2}{\sum_{i=1}^{n}(O_i - \overline{O})^2}$	$-\infty < E_{NS} \leq 1$; Perfect: 1	Nash and Sutcliffe (1970); Moriasi et al. (2007); Javan et al. (2015); Jimeno-Sáez et al. (2018)
Percent Bias (PBIAS)	$\dfrac{\sum_{i=1}^{n}(O_i - S_i)}{\sum_{i=1}^{n}O_i} \times 100$	$|PBIAS| \leq 25\%$ very good	Moriasi et al. (2007); Jimeno-Sáez et al. (2018)
Scatter Index (SI)	$\sqrt{\dfrac{\sum_{i=1}^{n}[(S_i - \overline{S}) - (O_i - \overline{O})]^2}{\sum_{i=1}^{n}O_i^2}}$	Perfect: SI < 20%; Operational: SI < 60%	Janssen and Komen (1984); Moriasi et al. (2007)

*Note. n is the number of data pairs; O_i represent observed MODFLOW2005-MT3DMS results, and S_i represent estimated values; $\overline{O}$ is the mean observed value; $\overline{S}$ is the mean estimated value.

Appendix B. Red Butte Creek flow data and vertical hydraulic conductivities of streambed

Table B.1

Observed inflow data of Red Butte Reservoir from USGS 10172200 Red Butte Creek at Fort Douglas, near Salt Lake City, Utah (cfs)

Monthly Avg. Inflow (cfs) to Red Butte Reservoir	Jan.	Feb.	Mar.	Apr.	May	June	July	Aug.	Sep.	Oct.	Nov.	Dec.
Year / Month	1	2	3	4	5	6	7	8	9	10	11	12
2009	1.4281	2.1629	3.9852	14.0357	15.1777	6.7020	3.3332	1.9561	1.4753	1.7058	1.7077	1.6629
2010	1.7777	1.6832	2.2213	5.8943	8.4623	6.3763	2.9584	1.7981	1.4397	1.5061	1.6980	2.3952
2011	2.6571	2.5914	6.7058	19.0507	37.4065	24.2200	8.3355	4.7400	2.9790	3.2087	3.0587	2.5797
2012	2.4010	2.1714	3.2216	4.1637	3.0365	1.8460	1.3355	0.9658	0.9183	1.1448	1.4123	1.4303
2013	1.5500	2.0668	2.5687	3.7663	2.6019	1.5003	0.9435	0.6784	0.8043	0.9371	1.0740	0.9226
2014	1.1287	1.4029	1.9842	2.9633	2.7477	1.6253	0.9832	0.8561	0.8733	1.0468	1.1153	1.1097
2015	1.0997	1.4175	1.3445	1.6437	4.9374	2.7397	1.2906	0.8481	0.6920	0.8561	0.8957	0.8997
2016	1.0045	1.3338	2.2948	3.8550	4.7600	2.1873	1.0684	0.6503	0.6903	0.9042	1.0620	1.2510
2017	0.9713	3.0457	6.7713									
Average monthly values from 2009 to 2016	1.6308	1.8537	3.0408	6.9216	9.8913	5.8996	2.5310	1.5616	1.2340	1.4137	1.5030	1.5314

Table B.2

Monthly observed and estimated tributary inflows of Connor Road storm drain into RBC from 2009 to 2017 (cfs)

Storm Drain Name	Year	Month	Inflow to RBC (cfs)	Year	Month	Inflow to RBC (cfs)
Connor Road	2009 to 2015	Jan.	0.0662	2016	Apr.	0.1384
Connor Road	2009 to 2015	Feb.	0.0844	2016	May	0.1117
Connor Road	2009 to 2015	Mar.	0.1345	2016	June	0.0536
Connor Road	2009 to 2015	Apr.	0.1705	2016	July	0.0642
Connor Road	2009 to 2015	May	0.0945	2016	Aug.	0.0540
Connor Road	2009 to 2015	June	0.0546	2016	Sep.	0.1118
Connor Road	2009 to 2014	July	0.1833	2016	Oct.	0.0798
Connor Road	2009 to 2014	Aug.	0.2023	2016	Nov.	0.0803
Connor Road	2009 to 2014	Sep.	0.4798	2016	Dec.	0.0635
Connor Road	2009 to 2014	Oct.	0.2178	2017	Jan.	0.0813
Connor Road	2009 to 2014	Nov.	0.2264	2017	Feb.	0.1098
Connor Road	2009 to 2014	Dec.	0.2495	2017	Mar.	0.1736
Connor Road	2015	July	0.2953	2017	Apr.	0.2026
Connor Road	2015	Aug.	0.0486	2017	May	0.0774
Connor Road	2015	Sep.	0.5576	2017	June	0.0556
Connor Road	2015	Oct.	0.0189	2017	July	0.1903
Connor Road	2015	Nov.	0.0086	2017	Aug.	0.5042
Connor Road	2015	Dec.	0.1461	2017	Sep.	0.7698
Connor Road	2016	Jan.	0.0511	2017	Oct.	0.5546
Connor Road	2016	Feb.	0.0591	2017	Nov.	0.5903
Connor Road	2016	Mar.	0.0954	2017	Dec.	0.5389

Table B.3

Monthly observed and estimated tributary inflows of GIRF storm drain into RBC from 2009 to 2017 (cfs)

Storm Drain Name	Year	Month	Inflow to RBC (cfs)	Year	Month	Inflow to RBC (cfs)
GIRF	2009 to 2014	Jan.	0.4663	2015	Nov.	0.0180
GIRF	2009 to 2014	Feb.	0.0484	2015	Dec.	0.3368
GIRF	2009 to 2014	Mar.	0.0079	2016	Jan.	0.9006
GIRF	2009 to 2014	Apr.	0.0061	2016	Feb.	0.1179
GIRF	2009 to 2014	May	0.0065	2016	Mar.	0.0071
GIRF	2009 to 2014	June	0.0022	2016	Apr.	0.0052
GIRF	2009 to 2014	July	0.0036	2016	May	0.0046
GIRF	2009 to 2013	Aug.	0.0058	2016	June	0.0020
GIRF	2009 to 2013	Sep.	0.0142	2016	July	0.0032
GIRF	2009 to 2013	Oct.	0.0040	2016	Aug.	0.0024
GIRF	2009 to 2013	Nov.	0.0113	2016	Sep.	0.0074
GIRF	2009 to 2013	Dec.	0.1201	2016	Oct.	0.0026
GIRF	2014	Aug.	0.0168	2016	Nov.	0.0032
GIRF	2014	Sep.	0.0346	2016	Dec.	0.1165
GIRF	2014	Oct.	0.0107	2017	Jan.	0.3921
GIRF	2014	Nov.	0.0206	2017	Feb.	0.0062
GIRF	2014	Dec.	0.0247	2017	Mar.	0.0074
GIRF	2015	Jan.	0.1063	2017	Apr.	0.0084
GIRF	2015	Feb.	0.0211	2017	May	0.0017
GIRF	2015	Mar.	0.0093	2017	June	0.0029
GIRF	2015	Apr.	0.0048	2017	July	0.0044
GIRF	2015	May	0.0131	2017	Aug.	0.0016
GIRF	2015	June	0.0017	2017	Sep.	0.0096
GIRF	2015	July	0.0032	2017	Oct.	0.0013
GIRF	2015	Aug.	0.0024	2017	Nov.	0.0033
GIRF	2015	Sep.	0.0052	2017	Dec.	0.0022
GIRF	2015	Oct.	0.0016			

Table B.4

Monthly observed and estimated tributary inflows of Fort Douglas storm drain into RBC from 2009 to 2017 (cfs)

Storm Drain Name	Year	Month	Inflow to RBC (cfs)	Year	Month	Inflow to RBC (cfs)
Fort Douglas	2009 to 2014	Jan.	0.0022	2015	Nov.	0.0000
Fort Douglas	2009 to 2014	Feb.	0.0018	2015	Dec.	0.0006
Fort Douglas	2009 to 2014	Mar.	0.0065	2016	Jan.	0.0002
Fort Douglas	2009 to 2014	Apr.	0.0075	2016	Feb.	0.0008
Fort Douglas	2009 to 2014	May	0.0093	2016	Mar.	0.0071
Fort Douglas	2009 to 2014	June	0.0010	2016	Apr.	0.0070
Fort Douglas	2009 to 2014	July	0.0034	2016	May	0.0055
Fort Douglas	2009 to 2013	Aug.	0.0052	2016	June	0.0008
Fort Douglas	2009 to 2013	Sep.	0.0120	2016	July	0.0000
Fort Douglas	2009 to 2013	Oct.	0.0010	2016	Aug.	0.0006
Fort Douglas	2009 to 2013	Nov.	0.0009	2016	Sep.	0.0078
Fort Douglas	2009 to 2013	Dec.	0.0024	2016	Oct.	0.0024
Fort Douglas	2014	Aug.	0.0170	2016	Nov.	0.0031
Fort Douglas	2014	Sep.	0.0217	2016	Dec.	0.0016
Fort Douglas	2014	Oct.	0.0006	2017	Jan.	0.0001
Fort Douglas	2014	Nov.	0.0005	2017	Feb.	0.0044
Fort Douglas	2014	Dec.	0.0074	2017	Mar.	0.0102
Fort Douglas	2015	Jan.	0.0064	2017	Apr.	0.0067
Fort Douglas	2015	Feb.	0.0002	2017	May	0.0009
Fort Douglas	2015	Mar.	0.0022	2017	June	0.0008
Fort Douglas	2015	Apr.	0.0089	2017	July	0.0080
Fort Douglas	2015	May	0.0215	2017	Aug.	0.0000
Fort Douglas	2015	June	0.0014	2017	Sep.	0.0116
Fort Douglas	2015	July	0.0021	2017	Oct.	0.0000
Fort Douglas	2015	Aug.	0.0031	2017	Nov.	0.0000
Fort Douglas	2015	Sep.	0.0071	2017	Dec.	0.0000
Fort Douglas	2015	Oct.	0.0010			

Table B.5

Monthly observed and estimated tributary inflows of Dentistry storm drain into RBC from 2009 to 2017 (cfs)

Storm Drain Name	Year	Month	Inflow to RBC (cfs)	Year	Month	Inflow to RBC (cfs)
Dentistry	2009 to 2015	Jan.	0.0819	2016	June	0.0091
Dentistry	2009 to 2015	Feb.	0.0272	2016	July	0.0017
Dentistry	2009 to 2015	Mar.	0.0670	2016	Aug.	0.0140
Dentistry	2009 to 2015	Apr.	0.0567	2016	Sep.	0.0266
Dentistry	2009 to 2015	May	0.0327	2016	Oct.	0.0415
Dentistry	2009 to 2015	June	0.0120	2016	Nov.	0.0552
Dentistry	2009 to 2015	July	0.0713	2016	Dec.	0.0255
Dentistry	2009 to 2015	Aug.	0.0204	2017	Jan.	0.0353
Dentistry	2009 to 2014	Sep.	0.0449	2017	Feb.	0.0463
Dentistry	2009 to 2014	Oct.	0.0205	2017	Mar.	0.0841
Dentistry	2009 to 2014	Nov.	0.0454	2017	Apr.	0.0677
Dentistry	2009 to 2014	Dec.	0.0259	2017	May	0.0135
Dentistry	2015	Sep.	0.0223	2017	June	0.0149
Dentistry	2015	Oct.	0.0193	2017	July	0.1409
Dentistry	2015	Nov.	0.0594	2017	Aug.	0.0269
Dentistry	2015	Dec.	0.0283	2017	Sep.	0.0860
Dentistry	2016	Jan.	0.1284	2017	Oct.	0.0008
Dentistry	2016	Feb.	0.0081	2017	Nov.	0.0216
Dentistry	2016	Mar.	0.0498	2017	Dec.	0.0239
Dentistry	2016	Apr.	0.0456			
Dentistry	2016	May	0.0519			

Table B.6

Estimated inflow of hypothetical groundwater spring (cfs) into RBC

Month	Month no.	Proportion	Estimated Inflow (cfs)
January	4	0.0584	0.0952
February	3	0.0653	0.1210
March	2	0.0722	0.2194
April	1	0.0790	0.5471
May		0.0859	0.8500
June		0.0102	0.0600
July	10	0.0171	0.0432
August	9	0.0239	0.0374
September	8	0.0308	0.0380
October	7	0.0377	0.0533
November	6	0.0446	0.0670
December	5	0.0515	0.0789

Notes. a) values of assumed hypothetical groundwater spring for the calibration in May and June 2016 are 0.85 and 0.06 cfs respectively.

b) proportions of May and June are based upon dividend of the assumed spring value in Table 4.3 and the average monthly value in Table B.1. Here, proportions of May and June are 0.0859 and 0.0102 respectively.

c) proportions of other months are [May proportion - ((May proportion - June proportion) * Month no.) / 11].

d) estimated inflow for a month is proportion of the month multiplied by the average monthly value in Table B.1.

Table B.7

Estimated inflow of groundwater springs (cfs) into RBC

Month	Month no.	Proportion	Estimated Inflow (cfs)
January	4	0.0674	0.1099
February	3	0.0599	0.1111
March	2	0.0524	0.1595
April	1	0.0450	0.3113
May		0.0375	0.3710
June		0.1197	0.7060
July	10	0.1122	0.2840
August	9	0.1047	0.1635
September	8	0.0973	0.1200
October	7	0.0898	0.1269
November	6	0.0823	0.1237
December	5	0.0749	0.1146

Notes. a) values of observed groundwater springs (Gabor et al., 2017) for the calibration in May and June 2016 are 0.371 and 0.706 cfs respectively.

b) proportions of May and June are based upon dividend of the observed spring value in Table 4.3 and the average monthly value in Table B.1. Here, proportions of May and June are 0.0375 and 0.1197 respectively.

c) proportions of other months are [May proportion - ((May proportion - June proportion) * Month no.) / 11].

d) estimated inflow for a month is proportion of the month multiplied by the average monthly value in Table B.1.

Table B.8

Monthly mean observed streamflow at Canyon Mouth of Emigration Creek (cfs)

streamflow in cfs / Date	Jan.	Feb.	Mar.	Apr.	May	June	July	Aug.	Sep.	Oct.	Nov.	Dec.
2009	1.00	1.44	6.02	34.10	32.60	21.20	14.50	3.97	1.62	3.80	4.16	3.29
2010	3.33	3.36	3.84	11.60	19.30	13.40	4.66	2.39	2.94	3.71	3.90	6.13
2011	7.51	4.61	17.30	44.50	75.40	57.40	20.60	8.79	4.92	4.45	4.09	2.77
2012	2.89	2.46	4.28	4.74	1.90	1.80	1.36	1.52	1.40	1.27	0.05	0.07
2013	0.42	0.01	1.41	5.41	4.20	2.04	1.27	0.94	0.17	1.21	2.16	2.15
2014	2.67	3.24	3.51	5.93	4.94	4.90	3.41	1.67	1.42	1.60	1.53	1.13
2015	1.72	2.59	1.12	1.47	9.69	4.82	1.96	1.56	1.29	1.12	0.97	0.96
2016	0.86	0.74	2.72	6.54	7.92	4.14	2.17	0.87	0.58	0.67	0.67	0.74
2017	0.89	7.28	18.39									

Table B.9

Monthly mean observed streamflow at Canyon Mouth of Parleys Creek (cfs)

streamflow in cfs / Date	Jan.	Feb.	Mar.	Apr.	May	June	July	Aug.	Sep.	Oct.	Nov.	Dec.
2009	4.53	5.76	6.28	30.90	38.00	18.00	9.21	4.72	3.86	4.31	5.45	5.85
2010	4.76	3.91	11.10	11.30	13.80	23.70	6.97	4.35	3.55	3.52	3.67	5.21
2011	4.22	3.08	10.10	111.00	159.00	134.00	58.20	24.60	9.60	41.70	23.20	12.90
2012	7.31	6.92	6.86	6.72	6.44	6.16	1.90	1.61	1.39	1.65	2.15	2.45
2013	2.36	2.21	3.89	6.77	5.48	3.75	3.55	3.12	3.23	2.07	2.48	2.03
2014	2.31	3.47	3.21	3.14	4.85	3.22	2.50	1.36	1.28	2.20	2.43	2.54
2015	3.21	2.99	2.94	3.32	5.91	4.33	2.67	2.55	2.45	1.69	1.80	3.57
2016	3.49	3.67	5.04	6.45	7.14	4.80	2.81	2.05	1.76	1.52	1.63	1.99
2017	2.80	5.12	46.62									

Table B.10

Length, bottom width, and streambed vertical hydraulic conductivity values of RBC segments/reaches

Flow or Streamflow Measurement Station modeled in HyperRBC	Segment/Reach No.	Conveyance type	Segment/Reach length (ft.)	Bottom Width (ft.)	Calibrated vertical hydraulic conductivity (K_v) of Streambed (ft/d)
Headwater (inflow from Red Butte Reservoir)	1	Stream	189.433	1.969	2.608
	2	Stream	325.948	1.969	2.608
	3	Stream	314.244	1.969	2.608
	4	Stream	218.456	1.969	2.608
	5	Stream	138.635	1.969	2.608
	6	Stream	357.392	1.969	2.608
	7	Stream	130.828	1.969	2.608
	8	Stream	271.597	1.969	2.608
	9	Stream	145.134	1.969	2.608
	10	Stream	346.257	1.969	2.608
	11	Stream	180.055	1.969	2.608
	12	Stream	173.408	1.969	2.608
	13	Stream	285.564	1.969	2.608
	14	Stream	281.002	1.969	2.608
	15	Stream	209.427	1.969	2.608
	16	Stream	348.524	1.969	2.608
	17	Stream	256.183	1.969	1.036
	18	Stream	245.766	1.969	1.036
	19	Stream	401.153	1.969	1.036
	20	Stream	224.006	1.969	1.036
	21	Stream	429.551	1.969	1.036
	22	Stream	209.029	1.969	1.036
	23	Stream	413.024	1.969	1.036
	24	Stream	223.345	1.969	1.036
	25	Stream	394.363	1.969	1.036
	26	Stream	199.578	1.969	1.036
	27	Stream	366.518	1.969	1.036
	28	Stream	227.674	1.969	1.036
	29	Stream	181.992	1.969	6.635
	30	Stream	345.054	1.969	6.635
	31	Stream	164.833	1.969	6.635
Cottam Grove	32	Stream	227.452	1.969	6.635
	33	Stream	309.546	16.404	0.992
Conner Road SD inflow	34	Stream	317.304	16.404	0.992
	35	Stream	262.244	16.404	0.992
	36	Stream	124.048	16.404	0.992
GIRF SD inflow	37	Stream	368.031	16.404	0.050
	38	Stream	197.379	16.404	0.050

Table B.10

Length, bottom width, and streambed vertical hydraulic conductivity values of RBC segments/reaches (continued)

Flow or Streamflow Measurement Station modeled in HyperRBC	Segment/Reach No.	Conveyance type	Segment/Reach length (ft.)	Bottom Width (ft.)	Calibrated vertical hydraulic conductivity (K_v) of Streambed (ft/d)
	39	Stream	308.663	16.404	0.050
	40	Stream	192.029	16.404	0.050
Fort Douglas SD inflow	41	Stream	251.979	16.404	0.050
Dentistry SD inflow	42	Stream	341.15	16.404	0.050
	43	Stream	193.876	16.404	0.050
	44	Stream	360.646	16.404	0.050
Foothill Drive SMS	45	Stream	194.853	16.404	0.050
Tributary 1: Mount Olivet Ditch inflow; spring inflow	46	Stream	271.795	9.843	12.260
Spring inflow	47	Stream	163.272	9.843	12.260
	48	Stream	186.275	9.843	0.027
	49	Stream	281.019	9.843	0.027
	50	Stream	362.585	9.843	0.027
	51	Stream	214.444	9.843	0.027
	52	Stream	405.607	9.843	0.027
	53	Stream	206.432	9.843	0.027
	54	Stream	362.28	9.843	0.027
	55	Stream	214.132	9.843	0.027
	56	Stream	132.897	9.843	0.027
Diversion 1: Mount Olivet Cemetery	57	Stream	200.000	9.843	0.000
	58	Stream	368.248	9.843	0.027
	59	Stream	226.278	9.843	0.027
	60	Stream	360.662	9.843	0.027
	61	Stream	193.359	9.843	0.027
	62	Stream	333.367	9.843	0.027
	63	Stream	211.206	9.843	0.027
	64	Stream	270.366	9.843	0.027
	65	Stream	108.965	9.843	0.027
Miller Park SMS (near 1600 E)	66	Stream	342.456	9.843	0.027
	67	Stream	143.762	9.843	0.018
	68	Stream	229.784	9.843	0.018
	69	Stream	211.487	9.843	0.018
	70	Stream	349.885	9.843	0.018

Table B.10

Length, bottom width, and streambed vertical hydraulic conductivity values of RBC segments/reaches (continued)

Flow or Streamflow Measurement Station modeled in HyperRBC	Segment/Reach No.	Conveyance type	Segment/Reach length (ft.)	Bottom Width (ft.)	Calibrated vertical hydraulic conductivity (K_v) of Streambed (ft/d)
	71	Stream	231.425	9.843	0.018
	72	Stream	89.449	9.843	0.018
	73	Stream	360.947	9.843	0.018
	74	Stream	329.949	9.843	0.018
	75	Stream	311.387	9.843	0.018
	76	Stream	153.149	11.483	0.018
	77	Stream	177.705	11.483	0.018
	78	Stream	310.527	11.483	0.018
	79	Stream	158.363	11.483	0.018
1300 E SMS	80	Stream	153.712	11.483	0.018
	81	Stream	311.822	11.483	0.2725
	82	Stream	311.965	11.483	0.2725
	83	Stream	199.705	11.483	0.2725
	84	Underground pipe	308	11.483	0.2725
	85	Underground pipe	308	11.483	0.2725
	86	Underground pipe	308	11.483	4.215
	87	Underground pipe	308	11.483	4.215
	88	Underground pipe	308	11.483	4.215
	89	Underground pipe	308	11.483	4.215
	90	Underground pipe	308	11.483	4.215
	91	Underground pipe	308	11.483	4.215
	92	Underground pipe	308	11.483	4.215
	93	Underground pipe	308	11.483	0.00528
	94	Underground pipe	308	11.483	0.00528
	95	Underground pipe	308	11.483	0.00528
	96	Underground pipe	308	11.483	0.00528
	97	Underground pipe	308	11.483	0.00528
	98	Underground pipe	308	11.483	0.00528
Tributary 2: Emigration Creek inflow	99	Underground pipe	308	11.483	0.00528
	100	Underground pipe	308	164.042	0.00528
	101	Underground pipe	308	164.042	0.00528
	102	Underground pipe	308	11.483	0.0045
	103	Underground pipe	308	11.483	0.0045
	104	Underground pipe	308	11.483	0.0045
	105	Underground pipe	308	11.483	0.0045
	106	Underground pipe	308	11.483	0.0045
	107	Underground pipe	308	11.483	0.0045
	108	Underground pipe	308	11.483	0.0045

Table B.10

Length, bottom width, and streambed vertical hydraulic conductivity values of RBC segments/reaches (continued)

Flow or Streamflow Measurement Station modeled in HyperRBC	Segment/Reach No.	Conveyance type	Segment/Reach length (ft.)	Bottom Width (ft.)	Calibrated vertical hydraulic conductivity (K$_v$) of Streambed (ft/d)
	109	Underground pipe	308	11.483	0.0045
	110	Underground pipe	308	11.483	0.0045
	111	Underground pipe	308	11.483	0.0045
	112	Underground pipe	308	11.483	0.0045
	113	Underground pipe	308	11.483	0.0045
	114	Underground pipe	308	11.483	0.0045
Tributary 3: Parleys Creek inflow	115	Underground pipe	308	11.483	0.0045
	116	Underground pipe	308	11.483	0.0045
	117	Underground pipe	308	11.483	0.0045
	118	Underground pipe	308	11.483	0.0045
	119	Underground pipe	308	11.483	0.0045
	120	Underground pipe	308	11.483	0.0045
	121	Underground pipe	308	11.483	0.0045
	122	Underground pipe	308	11.483	0.0045
	123	Underground pipe	308	11.483	0.0045
	124	Underground pipe	308	11.483	0.0045
	125	Underground pipe	308	11.483	0.0045
	126	Underground pipe	308	11.483	0.0045
	127	Underground pipe	308	11.483	0.0045
	128	Underground pipe	308	11.483	0.0045
	129	Underground pipe	308	11.483	0.0045
	130	Underground pipe	308	11.483	0.0045
	131	Underground pipe	308	11.483	0.0045
	132	Underground pipe	308	11.483	0.0045
	133	Underground pipe	308	11.483	0.0045
	134	Underground pipe	308	11.483	0.0045
	135	Underground pipe	308	11.483	0.0045
	136	Underground pipe	308	11.483	0.0045
	137	Underground pipe	308	11.483	0.0045
	138	Underground pipe	308	11.483	0.0045
	139	Underground pipe	308	11.483	0.0045
	140	Underground pipe	308	11.483	0.0045
900 W SMS Diversion 2: RBC into the Jordan River (Three Creeks Confluence Park)	141	Underground pipe	308	11.483	0.0045
	142	Stream	308	11.483	0.0000

CURRICULUM VITAE

Saeid Masoudiashtiani

SUMMARY

As a Water Resources Engineer with a PhD in Civil Engineering from Utah State University, I have extensive experience in groundwater and surface water modeling, optimization methods, and statistical analyses. I am highly proficient in programming languages such as Python, C#, C++, FORTRAN, and R, which enables me to conduct effective groundwater simulation and manage aquifer recharge, including aquifer storage and recovery (ASR) and aquifer recharge (AR). I have successfully used PEST and UCODE_2014 software for calibration processes in relevant projects, and I have practical experience in irrigation engineering and the use of treated domestic wastewater for irrigation.

EDUCATION

- **Ph.D., Civil Engineering - Water Resources Engineering**
  Dissertation title: Groundwater-Surface water interaction to increase Groundwater Availability
  - ✓ Funded by **EPA-STAR 83582401** project (i.e., Assessment of Stormwater Harvesting via Manage Aquifer Recharge (MAR) to Develop New Water Supplies in the Arid West: The Salt Lake Valley Example) that is published at:
    https://digitalcommons.usu.edu/cee_facpub/3608/
    or
    https://cfpub.epa.gov/ncer_abstracts/index.cfm/fuseaction/display.abstractDetail/abstract_id/10497/report
  Utah State University, USA, May 2022
- **M.Sc., Agricultural Engineering - Irrigation Engineering**,
  Thesis title: Effects of Urban Wastewater on Physical Properties of Soils
  University of Tehran, Tehran, Iran, September 2009
- **B.Sc., Agricultural Engineering - Irrigation and Drainage Engineering**,
  Shiraz University, Shiraz, Iran, May 2005

RESEARCH INTERESTS

- Groundwater and surface water interaction

- Groundwater flow and solute transport modeling

- Optimization models

- Irrigation engineering

RESEARCH EXPERIENCES

Reconnaissance Prediction of ASR Well Recovery Effectiveness in Unconfined Aquifers

- Obtaining Recovery Effectiveness (REN) is how much injectate is within extracted water of a simple aquifer storage and recovery (ASR) system for unconfined freshwater aquifers.
- Employing groundwater flow (**MODFLOW2005**) and solute transport (**MT3DMS**) simulations to quantify REN.
- Implementing **parallel processing** on node clusters of the Center for High-Performance Computing (CHPC) at the University of Utah by using **MPI libraries** in **C++** programming language to run 48000 **MODFLOW2005-MT3DMS** simulations.
- Developing specific-porosity polynomial REN estimators for steady injection and extraction rates (61-day injection and 91-day extraction durations with equal rates) by applying the results of the simulations and an optimization method via **Excel** and **R** software.
- Developing **ANN-based** (**artificial neural net**) predictors to estimate REN for steady injection and extraction rates (61-day injection and 91-day extraction durations with equal rates) by executing the **neural net package** of **R** software.

Managed Aquifer Storage for Effective Recovery (MASER) Software

- Developing a graphical user interface (GUI) in **Python** programming language including a stand-alone executable under the Windows 10 operating system, Managed Aquifer Storage for Effective Recovery (MASER). MASER simplifies evaluating and designing aquifer storage and recovery (ASR) or aquifer recharge (AR) well suitability from water supply and environmental protection perspectives.
- Using unsteady stormwater runoff of a residential area by simulating daily varying stormwater runoff that results from varying daily rainfall in **WinSLAMM 10.4.1** software and applying it for ASR injection in a selected area for water use.
- Applying the injection volume that could be diverted by stream to provide ASR steady injection.
- Comparing REN values that result from the ASR unsteady and steady injections, obtaining blended water quality of the extracted water, and providing row and column maps of groundwater quality for water users and environmental protection agencies.

Modeling Groundwater and Surface Water within Red Butte Watershed in Utah, USA

- Including a part of Salt Lake Valley around Red Butte Creek (RBC) from just downstream of Red Butte Reservoir to and including part of the Jordan River.
- Employing aquifer data primarily from the USGS Salt Lake Valley, groundwater numerical model in MODFLOW.
- Constructing a sub-system groundwater numerical model for Red Butte Watershed (HyperRBC) in **MODFLOW2005**.
- Building RBC distribution network including headwater, tributary inflows, and diversion outflows.
- Applying **Streamflow-Routing** (**SFR**) package to represent RBC and outflow of Red Butte Reservoir as headwater for the model.
- Calibrating vertical hydraulic conductivity of RBC streambed by providing a **C#** code for hundreds of calibration runs that execute the HyperRBC numerical model and parameter estimation (**PEST**) software in **parallel processing**.
- Investigating changes of stream-aquifer seepages resulting from green infrastructure (e.g., grass swale) infiltration around RBC and the Jordan River in SLV, Utah.
- Providing **QUAL2kw** surface water model of RBC to use stream-aquifer seepages of **MODFLOW2005** and simulate water-depth changes for a short period.

Radial Collector Wells

- Investigating analytical equations of Radial Collector wells and publishing a conference paper that compares the results of the equations.
- Providing/Writing **C#** Console and Windows Form codes to connect **Feflow** simulator to SOMOS (Simulation/Optimization Modeling System) software. Originally, SOMOS connects MODFLOW simulator to optimizers such as **GAMS**.
- Providing some simple numerical models in Feflow for Radial Collector wells.
- Modifying I/O files and compiled Analytical Element Method (**AEM**) code of 1989 (written in Fortran-77 programming language) to simulate Radial Collector wells by using Sink lines.

Effects of Urban Wastewater on Physical Properties of Soils (M.Sc. thesis)

- Applying freshwater and urban wastewater for sorghum irrigation to investigate changes in certain soil's physical properties.
- Estimating values of coefficients for a soil-water retention equation to plot its curves by using **RETC** software.
- Showing: i) the increase of the available water capacity of soils by 4% (volumetric), and ii) 24% relative value on average.

TECHNICAL EXPERTISE

Programming Languages: C# console and Windows Form, C++ integrated with MPI libraries for parallel processing under the Windows and Linux operating systems, Python, FORTRAN, R (applied for statistical analyses and Artificial Neural Net), GAMS, and LINGO/LINDO.

Water Resources Engineering Software: ArcMap, QGIS, MODFLOW-2005, MODFLOW 6, MODPATH, MT3DMS, MT3D, PEST, UCODE_2014, GMS, GWV, ModelMuse, Feflow, AEM, HEC-HMS, WinSLAMM, QUAL2K, QUAL2kw, and RETC.

TEACHING EXPERIENCE

Teacher Assistant (TA)

 Utah State University, Logan, Utah [2015, 2016, & 2021]:

- ✓ Developed curriculum for the course "CEE 5450 & CEE 6450, Hydrologic Modeling," which involved creating instructional materials, administering, and grading tests (including quizzes and midterms), holding office hours, and assigning final grades for three semesters.

PUBLICATIONS

- Masoudi Ashtiani, S., Ghasemi, A. R., & Kamgar Haghighi, A. A. (2009). Investigations of Temporal and Spatial Variability of the Minimum Temperature to Estimate Minimum Temperature for Application in Frost Protection a Case Study an Apple Orchard in the Agricultural of College of Shiraz University. The Scientific Journal of Agriculture (SJA), 31(2), 49-58.
  https://www.sid.ir/en/journal/ViewPaper.aspx?ID=181401

- Masoudiashtiani, S., Parsinejad, M., & Abbasi, F. (2011). Effect of Applying Urban Wastewater in Irrigation of Sorghum on Some Soil Physical Properties. Iranian Journal of Soil Research (Formerly Soil and Water Sciences), 25(3), 243-253.
  https://www.sid.ir/en/Journal/ViewPaper.aspx?ID=234889

- Masoudiashtiani, S., & Peralta, R. C. (2022). Managed Aquifer Storage for Effective Recovery (MASER) software, HydroShare,
  http://www.hydroshare.org/resource/3186303590a846e484f4c67d1a336511

- Thayer, B., Masoudiashtiani, S., & Peralta, R. C. (2022). Editing and Running QUAL2KWv6-MODFLOW2005 (ERQMS) integrated software, HydroShare,
  http://www.hydroshare.org/resource/837619c3080b4ee7aaeea81d402c1946

CONFERENCES

- Masoudiashtiani, S., Peralta, R. C., & Banihabib, M. E. (2016). Radial Collector Well Empirical Equations Comparison. 2nd International Conference on Sustainable Development, Strategies, and Challenges with a Focus on Agriculture, Natural Resources, Environment and Tourism, Tabriz, Iran.
  https://www.researchgate.net/publication/299397873_challenges_strategies_and_sustainable_development_International_conference_on_nd_2_With_a_focus_on_Agriculture_Natural_Resources_Environment_and_Tourism_23-25_Feb_2016_Tabriz_Iran_Radial_Collector_Wel

- Masoudiashtiani, S., & Peralta, R. C. (2017). Radial Collector Well Design Optimization. Poster Presentation. Spring Runoff Conference, Logan, Utah, USA.
  https://digitalcommons.usu.edu/runoff/2017/2017Posters/23/

- Masoudiashtiani, S., & Peralta R. C. (2019). Improving stormwater and ASR application to fulfill turf irrigation demand. Poster Presentation H13N-1905, American Geophysical Union, Fall Meeting.
  https://agu.confex.com/agu/fm19/meetingapp.cgi/Paper/607178

- Masoudiashtiani, S., & Peralta, R. C. (2019). Increasing Sustained Water Supply by Optimizing Stormwater and ASR Use to Provide Secondary Water for Turf Irrigation. Oral Presentation. 2019 Annual Conference, American Water Resources Association (AWRA). Salt Lake City, Utah.
  https://aquadoc.typepad.com/files/2019-ac-abstracts_final-2.pdf

- Masoudiashtiani, S., & Peralta, R. C. (2020). Evaluating Surface water and Groundwater Network in Red Butte Watershed to Obtain Sustainable Groundwater Yield and Availability. Oral Presentation. Groundwater Protection Council (GWPC), Virtual Annual Forum.